MODELING MAT CONSOLIDATION OF STRAND-BASED WOOD COMPOSITES DURING HOT PRESSING

by

CHENG ZHOU

B.Sc., Southeast University, 1998
M.Sc., Southeast University, 2001

A THESIS SUBMITTED IN PARTIAL FULFILLMENT OF
THE REQUIREMENTS FOR THE DEGREE OF

DOCTOR OF PHILOSOPHY

in

THE FACULTY OF GRADUATE STUDIES

(Forestry)

THE UNIVERSITY OF BRITISH COLUMBIA

(Vancouver)

April 2010

ABSTRACT

During the manufacturing of wood composites, mats of resinated fibers, particles or strands are consolidated under heat and pressure to produce panels with the necessary strength and stiffness properties. As the mat consolidates a vertical density profile (VDP) is established and it has a significant impact on panel properties. In order to tailor the VDP of the panel to various end-use applications, a means of describing of the effect of pressing variables on the development of the VDP is needed.

This study examined the role of environmental factors, i.e., temperature and moisture content (MC), on the compression and viscoelastic behavior of wood strands. The strand stress-strain relationship during hot pressing was modeled using a modified Hooke's law, in which the compression modulus as a function of temperature and MC was quantitatively obtained using a regression approach. Similarly, the viscoelastic behavior of strands was investigated for various temperatures and MCs and the results were used to develop a model for predicting the stress relaxation response of the strands. The results showed that the relaxation modulus as a function of time follows a linear relationship on a log-log plot; it is important to note that the response was affected by strain level and environmental conditions.

Based on the strand compression properties and mat structure, a comprehensive model was established that simulated the VDP development and was found to be a good description of the experimental results. The effects of mat elastoplasticity and springback on the formation of the VDP were also discussed. In addition, a generalized model based

on the beam bending of the wood elements was developed to predict the mat pressure-density relationship of wood composites. This is valuable for improving the fundamental understanding of the relationship between pressing variables and panel properties for process optimization.

TABLE OF CONTENTS

Abstract ..... **ii**

Table of Contents ..... **iv**

List of Tables ..... **vii**

List of Figures ..... **viii**

List of Symbols ..... **xii**

Acknowledgements ..... **xvi**

Dedication ..... **xvii**

Co-Authorship Statement ..... **xviii**

CHAPTER 1 Introduction **1**

1.1 Introduction 1
1.2 Objectives 6
1.3 Research Hypotheses and Methodology 7
1.4 Outline of the Dissertation 8
1.5 Bibliography 11

CHAPTER 2 A Generalized Mat Consolidation Model for Wood Composites **16**

2.1 Introduction 16
2.2 Models 19
2.2.1 A Bending Model for Three-dimensional (3D) Mat Structure 19
2.2.2 A Bending Model for Two-dimensional (2D) Mat Structure 22
2.2.3 A Generalized Model for Wood Composite Mat Consolidation 25
2.3 Experimental 26
2.3.1 Materials 26
2.3.2 Methods 27
2.4 Results and Discussion 28
2.4.1 Fiber Mat Consolidation 29
2.4.2 Strand Mat Consolidation 30
2.4.3 Particle Mat Consolidation 32
2.4.4 Effect of Parameter K and Young's Modulus E 33
2.5 Summary and Conclusions 34
2.6 Bibliography 46

CHAPTER 3 Characterizing Hydro-thermal Compression Behavior of Aspen Wood Strands 51

3.1 Introduction 51
3.2 Literature Review: Dependence of Wood Softening on Temperature and MC 54
3.3 Model Development 56
3.4 Experimental 58
3.4.1 Materials 58
3.4.2 Methods 59
3.5 Results and Discussion 61
3.5.1 Effects of Temperature and MC on Strain Function $\varphi(\varepsilon)$ 61
3.5.2 Effects of Temperature and MC on Compression Modulus E 64
3.6 Summary and Conclusions 67
3.7 Bibliography 82

CHAPTER 4 Viscoelasticity of Aspen Wood Strands during Hot Pressing 87

4.1 Introduction 87
4.2 Background 89
4.2.1 Stress Relaxation Behavior of Cellular Materials in Compression 89
4.2.2 Extension of Boltzmann Superposition Principle 92
4.3 A Model for Predicting Stress Relaxation of Wood Strands in Compression 94
4.4 Experimental 96
4.4.1 Materials 96
4.4.2 Methods 97
4.5 Results and Discussion 100
4.5.1 Effect of Strain Level on Stress Relaxation 101
4.5.2 Effect of Temperature on Stress Relaxation 103
4.5.3 Effect of MC on Stress Relaxation 105
4.5.4 Model Validation 106
4.6 Summary and Conclusions 109
4.7 Bibliography 121

CHAPTER 5 Modeling Vertical Density Profile Formation of Strand-based Wood Composites during Hot Pressing 126

5.1 Introduction 126
5.2 Literature Review: Modeling of Heat and Mass Transfer during Hot Pressing 131
5.3 Model Development 134
5.3.1 Mat Formation 135
5.3.2 Heat and Mass Transfer 136
5.3.3 Mat Consolidation and VDP Formation 138
5.3.4 Mat Stress Relaxation 142
5.3.5 Mat Elastoplasticity 144

5.4 Experimental 145
5.4.1 Panel Manufacture 145
5.4.2 VDP Measurement 148
5.4.3 Elastoplasticity of Strand Mat 148
5.5 Results and Discussion 150
5.5.1 Predicted Temperatures and MCs inside the Mat 150
5.5.2 VDP Model Validation 153
5.5.3 Predictive Effects of Pressing Variables on VDP Formation 157
5.5.4 Sensitivity Analysis of VDP Model 158
5.5.5 Mat Stress Relaxation 160
5.5.6 Mat Elastoplasticity and Springback 161
5.6 Summary and Conclusions 163
5.7 Bibliography 191

CHAPTER 6 Concluding Remarks and Recommendations 199

6.1 General Summary and Conclusions 199
6.2 Recommendations and Further Research Work 202
6.3 Bibliography 205

LIST OF TABLES

Table 3.1 The glass transition temperatures of wood components and water and the best fit values of k and q used for the Kwei model (Kelley et al. 1987) 69
Table 3.2 Relative humidity and EMC values for selected saturated salt solutions 70
Table 3.3 Compression modulus E (MPa) of wood strands at various combinations of temperatures and MCs (Standard deviation in parentheses) 71
Table 4.1 Relative humidity and EMC values for selected saturated salt solutions ... 110
Table 5.1 Parameters for mat formation model 165
Table 5.2 Parameters for heat and mass transfer model 166
Table 5.3 Mat strain and springback at σ = 1.1 MPa during unloading 167

LIST OF FIGURES

Figure 2.1 (a) A typical structural unit in a fiber mat. (b) A fiber in a Cartesian coordinate system. 36
Figure 2.2 (a) Schematic of a fiber supported by crossing fibers. (b) A fiber bending unit. 37
Figure 2.3 (a) A typical structural unit in a strand mat. (b) A strand in a Cartesian coordinate system. 38
Figure 2.4 Schematics of the proposed strand geometry in the mat and the idealized loading conditions. 39
Figure 2.5 Comparison of the mat pressure-density responses of fiber, strand and particle mat. 40
Figure 2.6 Comparison between experimental result and model prediction of fiber mat pressure-density relationship. 41
Figure 2.7 Comparison between experimental result and predictions of bending model and compression model for strand mat pressure-density relationship. 42
Figure 2.8 Comparison between experimental result and model prediction of particle mat pressure-density relationship. 43
Figure 2.9 Effect of the parameter K in the bending model on the predicted mat pressure in the low-density range 44
Figure 2.10 Effect of wood strand modulus E in the bending model on the predicted mat pressure in the low-density range 45
Figure 3.1 Predictive effects of moisture content on the glass transition temperature of lignin and hemicellulose from the Kwei model 72
Figure 3.2 (a) An idealized stress-strain relationship of wood in transverse compression; (b) Strain function $\varphi(\varepsilon)$ corresponding to the stress-strain relationship in (a)…. 73
Figure 3.3 Schematic drawing of the test apparatus for strand compression 74
Figure 3.4 Strain function $\varphi(\varepsilon)$ at different temperatures and MCs 75
Figure 3.5 Typical comparisons between experimental results and model prediction of strand stress-strain relationship. 76

Figure 3.6 Compressive stress-strain relationship of wood strands at different temperatures (MC = 0%)..... 77
Figure 3.7 Effect of temperature on the normalized modulus E of wood strands (normalized using E at T = 20°C and MC = 0% as the reference point)..... 78
Figure 3.8 Compressive stress-strain relationship of wood strands at different MCs (T = 20°C)..... 79
Figure 3.9 Effect of moisture content on the normalized modulus E of wood strands (normalized using E at T = 20°C and MC = 0% as the reference point)..... 80
Figure 3.10 Comparison between experimental results and model prediction of E values …..... 81
Figure 4.1 A linear loading strain history for strand columns in compression. t_i is the time needed for the i-strand column to reach the target strain ε_i 111
Figure 4.2 (a) The selected strain levels for strand stress relaxation tests as indicated in a typical stress-strain curve. (b) The stress relaxation vs. time at selected strain levels in (a). (c) Double logarithm plots of stress relaxation modulus vs. time corresponding to (b). (d) The stress relaxation rate at selected strain levels obtained from (c). Test condition: T = 20°C, MC = 9%..... 112
Figure 4.3 Effect of temperature on the stress relaxation of wood strands under transverse compression for ovendry samples..... 113
Figure 4.4 Effect of temperature on the stress relaxation rate of wood strands under transverse compression at different MCs..... 114
Figure 4.5 Effect of MC on the stress relaxation of wood strands under transverse compression..... 115
Figure 4.6 Effect of MC on the stress relaxation rate of wood strands under transverse compression at different temperatures..... 116
Figure 4.7 Comparison between experimental results and model prediction of stress relaxation rate ξ..... 117
Figure 4.8 Comparison between experimental results and model prediction of logK values..... 118
Figure 4.9 Comparison between experimental results and model prediction of stress relaxation response at various strain levels..... 119

Figure 4.10 Effect of loading rate v on the stress relaxation for different combinations of temperatures and MCs..... 120
Figure 5.1 An idealized press cycle for OSB hot pressing 168
Figure 5.2 Schematic of a strand positioned in a mat forming area viewed as a grid system 169
Figure 5.3 Schematic of a mat consisting of strand columns with different overlap number 170
Figure 5.4 Schematic of a mat consisting of strand columns with N_z layers 171
Figure 5.5 Schematic of a strand mat structure for heat and mass transfer model 172
Figure 5.6 Schematics of a strand column in compression at different time steps during press closing 173
Figure 5.7 Schematic of linear loading strain histories for strand columns in compression 174
Figure 5.8 Comparison of predicted temperatures in face and core layers of a strand mat with experimental results 175
Figure 5.9 Predicted MC changes in different layers during hot pressing 176
Figure 5.10 Predicted temperature distributions inside the mat at various stages during hot pressing 177
Figure 5.11 Predicted MC distributions inside the mat at various stages during hot pressing 178
Figure 5.12 Development of the VDP in a strand mat at different times during press closing as predicted by the model (MC = 6%) 179
Figure 5.13 Horizontal density distribution within the mat at the target thickness (MC = 6%)..... 180
Figure 5.14 Comparison of predicted local VDP in Figure 5.13 with the measured data from 50 × 50 mm samples. (a) average local density = 591 kg m^{-3}, (b) average local density = 656 kg m^{-3}, (c) average local density = 713 kg m^{-3}, (d) overall mat density = 680 kg m^{-3}..... 181
Figure 5.15 Comparison of the predicted VDP for a panel made from ovendry strands and the measured results from a panel made under the same conditions 182
Figure 5.16 Comparison of the shape of the panel VDP for three press closing times.. 183

Figure 5.17 Comparison of the shape of the panel VDP for three initial mat temperatures..... 184
Figure 5.18 The effect of a 20% change in core temperatures on the shape of the panel VDP 185
Figure 5.19 The effect of a 30% change in core MCs on the shape of the panel VDP.. 186
Figure 5.20 Stress relaxation behaviour of mat during hot pressing. (a) experimental results, (b) model predictions 187
Figure 5.21 The mat pressure decrease as a coupled response of thermal softening and viscoelastic stress relaxation 188
Figure 5.22 The elastoplastic behaviour of a strand mat at various moisture levels 189
Figure 5.23 Comparison of stress-strain relationship during unloading between experimental results and model predictions 190

LIST OF SYMBOLS

		Units
a_i	Total area of columns with i strands	mm^2
b	Coefficient of stress relaxation	
b_i	Constants of coefficient in the nonlinear strain function	
c_p	Coefficient for characterizing mat elastoplasticity	
d	Fiber diameter	m
$\overline{d}$	Imaginary fiber diameter	m
h	Thickness of a volume with unit area in a mat	m
i	Number of strands covered at a given point in mat area	
j	The jth layer of the column	
i_m	Maximum number of strands in columns	
k	Parameter accounting for molecular interactions	
l_f	Distance between adjacent fiber contacts	m
$\bar{l}_f$	Mean distance between fiber contacts	m
$\bar{l}_s$	Mean distance between strand contacts	m
m	Mat mass	kg
m_{dj}	Dry wood mass in the jth layer	kg
n	Number of layers in a mat	
n_c	Parameter for different mat type	
p	Mat pressure	MPa
$p(i)$	Probability of a point in mat area covered by i strands	
q	Parameter accounting for free volume	
t	Current time	s
t_0	A given initial time	s
t_1	The time from the moment at which the load is applied on the mat to the moment at which the i-strand columns starts compression	s

t_2	Time needed for *i*-strand columns to reach the target mat thickness	s
t_i	Time needed for strand column to reach the target thickness	s
t_m	Time needed for all strand columns to reach the target mat thickness	s
t'	Past time	s
v	Loading speed	mm s^{-1}
A	Mat area	mm^2
E	Young's modulus	MPa
E_c	Young's modulus of wood constituent	MPa
E_f	Young's modulus of fiber	MPa
$E_r(t)$	Relaxation modulus	MPa
$E_r'(t)$	Relaxation modulus of linear viscoelastic material	MPa
E_s	Young's modulus of strand	MPa
E_w	Young's modulus of cell wall material	MPa
E_w^0	Young's modulus of cell wall material at 0°C	MPa
F	Force applied on the midpoint of the fiber segment	N
H	Target strand column thickness	mm
$H(t)$	Mat thickness at time t	mm
$H_i(t_0)$	Strand column thickness at time t_0	mm
H_0	Initial mat thickness	mm
H_m	Target mat thickness	mm
H_{l0}	Initial layer thickness in a column	mm
I	Moment of inertia of wood element cross-section	m^4
K	Specific relaxation modulus at t = 1 s	MPa
K_c	Dimensionless parameter for general mat	
K_f	Dimensionless parameter for fiber mat	
K_s	Dimensionless parameter for strand mat	
L	Total length of wood constituents in the mat	m

L_m	Mat length	mm
MC	Moisture content	%
N_s	Total number of strands in a mat	
N_x	Number of mesh elements in x axis	
N_y	Number of mesh elements in y axis	
N_z	Number of layers in a mat	
$P(t)$	A force applied on a mat at time t	N
T	Temperature	°C
T_g	Glass transition temperature	°C
T_{g1}	Glass transition temperature of polymer	°C
T_{g2}	Glass transition temperature of moisture	°C
T_m	Mat thickness	mm
V	Mat volume	m^3
V_0	Initial mat volume	m^3
W_1	Weight fraction of polymer	
W_2	Weight fraction of moisture	
W_m	Mat width	mm
X_1, X_2, X_3	Axis in a Cartesian coordinate system	
α	Constant coefficient	
α_m	Parameter accounting for temperature effect	
β	Constant coefficient	
γ	Constant coefficient	
ε	Strain	mm/mm
ε_0	Initial imposed strain	mm/mm
ε_i	Strain of i-strand column	mm/mm
ε_j	Strain of the jth layer in a column	mm/mm
$\varepsilon_i(t)$	Strain of i-strand column at time t	mm/mm
δ	Deflection of the fiber segment	m
θ	Angle between a fiber and X_3 axis	degree
λ	Strand length	mm

ξ	Stress relaxation rate	
ξ_i	Stress relaxation rate for i-strand column	
ρ_0	Initial mat density	kg m^{-3}
ρ_c	Wood constituent density	kg m^{-3}
ρ_{ds}	Dry strand density	kg m^{-3}
ρ_f	Fiber density	kg m^{-3}
ρ_j	Density of the *j*th layer in a column	kg m^{-3}
ρ_m	Mat density	kg m^{-3}
ρ_s	Strand density	kg m^{-3}
σ	Stress	MPa
σ_0	Initial stress	MPa
σ_i	Stress of *i*-strand column	MPa
σ_n	Overall mat stress	MPa
$\sigma(t)$	Stress at time *t*	MPa
$\sigma_i(t)$	Stress of columns with *i* strands at time *t*	MPa
τ	Strand thickness	mm
φ	Angle between X_1 axis and the normal projection of a fiber onto the X_1X_2 plane	degree
$\varphi(\varepsilon)$	Nonlinear strain function	
ω	Strand width	mm

ACKNOWLEDGEMENTS

First of all, I would like to express sincere and deep gratitude to my research supervisor, Dr. Chunping Dai, FPInnovations – Forintek Division, and academic supervisor, Dr. Gregory D. Smith, Department of Wood Science, UBC, for their continuing guidance and support. Without their invaluable advice, encouragement and patience, this work would never have come true.

Appreciation also goes to my supervisory committee members, Dr. Stavros Avramidis, Department of Wood Science, UBC, and Dr. Reza Vaziri, Department of Civil Engineering, UBC, for their helpful feedback in this research.

I owe my special thanks to the following scientists and technologists during the course of my stay at FPInnovations – Forintek Division, Visiting Professor Changming Yu for his advice on code writing and debugging, Mr. Paul Symons, Mr. Tony Thomas, Mr. Kevin Groves, Mr. Peter Ens, Mr. Axel Andersen, Mr. Bob Daniels, and Mr. Jules Gardy for their technical assistance in the experimental study, Dr. Liping Cai for his statistical software, Dr. Brad J. Wang, Dr. Heng Xu, Mr. Martin Feng, and Dr. Guangbo He for their helpful discussions and suggestions.

I would also like to thank Dr. Cindy Prescott and Ms. Gayle Kosh, Faculty of Forestry, UBC, and Ms. Debbie Wong, Department of Wood Science, UBC, for their administrative help during my educational study at UBC. In addition, financial support from National Sciences and Engineering Research Council of Canada through a discovery research grant is gratefully acknowledged.

My thanks also go to the publisher De Gruyter for their permission to use the papers published in their journal Holzforschung in my dissertation.

Last but not least, my deepest love and thanks go to the family members, my parents, my wife Lin, and my daughter Iris, who provide the endless love, support and sacrifice throughout all my life.

DEDICATION

To my parents

To my wife Lin

To my daughter Iris

CO-AUTHORSHIP STATEMENT

I identified and designed the research program based on the discussion with my research supervisor Dr. Chunping Dai. I conducted the experimental studies, performed the data analyses, developed the simulation models, and prepared the manuscripts. My research supervisor Dr. Chunping Dai and academic supervisor Dr. Gregory D. Smith both reviewed and approved these manuscripts.

CHAPTER 1 INTRODUCTION

1.1 Introduction

Wood composite panels can be classified into two major categories: veneer type such as plywood and laminated veneer lumber (LVL) and non-veneer type such as oriented strand board (OSB), particleboard and medium-density fiberboard (MDF). Plywood and LVL are made of solid veneer sheets coated with continuous gluelines. As a result, a relatively low pressure is needed for this layered structure to create adequate veneer-to-veneer contacts for bonding, which leads to the desired strength and stiffness of final products (Bowyer et al. 2002). In contrast, non-veneer-based panels have a more complex structure as they are made of short and discontinuous wood elements (e.g., strands, particles and fibers). Due to the small quantities of resin used in the panel manufacture, which is usually in the range of 3 to 15% of total weight of wood elements, the wood constituent surfaces are covered with discrete resin spots. In addition, the initial mat structure is generally loose and porous after the furnish is deposited onto the forming belt. As such, a high degree of mat consolidation is required to reduce the voids between elements and then create adequate contacts for bonding development (Dai et al. 2007). This mat densification process makes the mechanical strength properties of OSB panels comparable to those of structural plywood and results in a greater overall panel density.

Therefore, hot pressing is a critical operation in the manufacture of wood-based composites. During this process, heating not only accelerates resin curing for bonding

development but also softens the woody materials to facilitate mat densification. Due to the variations of temperature and moisture content (MC) from surface layers to core layers, mat deformation is usually not uniform across the mat thickness, which leads to the formation of vertical density profile (VDP). Furthermore, hot pressing is a very complicated process, which combines physical, mechanical and chemical responses involving a number of manufacturing variables (e.g., press platen temperature, press cycle, and press closing time). It not only affects the productivity and cost but also determines the panel properties and its performance (e.g., bending strength, stiffness, internal bond, and thickness swell). As a result, the necessity for improving productivity or producing high-performance products requires a clear understanding of the mechanisms occurring in wood composites manufacture.

Traditionally, hot pressing of wood composites was studied by empirical methods and a large amount of experimental results have been reported (Strickler 1959, Kelly 1977, Smith 1982, Kamke and Casey 1988, Winistorfer et al. 2000, Wang and Winistorfer 2000, Wang et al. 2004). Although these investigations gave some general knowledge about the relationship between production parameters and panel properties, they could not provide a fundamental and systematic analysis for the manufacturing process. Consequently, modeling work that is more analytical and rigorous is required for this subject.

Suchsland (1959, 1967) appeared to be the first to conceptualize the mat formation and deformation processes by treating the mat as a system of wood particle columns. His

ground-breaking work provided valuable insight into the randomness in wood composite structures, which was closely associated with the mat compression behavior. Humphrey and Bolton (1989) were among the first to develop a heat and mass transfer model for wood composites during hot pressing, which treated the composite mat as a continuous and homogenous material. This model significantly improved the understanding of the hot pressing process and revealed the need for further research. In combination with the viscoelasticity theories of amorphous polymers, Wolcott et al. (1990, 1994) applied theories of cellular solids (Gibson and Ashby 1988) to model the transverse compression behavior and viscoelasticity of wood flakes. The significance of these theories is to separate the response of the cell wall polymers from the geometrical response of the cellular structure.

Dai and Steiner (1994a, b), for the first time, developed a theoretical model to describe the characteristics of random flake mat structure using the geometric probability theory. This model was then applied to predict the overall mat consolidation behavior under ambient conditions based on the compression characteristics of wood flakes (Dai and Steiner 1993). Furthermore, the mat structure model was also applied to predict the horizontal density variations within the plane of the panel (Dai and Steiner 1997). Based on the viscoelastic properties of wood flakes in transverse compression and random mat structure, a model was developed to predict the viscoelastic consolidation of wood composite mats (Dai 2001). As well, the concept of elastoplasticity was proposed to characterize the springback and permanent deformation of wood strand mats during pressing (Dai et al 2000). More recently, Dai and Yu (2004) developed a theoretical

model for heat and mass transfer in wood composite mats during hot pressing. In this model, the manufacturing variables, e.g., mat temperature, MC, and gas pressure, were linked to the mat material properties such as mat density, thermal conductivity, and permeability.

Based on the approach developed by Dai and Steiner (1993, 1994a, b), several models were further established to investigate mat formation and the compression behavior of strand mats (Lang and Wolcott 1996a, b, Lenth and Kamke 1996a, b, Oudjehane et al. 1998, Zombori et al. 2001, 2003, Painter et al. 2006, Lee et al. 2007). In addition, Godbille (2002) adapted Dai and Steiner's model to investigate the consolidation process of particle mats during hot pressing.

Following a similar concept proposed by Humphrey and Bolton (1989), Thoemen and Humphrey (2003, 2006), Thoemen et al. (2006), and Thoemen and Ruf (2008) presented a simulation model to predict the temperature and moisture distributions, and vertical density distribution of an MDF mat during continuous hot pressing. Their approach for fiber mat consolidation was based on a spring-dashpot model with the appropriate selection of the rheological coefficients to simulate the VDP development.

Although these established models greatly improved the understanding of the wood composite manufacturing process, there still exist a number of knowledge gaps in mat consolidation due to the complexity of hot pressing. As Dai and Steiner (1993) pointed out, the early stage of strand mat consolidation is dominated by the strand bending rather

than strand compression. Based on the compressive characteristics of wood flakes, their model cannot predict accurately the bending response of a mat under low pressure. As such, further research is needed to clarify this bending mechanism during mat consolidation and this is especially true for the manufacture of low-density panel products. In addition, their consolidation model does not work well for fiber mats due to the size difference between strand and fiber as well as the mat consolidation mechanism. It is necessary to develop a model for predicting the fiber mat pressure-density relationship based on the fiber properties and mat structure.

Most of the existing models are based on a system of dashpot and spring elements to represent the mat material and simulate its densification (Thoemen and Humphrey 2003, 2006, Painter et al. 2006, Thoemen et al. 2006, Lee et al. 2007, Thoemen and Ruf 2008), in which the rheological coefficients were obtained from empirical equations based on the experimental data (von Hass et al. 1998, von Hass and Frühwald 2000, 2001). This study provided valuable information of mat material properties such as permeability, compressibility, and viscoelasticity for different mat densities, temperatures, and MCs. However, due to the limited number of parameters used in these tests, it is doubtful that they accurately represent the actual manufacturing process. In addition, they did not take into account the structural factors such as wood element size and wood species which are very important for OSB panels. In addition, the plastic deformation of mats which affects springback after the press opens has not been well studied. The lack of the above-mentioned knowledge makes it difficult to fully understand the consolidation behavior of wood composite mats during hot pressing.

Due to the complexity of mat structure and the heterogeneity of wood strands, it is difficult to adequately describe a mat during compression. In addition, special equipment and techniques are needed to achieve uniform temperature and moisture content distributions at elevated temperatures and moisture conditions prior to mat consolidation. As such, it is more convenient to investigate the mat constituents, i.e., the wood strands, directly and link their properties to the mat properties. Thus, more work is needed to characterize the compression behavior of individual wood strands at various temperatures and MCs. Also needed is a means of taking the mat structure into account, and combining this with the compression behaviour of individual strands during hot pressing to predict the compression behavior of wood strand mats as a whole.

1.2 Objectives

The overall objective of this study is to improve fundamental understanding of wood composites manufacturing process. The specific objectives are:

1) to develop a generalized model to predict the mat pressure-density relationship of strand-based wood composites;

2) to predict the entire strand mat consolidation process with the generalized model and combine it with the existing model;

3) to conduct the transverse compression tests on wood strands at different temperatures and MCs and quantitatively establish the relationship between the strand compression modulus and environmental conditions;

4) to develop a model to predict the stress-strain response of wood strands in transverse compression during hot pressing;

5) to experimentally investigate the viscoelastic behavior of wood strands in compression over a range of temperatures and MCs;

6) to develop a model to predict the viscoelastic response of wood strands in compression during hot pressing;

7) to simulate the VDP formation based on the strand compression properties and the random mat structure; and

8) to investigate the elastoplastic behavior of the mat and its implication for VDP formation.

1.3 Research Hypotheses and Methodology

Wood is a cellular material and it is believed that the environmental conditions only affect the properties of cell wall material (e.g., elastic modulus) and do not compromise the integrity of the cellular structure (Wolcott et al. 1990, 1994, Dai and Steiner 1993). Like any other materials, the mechanical behavior of wood composite panels should be determined by the properties of wood constituents and the spatial organization of these elements within the panels (Dai and Steiner 1993). Thus, the general hypothesis of this study is that the overall mechanical response of strand-based wood composite mats can be predicted if the properties of individual wood strands, the mat structure, initial mat environmental conditions (e.g., temperature and MC), and the hot pressing parameters are all known. It should be noted that the effect of resin curing on mat consolidation is not

taken into account in this study. The resin is assumed to be fully cured when the mat reaches its target thickness. In addition, the mat formation is assumed to be a random process which allows the mat structure to be characterized by probability theories (Dai and Steiner 1994a, b).

Generally, the methodology used for each chapter is to develop a model based on the existing knowledge in which some parameters need to be determined experimentally. The experimental work is then carried out and the proposed model validated. Specifically, three types of research methods, i.e., analytical, empirical, and numerical methods, are applied in this study. Based on some assumptions, an analytical approach is to use basic scientific principles to describe the relationship between variables, which is usually involved in deriving mathematical equations and analytical solutions. An empirical approach is to obtain the desired relationship between variables based on the observed experimental data, usually involving regression analysis. A numerical approach is to solve a large and complex problem with concepts of digitalization and iteration, usually involving computer programming. Depending on the specific research objectives, these three methods are complementary to each other throughout this study.

1.4 Outline of the Dissertation

This dissertation is organized in a manuscript-based style, in which a variation of the text and figures in a given chapter has been either previously submitted to, or will shortly be

submitted to a refereed journal. Chapter I gives a brief introduction to the research subject, presents the research objectives, and outlines the dissertation organization.

Chapter II presents a generalized model for predicting the mat pressure-density relationship of wood composites. Based on the concepts from the compression models for a fiber assembly, this model treats the composite mat as a system of bending units, which makes bending of wood elements the dominant mechanism during the early stage of mat consolidation. The consolidation behavior of fiber, strand, and particle mats are experimentally investigated and compared with the model prediction.

Chapter III investigates the wood strand properties during hot pressing. A range of temperatures and MCs were selected to simulate the environmental conditions inside the mat during panel manufacturing process. A regression approach is applied to describe the modulus-temperature-moisture relationship. The stress-strain relationship for wood strands during hot pressing used here was based on a modified Hooke's law.

Chapter IV focuses on the viscoelastic behavior of wood strands in transverse compression under the same environmental conditions as in Chapter III. The experimental results show that the strand stress relaxation modulus and time follows a linear relationship on a log-log plot. The strand stress relaxation rate is highly dependent on the imposed strain levels and environmental conditions. A model for predicting the stress relaxation behavior of wood strands is developed and compared with test results.

Chapter V presents a simulation model for the VDP formation in strand-based wood composites during hot pressing that combines an existing three-dimensional heat and mass transfer model. The overall mat consolidation behavior can be described by the models for wood strands described in Chapters III and IV in combination with the mat structure. The VDP model predictions are presented and compared with the experimental results. The effect of mat elastoplastictiy on VDP formation is also investigated and discussed.

Finally, main conclusions and contributions of this dissertation are summarized in Chapter VI. In addition, the comments on the limitations of the present work and the recommendations for further research are also presented in this chapter.

1.5 Bibliography

Bowyer, J.L., Shmulsky, R., Haygreen, J.G. Forest products and wood science: An introduction. Iowa State Press, Ames, IA. 2002.

Dai, C. (2001) Viscoelasticity of wood composite mats during consolidation. Wood Fiber Sci. 33: 353-363.

Dai, C., Steiner, P.R. (1993) Compression behavior of randomly formed wood flake mats. Wood Fiber Sci. 25: 349-358.

Dai, C., Steiner, P.R. (1994a) Spatial structure of wood composites in relation to processing and performance characteristics. Part 2. Modeling and simulation of a randomly-formed flake layer network. Wood Sci. Technol. 25: 135-146.

Dai, C., Steiner, P.R. (1994b) Spatial structure of wood composites in relation to processing and performance characteristics. Part 3. Modeling the formation of multi-layered random flake mats. Wood Sci. Technol. 28: 229-239.

Dai, C., Steiner, P.R. (1997) On horizontal density variations in randomly-formed short-fibre wood composite boards. Compos. Part A 28: 57-64.

Dai, C., Yu, C. (2004) Heat and mass transfer in wood composite panels during hot-pressing: Part I. A physical-mathematical model. Wood Fiber Sci. 36: 585-597.

Dai, C., Yu, C., Hubert, P. (2000) Modeling vertical density profile in wood composites during hot-pressing. In: Proceedings of 5th Pacific Rim Bio-based Composites Symposium. Canberra, Australia. pp. 220-226.

Dai, C., Yu, C., Zhou, C. (2007) Theoretical modeling of bonding characteristics and performance of wood composites. Part 1. Inter-element contact. Wood Fiber Sci. 39: 48-55.

Gibson, L.J., Ashby, M.F. Cellular Solids: Structure and Properties. Pergamon Press, New York, NY, 1988.

Godbille, F.D. (2002) A simulation model for the hot pressing of particleboard. Ph. D. dissertation, University of New Brunswick, Fredericton, New Brunswick.

Humphrey, P.E., Bolton, A.J. (1989) The hot pressing of dry-formed wood-based composites. Part II. A simulation model for heat and mass transfer and typical results. Holzforschung 43: 199-206.

Kamke, F.A., Casey, L.J. (1988) Fundamentals of flakeboard manufacture: Internal mat conditions. Forest Prod. J. 38: 38-44.

Kelly, M. (1977) Critical review of relationships between processing parameters and physical properties of particleboard. General Technical Report FPL-10. USDA Forest Service, Forest Products Laboratory, Madison, WI.

Lang, E.M., Wolcott, M.P. (1996a) A model for viscoelastic consolidation of wood-strand mats. Part I. Structural characterization of the mat via Monte Carlo simulation. Wood Fiber Sci. 28: 100-109.

Lang, E.M., Wolcott, M.P. (1996b) A model for viscoelastic consolidation of wood-strand mats. Part II. Static stress-strain behavior of the mat. Wood Fiber Sci. 28: 369-379.

Lee, J., Kamke, F.A., Watson, L.T. (2007) Simulation of the hot-pressing of a multi-layered wood strand composite. J. Compos. Mater. 41: 879-904.

Lenth, C.A., Kamke, F.A. (1996a) Investigations of flakeboard mat consolidation. Part I. Characterizing the cellular structure. Wood Fiber Sci. 28: 153-167.

Lenth, C.A, Kamke, F.A. (1996b) Investigations of flakeboard mat consolidation. Part II. Modeling mat consolidation using theories of cellular materials. Wood Fiber Sci. 28: 309-319.

Oudjehane, A., Lam, F., Avramidis, S. (1998) A continuum model of the interaction between manufacturing variables and the consolidation of wood composite mats. Wood Sci. Technol. 32: 381-391.

Painter, G., Budman, H., Pritzker, M. (2006) Predictions of oriented strand board properties from mat formation and compression operating conditions. Part 1. Horizontal density distribution and vertical density profile. Wood Sci. Technol. 40:139-158.

Smith, D.C (1982) Waferboard press closing strategies. Forest Prod. J. 32: 40-45.

Strickler, M.D. (1959) Effect of press cycles and moisture content on properties Douglas-fir flakeboard. Forest Prod. J. 9: 203-215.

Suchsland, O. (1959) An analysis of the particleboard process. Michigan Quarterly Bulletin. 42: 350-372.

Suchsland, O. (1967) Behavior of a particleboard mat during the press cycle. Forest Prod. J. 17: 51-57.

Thoemen, H., Humphrey, P.E. (2003) Modeling the continuous pressing process for wood-based composites. Wood Fiber Sci. 35: 456-468.

Thoemen, H., Humphrey, P.E. (2006) Modeling the physical process relevant during hot pressing of wood-based composites. Part I. Heat and mass transfer. Holz Roh-Werkst. 64: 1-10.

Thoemen, H., Haselein, C.R., Humphrey, P.E. (2006) Modeling the physical process relevant during hot pressing of wood-based composites. Part II. Rheology. Holz Roh-Werkst. 64: 125-133.

Thoemen, H., Ruf, C. (2008) Measuring and simulating the effects of the pressing schedule on the density profile development in wood-based composites. Wood Fiber Sci. 40: 325-338.

von Hass, G., Frühwald, A. (2000) Untersuchungen zum Verdichtungsverhalten von Faser-, Span-, und OSB-Matten. Holz Roh-Werkst. 58: 317-323.

von Hass, G., Frühwald, A. (2001) Untersuchungen zum rheologischen Verhalten von Faser-, Span-, und OSB-Matten. Holz Roh-Werkst. 58: 415-418.

von Hass, G., Steffen, A., Frühwald, A. (1998) Untersuchungen zur Permeabilität von Faser-, Span-, und OSB-Matten für Gase. Holz Roh-Werkst. 56: 386-392.

Wang, S., Winistorfer, P.M. (2000) Fundamentals of vertical density profile formation in wood composites. Part II. Methodology of vertical density formation under dynamic conditions. Wood Fiber Sci. 32: 220-238.

Wang, S., Winistorfer, P.M., Young, T.M. (2004) Fundamentals of vertical density profile formation in wood composites. Part III. MDF density formation during hot-pressing. Wood Fiber Sci. 36: 17-25.

Winistorfer, P.M., Moschler, J.W.W, Wang, S., DePaula, E., Bledsoe, B.L. (2000) Fundamentals of vertical density profile formation in wood composites. Part I. In-

situ density measurement of the consolidation process. Wood Fiber Sci. 32: 209-219.

Wolcott, M.P., Kamke, F.A., Dillard, D.A. (1990) Fundamentals of flakeboard manufacture: Viscoelastic behavior of the wood composite. Wood Fiber Sci. 22: 345-361.

Wolcott, M.P., Kamke, F.A., Dillard, D.A. (1994) Fundamental aspects of wood deformation pertaining to manufacture of wood-based composites. Wood Fiber Sci. 26: 496-511.

Zombori, B.G., Kamke, F.A., Watson, L.T. (2001) Simulation of the mat formation process. Wood Fiber Sci. 33: 564-580.

Zombori, B.G., Kamke, F.A., Watson, L.T. (2003) Simulation of the internal mat conditions during the hot-pressing process. Wood Fiber Sci. 35: 2-23.

CHAPTER 2 A GENERALIZED MAT CONSOLIDATION MODEL FOR WOOD COMPOSITES[1]

2.1 Introduction

Wood-based composites such as oriented strand board (OSB), particleboard and medium-density fiberboard (MDF) are typically manufactured by consolidating mats of resinated wood elements (e.g., strands, particles or fibers) under heat and pressure. Compared with other composite materials (e.g., polymer matrix composites), wood composites contain small quantities of resin, usually in the range of 3 to 15% of total weight of wood elements. Consequently, development of adequate product strength requires a high degree of mat consolidation. The mat consolidation process not only creates the contact between wood elements for bonding (Dai et al. 2007), but also results in permanent wood deformation (Kunesh 1961; Wolcott et al. 1994), both of which significantly affect the final product properties (e.g., bending strength, internal bond, and thickness swell). Hence, mat consolidation plays a critical role in the manufacture of wood composites.

Realizing the importance of mat compression, researchers have made efforts to elucidate the mechanisms in this process. Suchsland (1959, 1967) was among the early researchers investigating the mat consolidation behavior. He treated a random flake mat as a system of independent, horizontally stacked flake columns with different flake overlaps, which was assumed to follow a binominal distribution. This early work provided a valuable conceptual model for the flakeboard manufacturing progress. Dai and Steiner (1993)

[1] A version of this chapter has been published . Zhou, C., Dai, C., Smith, G.D. (2008) A generalized mat consolidation model for wood composites. Holzforschung. 62:201-208.

were the first to develop a theoretical model of mat consolidation behavior. Their model was based on the Poisson distribution of random strand overlaps (Dai and Steiner 1994a, 1994b) and a modified Hooke's Law for transverse wood compression (Wolcott et al. 1990). Following a similar approach, Lang and Wolcott (1996a, 1996b), Lenth and Kamke (1996a, 1996b), Oudjehane et al. (1998), Zombori et al. (2001, 2003), and Painter et al. (2006) developed further models to investigate this nonlinear compression behavior of strand mats. In addition, Godbille (2002) adapted the model by Dai and Steiner (1993) to simulate the consolidation process of a particle mat during hot pressing. For fiber composites earlier studies can be traced back to Jones (1963) who found the compression response of fiber beds was due to fiber deformation (i.e., bending) and slippage at contact points. More recently, Englund et al. (2004) reviewed and applied models for wood strand composites compression and metal powder compaction to describe the experimental data for consolidation of wood/thermoplastic fiber mats. They then developed a model based on the relationship between the instantaneous modulus and relative density of the mat, which provided a good fit for their mat compression data. Thoemen and Humphrey (2003, 2006), and Thoemen et al. (2006) developed a three-dimensional simulation model that accounted for heat and mass transfer in MDF during continuous hot pressing and mat densification that used the traditional springs and dashpot analogue to describe the mat compressive characteristics. However, their model did not take into account the effects of constituent geometry and the mat structure.

When a mat of fibers or strands is under unidirectional compression, several mechanical modes including bending, shear, and compression occur. Bending mode plays a key role

in the early stage of mat consolidation while transverse compression is the dominant component in the late stage (van Wyk 1946; Jones 1963; Dai and Steiner 1993; Lang and Wolcott 1996b; Englund et al. 2004). Most of these models only considered transverse compression of the strands during mat consolidation except Lang and Wolcott's model (1996b). Based on an empirical characterization of mat structure, their model took into account strand bending by treating each strand as a simply supported beam under a distributed load. Although transverse compression is the main mechanism encountered in wood composite manufacture, the behavior in the low-stress range has not been sufficiently quantified and more work in this area is required, especially for low-density panel products.

To date, little research has been conducted to analytically investigate the consolidation mechanism of fiber mats in the field of wood composites (Thoemen and Humphrey 2003, 2006; Englund et al. 2004; Thoemen et al. 2006). However, extensive work has been done on the compression behavior of fiber networks in textile and pulp and paper fields (Schofield 1938; van Wyk 1946; Kallmes and Corte 1960; Jones 1963; Komori and Makishima 1977; Pan 1993; Toll and Manson 1995; Neckar 1997; Toll 1998; Bell and Roberts 2002; Alkhagen, 2002; Lundquist et al. 2004; Pawlak and Keller 2005; Neagu et al. 2006). Consequently, the research here is based on these earlier contributions to fiber assembly compression.

The overall objective of this study was to improve the fundamental understanding of the mat consolidation process. The specific objectives were:

1) to develop a generalized model that predicts the overall mat pressure-density relationship of randomly-formed wood composite mats for low-stress consolidation;
2) to describe the pressure-density relationship over the whole consolidation process by combining this proposed model and an existing model for random strand mats; and
3) to experimentally measure the consolidation behavior of wood strand, particle, and fiber mats, and compare these results with the predictions of the proposed models.

2.2 Models

2.2.1 A Bending Model for Three-dimensional (3D) Mat Structure

Ideally, a three-dimensional (3D) structure can be defined as a mat in which the fibers are randomly distributed in all directions (Figure 2.1a). According to the approach used by Komori and Makishima (1977), consider a Cartesian coordinate system X_1, X_2, X_3 set in the fiber mat where the angle between the X_3 axis and the axis of an arbitrary fiber be θ, and that between the X_1 axis and the normal projection of the fiber axis onto the X_1X_2 plane be φ. Then the orientation of any fiber can be defined uniquely by a pair of (θ, φ), provided that $0 \leq \theta \leq \pi$ and $0 \leq \varphi \leq \pi$ (Figure 2.1b).

As van Wyk (1946) pointed out, there are several assumptions to simplify this modeling process: 1) fibers are straight rods of the same diameter; 2) the twisting, slippage, and extension of the fibers are neglected; 3) fibers are deposited and oriented at random; and 4) the fiber mass is uniformly packed and the frictional forces between the fibers are

neglected. Based on these assumptions and the density function of fiber orientations, the number of fiber-to-fiber contacts in such a fiber mat can be determined. The fiber mat can be regarded as a system of bending units in which fiber segments are rigidly supported by two other fibers and a third one loaded midway between the supports, as shown in Figure 2.2 (adapted from Pawlak and Keller 2005). According to the elementary beam theory, for a small elastic deformation, the relationship between the force and beam deflection is given by:

$$F = \frac{24 E_f I}{l_f^{\,3}} \delta \tag{2.1}$$

where F is the force acting on the midpoint of the fiber segment, E_f is Young's modulus of fiber, I is the moment of inertia of the fiber cross section, l_f is the distance between adjacent contact points, and δ is the deflection of the fiber segment.

Since the contact points are not necessarily evenly spaced along the fiber, a mean distance between adjacent contacts $\bar{l}_f$ rather than the actual spacing l_f is proposed. Consequently, the factor *24* in Eq. (2.1) will be collected into the unknown factor k and the derivative form of Eq. (2.1) can be written as:

$$dF = \frac{k E_f I}{\bar{l}_f^{\,3}} d\delta \tag{2.2}$$

The mean fiber contact distance can be expressed as follows (van Wyk 1946; Komori and Makishima 1977):

$$\bar{l}_f = \frac{2V}{\pi d L} \tag{2.3}$$

where V is mat volume, d is fiber diameter, L is the total length of fibers in the mat. In addition, van Wyk assumed that the increment in pressure dp was proportional to the increment in the force dF per unit area in a volume with thickness h:

$$dp = \frac{hL}{V\bar{l}_f} dF \tag{2.4}$$

Above, the change of mat volume was further assumed to be proportional to the deflection of the fiber segments:

$$\frac{dV}{V} = -\frac{d\delta}{h} \tag{2.5}$$

Eq. (2.5) together with Eqs. (2.2) and (2.4) yield:

$$dp = -\frac{kE_f I h^2 L}{\bar{l}_f{}^4 V^2} dV \tag{2.6}$$

With the fibers oriented at random, the mean value of h^2 may be replaced by the mean value of $\bar{l}_f{}^2/3$ (van Wyk 1946). Based on these key assumptions, the relationship between mat pressure and volume is obtained by substituting $\bar{l}_f$ from Eq. (2.3) into Eq. (2.6) and integrating:

$$p = \frac{K_f E_f m^3}{\rho_f{}^3}\left(\frac{1}{V^3} - \frac{1}{V_0{}^3}\right) \tag{2.7}$$

where p is mat pressure, K_f is a dimensionless parameter determined by experiment which includes the effects of factor k and other fiber characteristics, m is the mass of the fibers, ρ_f is the fiber density, V is the final mat volume, V_0 is the initial mat volume when pressure is zero. Furthermore, recalling that $\rho_m = m/V$, Eq. (2.7) can be rewritten as:

$$p = \frac{K_f E_f}{\rho_f{}^3}\left(\rho_m{}^3 - \rho_0{}^3\right) \tag{2.8}$$

where ρ_m is mat density, ρ_0 is initial mat density prior to compression. Thus, the relationship between fiber mat pressure and density is established.

2.2.2 A Bending Model for Two-dimensional (2D) Mat Structure

To some extent, a strand mat is similar to a fiber mat in that the strands are also randomly distributed within the mat except that the strands are rectangular while the fibers are cylindrical. However, due to their flat surfaces, the strands are most likely to lie flat against each other, i. e., the faces of the strands will be essentially parallel to the forming plane (i.e., $\theta = \pi/2$) and their positions can be described by only the angle φ (Figures 2.3a and 2.3b).

A 2D mat structure is somewhat simpler than the 3D case, as $\theta = \pi/2$ for all wood elements; i. e., all the elements are parallel to the X_1X_2 plane (Figure 2.3a). It is further assumed that the orientation of these elements in that plane is random as shown in Figure 2.3b. Similar definitions for the 2D case have been used by Komori and Makishima (1977); Toll and Manson (1995); Toll (1998); and Pawlak and Keller (2005).

Similar to a 3D mat structure, this 2D structure can also be regarded as a system of bending units as shown in Figure 2.4, where the strand segments are supported by two other strands with a third strand loaded midway between the contacts. Let strand length, width, and thickness be λ, ω, and τ, respectively, and let $\omega = \alpha\tau$, where α is a constant.

According to the elementary beam theory, a small elastic deformation can be described as follows:

$$dF = \frac{kE_s I}{\bar{l}_s^{\,3}} d\delta \tag{2.9}$$

where E_s is Young's modulus of wood strand, $\bar{l}_s$ is the mean distance between the centers of two neighboring strand contacts. Since the strands have rectangular cross sections, the theories for fibers with circular cross sections cannot be directly applied to strand mat.

Nevertheless, the principle of geometrical equivalence will be utilized to obtain the mean distance between strand contacts. Let the strand cross-section area equal to an imaginary fiber cross-section area with a diameter $\bar{d}$,

$$\omega\tau = \alpha\tau^2 = \frac{\pi\bar{d}^2}{4} \tag{2.10}$$

Replacing the factor $2\sqrt{\frac{\alpha}{\pi}}$ with β, the above expression becomes:

$$\bar{d} = 2\sqrt{\frac{\alpha}{\pi}}\tau = \beta\tau \tag{2.11}$$

Furthermore, let these fibers be oriented such that their long axes lie within the X_1X_2 plane and randomly distributed to form a mat. Because the fibers and the strands have the same number of longitudinal axes and the equivalent cross-section area, these two random structures are equivalent. Moreover, since the strand contact distance is the

distance between the longitudinal axes of neighboring strands, which is equivalent to that of fiber contacts, then $\bar{l}_s$ can be obtained from $\bar{d}$, i. e., Eq. (2.11).

For a planar fiber assembly, Komori and Makishima (1977) provided a solution for the mean distance between fiber contacts:

$$\bar{l}_s = \frac{\pi V}{4\bar{d}L} = \frac{\pi V}{4\beta\tau L} = \frac{V}{\gamma\tau L} \tag{2.12}$$

It is assumed that an increase in pressure *dp* is proportional to the increase *dF* in the force per unit area in a volume with thickness τ:

$$dp = \frac{\tau L}{V\bar{l}_s} dF \tag{2.13}$$

Similarly, the change of mat volume is assumed to be proportional to the deflection of the strand segments:

$$dV = -\frac{V}{\tau} d\delta \tag{2.14}$$

Rearranging Eqs. (2.13) and (2.14) and substituting into Eq. (2.12) yields:

$$dp = -\frac{kE_s I\tau^2 L}{\bar{l}_s{}^4 V^2} dV \tag{2.15}$$

Recalling that the moment of inertia of the strand cross-section can be expressed as

$$I = \frac{w\tau^3}{12} = \frac{\alpha\tau^4}{12} \tag{2.16}$$

and that the strand mass is given by:

$$m = \rho_s L w \tau = \alpha\rho_s L\tau^2 \tag{2.17}$$

where ρ_s is the strand density, Eq. (2.15) can be rewritten as:

$$dp = -\frac{\gamma^4 k E_s m^5}{12\alpha^4 \rho_s{}^5} \frac{dV}{V^6} \tag{2.18}$$

After integrating from the initial mat volume to the final mat volume, the relationship between mat pressure and volume for a 2D mat structure is obtained:

$$p = \frac{K_s E_s m^5}{\rho_s{}^5} \left(\frac{1}{V^5} - \frac{1}{V_0{}^5}\right) \tag{2.19}$$

where p is mat pressure, K_s is a dimensionless parameter determined by experiment, V is the final mat volume, V_0 is the initial mat volume when pressure is zero. As was the case for fiber mat (Eq. 2.8), Eq. (2.19) can be expressed in terms of mat density:

$$p = \frac{K_s E_s}{\rho_s{}^5} \left(\rho_m{}^5 - \rho_0{}^5\right) \tag{2.20}$$

where ρ_m is the mat density, ρ_0 is the initial mat density, and a bending model for predicting the pressure-density relationship of a 2D mat structure is established.

2.2.3 A Generalized Model for Wood Composite Mat Consolidation

Comparison of Eqs. (2.8) and Eq. (2.20) shows that these equations differ only in the power to which the densities are raised. Based on this, it is reasonable to assume that the pressure and density relationships for different wood composites will follow a power law relationship of similar form. Consequently, a generalized consolidation model can be written as:

$$p = \frac{K_c E_c}{\rho_c{}^{n_c}} \left(\rho_m{}^{n_c} - \rho_0{}^{n_c}\right) \tag{2.21}$$

where p is mat pressure, K_c is a parameter determined experimentally, E_c is Young's modulus of wood constituent, ρ_c is density of wood constituent, ρ_m is mat density during consolidation, ρ_0 is mat density when uncompressed, and n_c is a parameter for different mat types. In this case n_c can be treated as a characteristic of the low-stress consolidation of mat structures, i. e., 3 for fibers and 5 for strands. Other mat materials will have other characteristic values for n_c. Although this generalized model is far from perfect, it may provide some insights into the mechanism of wood composite consolidation. Furthermore, this model has only two adjustable parameters (K_c and n_c) and as such should be relatively easy to use.

2.3 Experimental

The following experiment was designed to investigate the mat pressure-density relationships and to verify the proposed consolidation model for fiber mat, particle mat and strand mat, respectively.

2.3.1 Materials

Aspen (*Populus tremuloides*) wood fibers were prepared through a thermal-mechanical pulping process by a mill in Quebec, Canada. During this process, the fibers were subjected to only limited chemical action and their chemical composition is similar to that of original wood (Kollmann et al. 1968). Therefore, as most of the lignin in the cell walls remained intact, one would expect their shape and integrity to be relatively

uncompromised. In addition, hardwood fibers tend to be rounded in cross-section and thick-walled as compared to softwood tracheids (Bowyer et al. 2002). As a result, a rod is a reasonable approximation of the fiber shape. Aspen strands were obtained from an OSB plant in Ontario, Canada. Some of the strands were ground into particles and those small enough to pass through a 5 mm mesh screen were used for particle mat furnish.

2.3.2 Methods

The fiber dimensions (average length 1.04 mm and average diameter 28.3 μm) were measured using the Fiber Quality Analyzer (OpTest Equipment Inc., ON, Canada). In this instrument, a dilute suspension of fibers is passed through a flow cell that orients the fibers into a thin plane (Robertson et al. 1999). Then the fiber properties (e. g., fiber length, width, shape, and average coarseness) can be analyzed by the optical and image processing systems. The average length (61.1 mm) and width (18.6 mm) of wood strands were obtained by an image analysis system (OSBVIEW, FPInnovations - Forintek Division), and the average thickness (0.7 mm) was measured by a digital caliper. The average moisture contents of the furnish prior to consolidation were 9.1, 8.9, and 8.5% for fiber, strand and particle mats, respectively. All mats were made by hand in a 152 mm by 152 mm forming box with 170 g wood constituents. In addition, efforts were made to ensure the randomness of mat structure during each formation process.

All mat consolidation tests were conducted on a universal servo-hydraulic MTS machine equipped with a 222.5 kN load cell at an ambient temperature of approximately 20°C.

The computer control and monitoring system can acquire the pressure and deformation data in real time. To minimize the variability in initial mat density, mats were pre-compressed to a thickness of 60 mm for fiber, 36 mm for strand, and 40 mm for particle mats based on their initial bulky volume. Very low stress (approximately 8 kPa) was detected when the mats were compressed from the initial thickness to the pre-compressed thickness, which is interpreted as the pre-compression having almost no effect on the later mat compression behavior. It is noted that the mat density corresponding to the pre-compressed thickness is the initial mat density ρ_0 used in this proposed model. The mats were then compressed at a loading rate of 25 mm min^{-1} until the compressive force reached the upper limit of the load cell. Six replicates were conducted for each furnish type for a total of 18 mats.

2.4 Results and Discussion

The pressure as a function of mat density for all 18 mats (6 for each mat type) is shown in Figure 2.5. The shape is similar for each mat type and differs only in the rate at which the pressure increases: fastest for strands and slowest for fibers. One can also see that the pressure-density responses for each mat type are very similar, indicating the consistent mat structure between replicates.

2.4.1 Fiber Mat Consolidation

For a wood fiber mat prior to pressing, wood fibers are distributed at random positions and orientations within the mat and it can be treated as a 3D structure. According to Eq. (2.8), if the E_f value is known, then K_f can be obtained by fitting the model prediction to the test data during low-stress mat consolidation. However, since it is very difficult to determine the elastic modulus of single aspen fiber, it is reasonable to obtain an estimate value for E_f from literature. According to Neagu et al. (2006), the fiber longitudinal Young's modulus varies between 21.0 and 39.0 GPa, depending on the wood species and pulping process. Therefore, a mid-range E_f value of 30.0 GPa was assumed for the fibers. This E_f value was then used to determine the value of K_f by performing a least-squares fit to the results, producing an estimate for K_f of 1.5×10^{-3}.

Model predictions are compared with experiment results in Figure 2.6. Due to its initially loose structure at the early stage of mat consolidation, the pressure increases slowly with relatively large increase in density. For mat density below 650 kg m^{-3}, the model prediction is in good agreement with the measured values. This initial close agreement suggests that bending is the dominant mechanism at densities below 650 kg m^{-3} for the fiber mat. At this stage, fiber-to-fiber contact develops with the increase of mat density, which will shorten the distances between contacts and produces a corresponding increase in consolidation force (i.e., Eq. 2.1).

At mat densities above 650 kg m^{-3}, the discrepancy between model prediction and experimental data becomes larger and increases with mat density. Obviously, there is a change in mechanism as more contacts occur between the fibers. The mat consolidation mechanism changes from one dominated by fiber bending to one where fiber compression becomes significant. In addition, at sufficiently high pressure, the fibers may be damaged by cell wall buckling or cell wall fracture, thus resulting in the pressures that are below those predicted by the bending model. Furthermore, as this model is based on the idealized random fiber assembly, it needs to be modified to include the effects of fiber diameter distribution, fiber orientation distribution, fiber bundles, fiber crimp, and the slippage between the fibers to improve its prediction ability.

2.4.2 Strand Mat Consolidation

The entire mat consolidation process can be divided into two stages as shown in Figure 2.7: the initial strand bending and the late strand compression.

Bending model

At the early stage of mat consolidation, according to Eq. (2.20), an E_s value of 11.2 GPa (Wood Handbook 1999) was used to determine the K_s value using a least-squares fit to the experimental results. The K_s value was estimated to be 2.0×10^{-4}. The bending model prediction is in reasonable agreement with the test results, indicating that strand bending indeed dominates the initial mat consolidation.

Compression model

Dai and Steiner (1993) proposed a model based on transverse compression properties of wood strands and random mat structure in which the mat was defined as a system of strand columns of infinitely small cross-sectional area. The distribution of the number of strands in a column could be described by the following Poisson distribution:

$$p(i) = \frac{e^{-n} n^{i}}{i!} \tag{2.22}$$

where $p(i)$ is the probability of a strand column over mat area covered by i strands, n is the mean strand number of all strand columns, i is the number of strands in a strand column. The overall mat pressure was obtained based on the modified Hooke's law to describe the nonlinear stress-strain relationship of wood strands (Wolcott et al. 1994):

$$\sigma_n = E e^{-n} \sum_{i=T_m/\tau}^{\infty} \varphi(\varepsilon_i)\varepsilon_i \frac{n^{i}}{i!} \tag{2.23}$$

where σ_n is the overall mat pressure, E is the compression modulus of wood strand, T_m is the mat thickness, τ is the strand thickness, ε_i is the strand strain in a column of i strands, $\varphi(\varepsilon_i)$ is the nonlinear strain function for the strand column and was described empirically by the following equation:

$$\varphi(\varepsilon) = \sum_{i=0}^{10} b_i \varepsilon^{i} \tag{2.24}$$

where b_i is obtained through a computer regression program, which was well described in a previous publication (Dai and Steiner 1993). The predictions from their model were in good agreement with the experimental data. Based on this close agreement, it was decided that this model could be used to describe strand compression. As can be seen from Figure 2.7, at the late stage of mat consolidation, good agreement was obtained with

the compression model. This is evidence that the strand transverse compression is the dominant mode. It is also evident in Figure 2.7 that the mat density, at which the transition from bending to compression occurs, is around 400 kg m^{-3}. Interestingly, this is approximately equal to the density of wood strands prior to compression.

2.4.3 Particle Mat Consolidation

Wood particles are different from fibers and strands not only in size but also in slenderness ratio (the ratio of length to thickness), which is much smaller than both fibers and strands. In addition, particles slip and reposition themselves more during consolidation than strands. As a result, it is difficult to determine whether the particle mat is a 3D or 2D structure. Before pressing, the mat appears to be three-dimensional. Therefore, some longitudinal compression of particles may also occur, causing the mat to be stiffer during consolidation. After the initial compression of the mat, it is more similar to 2D as the particles are stacked against each other, making it more similar to a strand mat.

Due to the small slenderness ratio, there is no justification for particles to bend likes fibers or strands during mat consolidation. In fact, due to particle shape and size, the particle mat consolidation seems to be similar to the powder compaction process involved with particle movement and rearrangement during packing. When the compaction behaviour of powders is described by the relationship of the compaction pressure and the relative density of the material, the trend of the powder compaction pressure-density

curve is very similar to that of particle mat pressure-density curve (Poquillon et al. 2002; Martin et al. 2003). However, one can still fit the model to the data to see if it is a reasonable description of the data. Using a value of 11.2 GPa for E_c, the values for n_c and K_c were adjusted gradually until the sum of the square of the difference between the observed and predicted results was minimized. It was found that the minimum corresponded to the values of $n_c = 2.2$ and $K_c = 1.7\times10^{-4}$ in Eq. (2.21) and was compared with the data in Figure 2.8. The model prediction appeared to agree well with the test data over the whole range. Consequently, it was concluded that this model could be utilized as a reasonable description of the mat pressure-density relationship although it cannot provide a clear explanation for the mechanism occurring during particle mat consolidation.

2.4.4 Effect of Parameter K and Young's Modulus E

The empirical parameter K_c in Eq. (2.21) is a structural factor which accounts for variations in distances between element contacts, variability of element length, and other characteristics. For instance, it is expected that this parameter will be different for randomly oriented strand mats compared with highly oriented ones, as the distribution of contact distances between strands is different in each case. It is noted that this parameter can only be determined by experiment. The changes in mat compressive behavior for different K_c values are compared in Figure 9, where the effect of increasing K_c only changes the rate of increase in mat pressure.

One of the key applications of the model is to predict vertical density profile of wood composites during hot pressing. Eq. (2.21) establishes a quantitative relationship between mat compression and elastic modulus of wood. It allows for the calculation of layered mat deformation assuming E_c is a function of moisture content and temperature. Figure 10 shows the effect of different E_c values on the strand mat pressure-density relationship (a lower E_c value due to the elevated temperature or moisture content within the mat). As is the case for the K_c value, increasing E_c value changes the rate of increase in mat pressure. In addition, this model can also predict the effect of different wood species on the mat compression behavior by using the appropriate E_c value for each species.

2.5 Summary and Conclusions

A generalized model is presented to understand and predict the mat consolidation behavior of wood composites. The composite mat is viewed as a system of bending units in which the compression load is transferred through the contact points between adjacent wood constituents. With knowledge of the statistical distribution of the distance between contact points in the fiber mat, the overall mat consolidation can be predicted based on bending forces on the individual wood elements using elementary beam theory. At moderate- and low-stress stage of mat consolidation, model predictions agree well with the experimental results for fiber mat. The entire consolidation process for a strand mat can be predicted by this model combined with the compression model (Dai and Steiner 1993). By adjusting coefficients, this model can also describe the experimental data of

particle mats. This model will be used to predict the hot pressing behavior of mats by expressing the modulus as a function of moisture content and temperature.

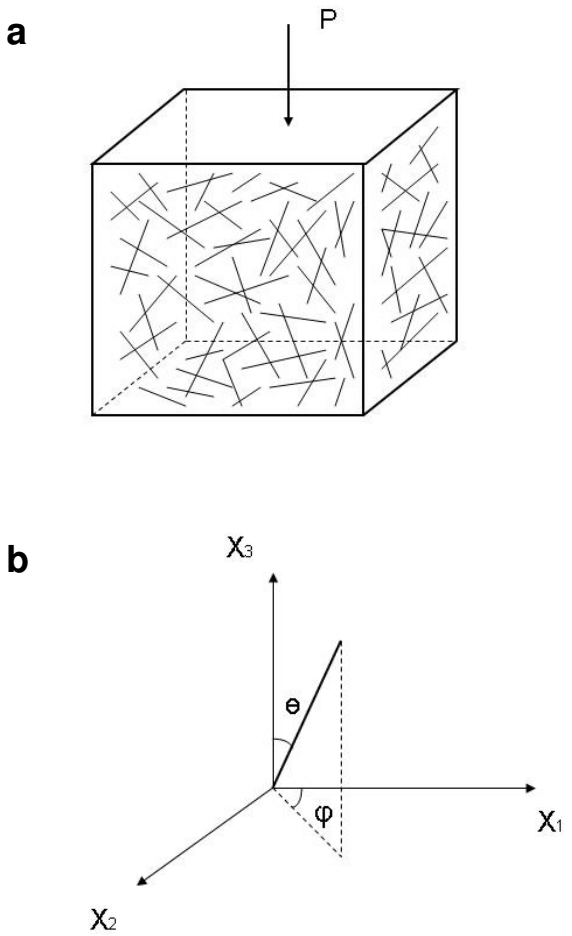

Figure 2.1 (a) A typical structural unit in a fiber mat. (b) A fiber in a Cartesian coordinate system.

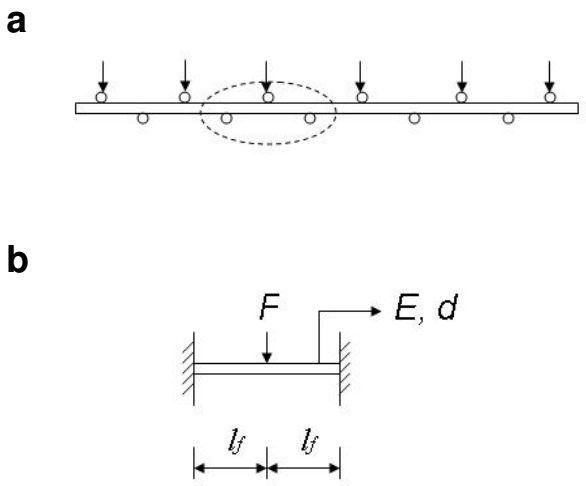

Figure 2.2 (a) Schematic of a fiber supported by crossing fibers. (b) A fiber bending unit.

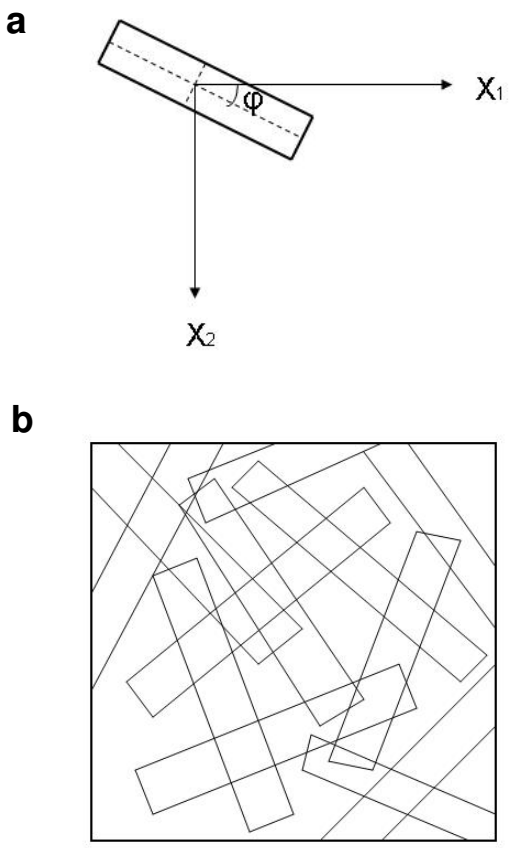

Figure 2.3 (a) A typical structural unit in a strand mat. (b) A strand in a Cartesian coordinate system.

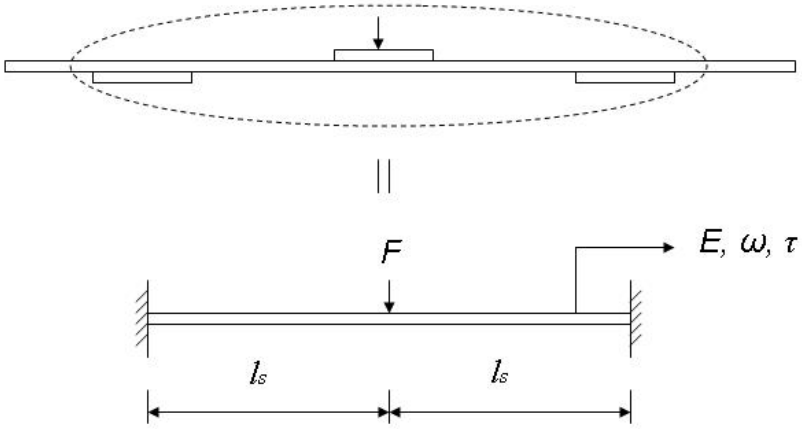

Figure 2.4 Schematics of the proposed strand geometry in the mat and the idealized loading conditions.

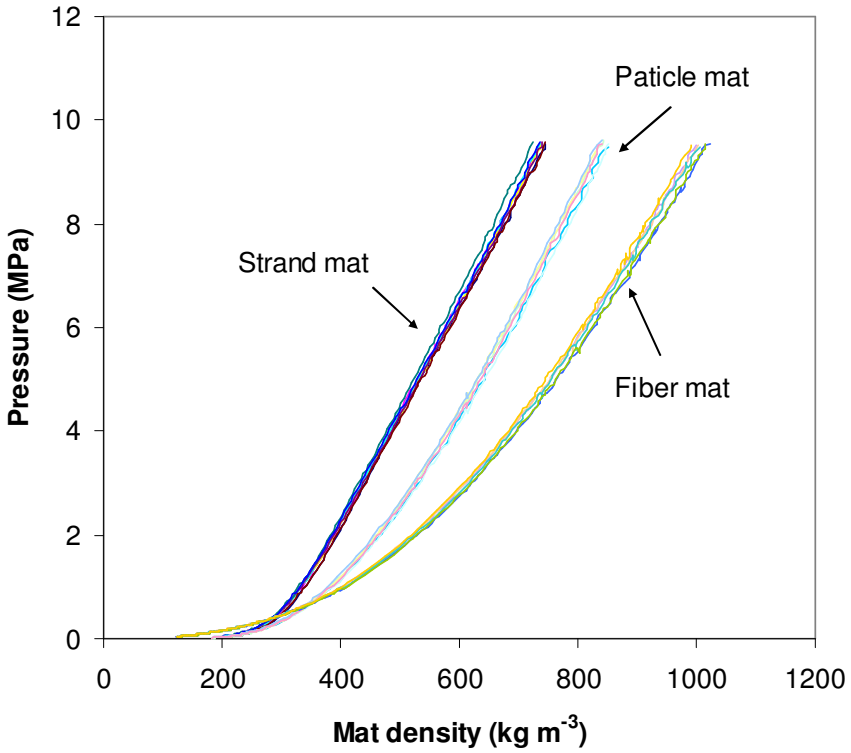

Figure 2.5 Comparison of the mat pressure-density responses of fiber, strand and particle mat.

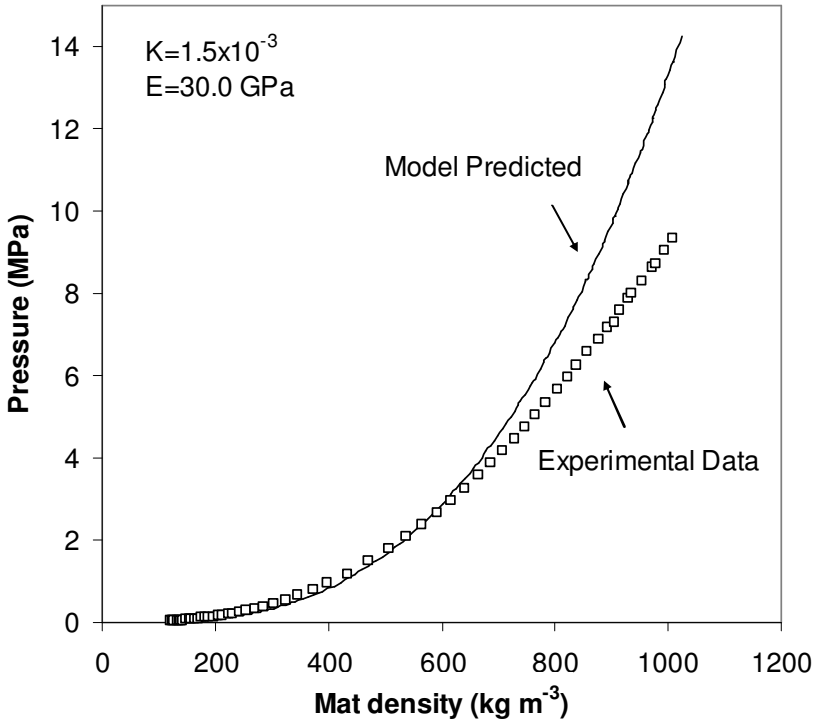

Figure 2.6 Comparison between experimental result and model prediction of fiber mat pressure-density relationship.

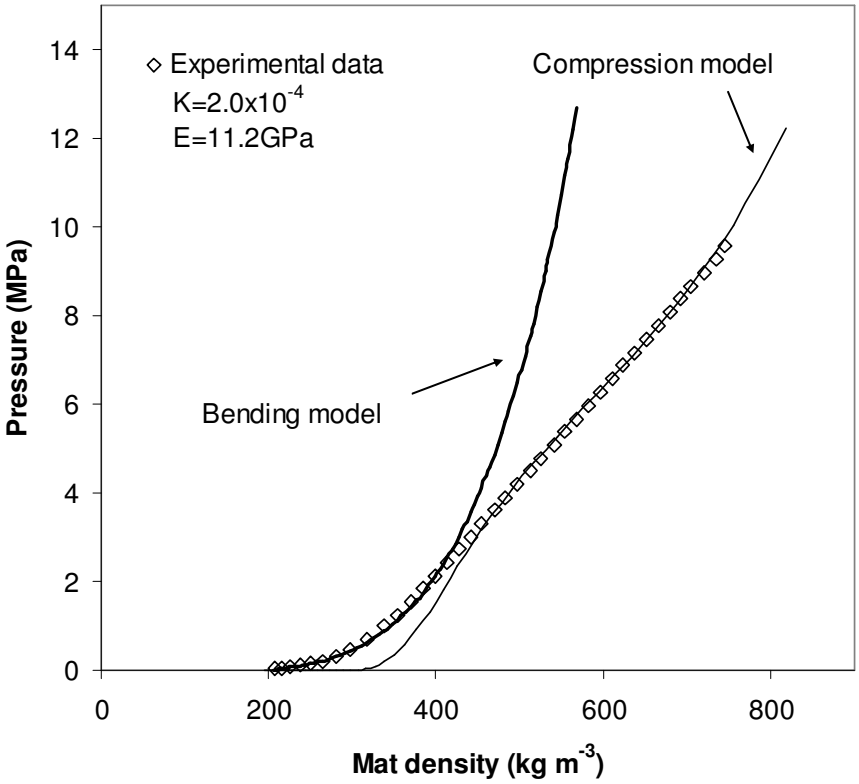

Figure 2.7 Comparison between experimental result and predictions of bending model and compression model for strand mat pressure-density relationship.

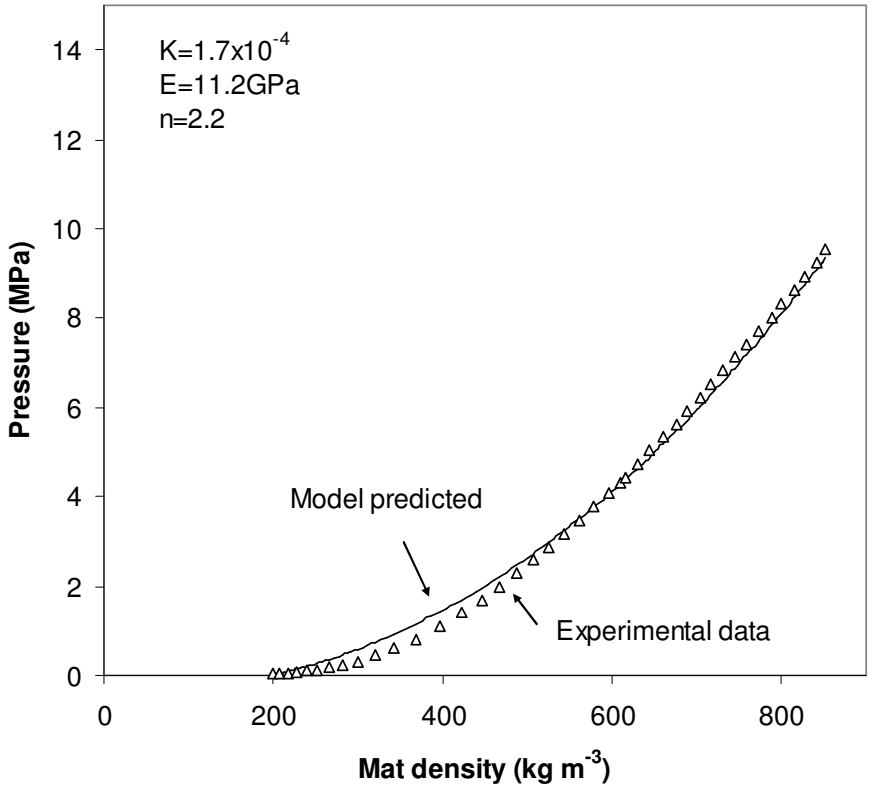

Figure 2.8 Comparison between experimental result and model prediction of particle mat pressure-density relationship.

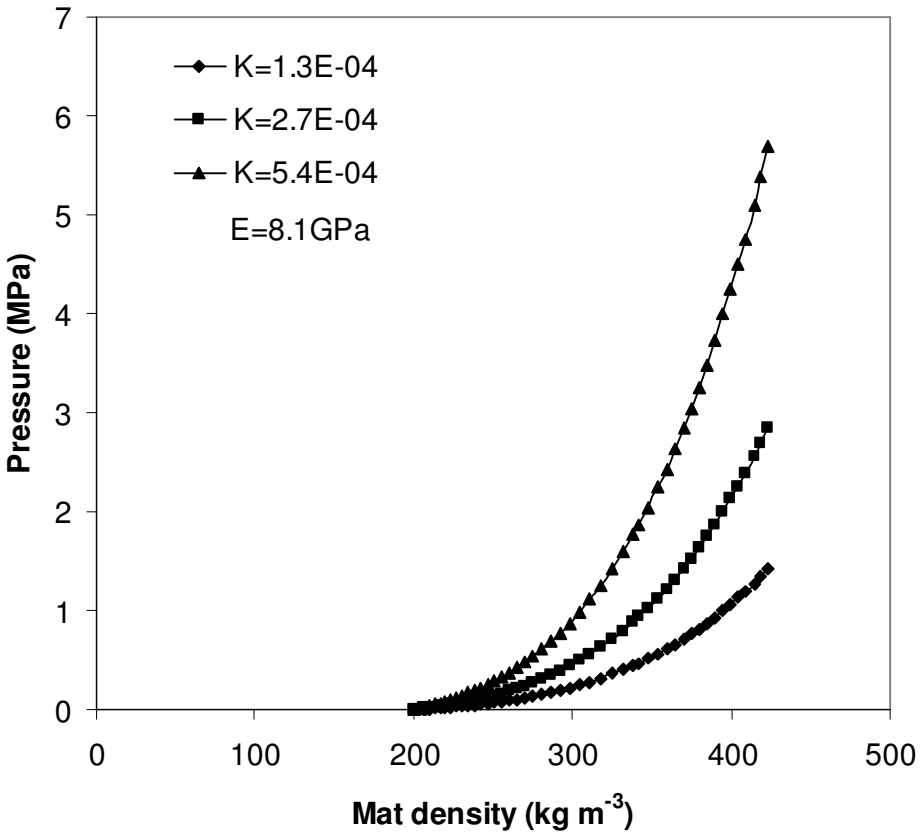

Figure 2.9 Effect of the parameter K in the bending model on the predicted mat pressure in the low-density range.

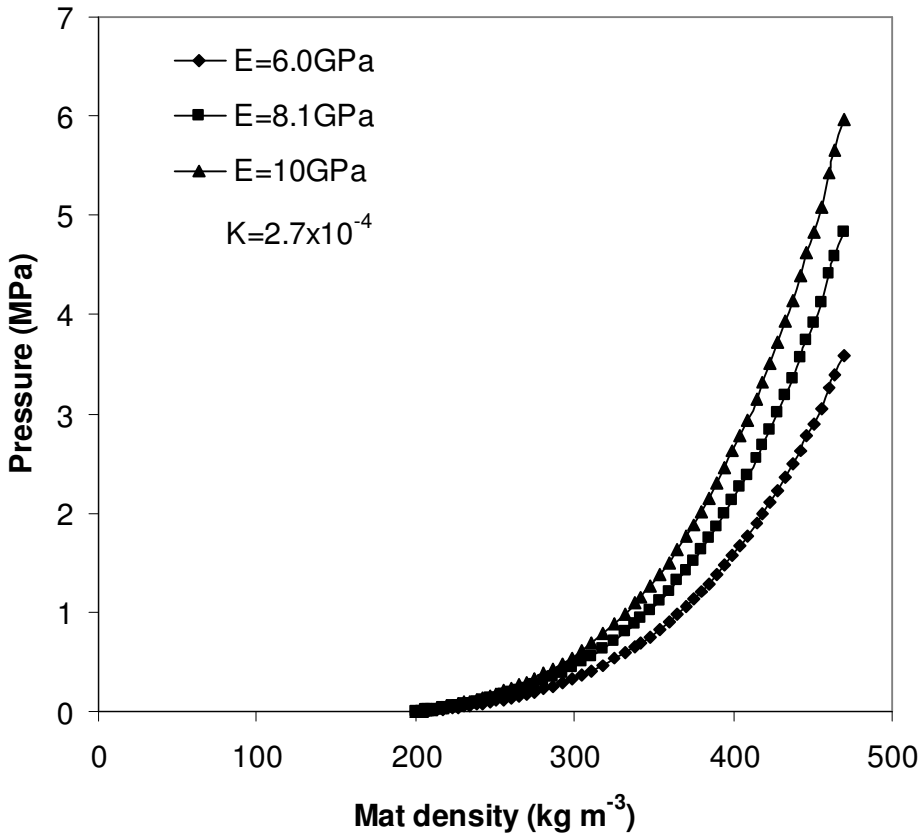

Figure 2.10 Effect of wood strand modulus E in the bending model on the predicted mat pressure in the low-density range.

2.6 Bibliography

Alkhagen, M.I. (2002) Nonlinear elasticity of fiber masses. Ph.D. dissertation, Chalmers University of Technology, Göteborg, Sweden.

Bell, N.B., Roberts, W.W. Jr. (2002) Modeling and computer simulation of the compressional behavior of fiber assemblies. Part I: Comparison to van Wyk's theory. Text. Res. J. 72: 341-351.

Bowyer, J.L., Shmulsky, R., Haygreen, J.G. Forest products and wood science: An introduction. Iowa State Press, Ames, Iowa. 2002.

Dai, C., Steiner, P.R. (1993) Compression behavior of randomly formed wood flake mats. Wood Fiber Sci. 25: 349-358.

Dai, C., Steiner, P.R. (1994a) Spatial structure of wood composites in relation to processing and performance characteristics. Part 2. Modeling and simulation of a randomly-formed flake layer network. Wood Sci. Technol. 25: 135-146.

Dai, C., Steiner, P.R. (1994b) Spatial structure of wood composites in relation to processing and performance characteristics. Part 3. Modeling the formation of multi-layered random flake mats. Wood Sci. Technol. 28: 229-239.

Dai, C., Yu, C. and Zhou, C. (2007) Theoretical modeling of bonding characteristics and performance of wood composites. Part 1. Inter-element contact. Wood Fiber Sci. 39: 48-55.

Englund, K.R., Wolcott, M.P., Hermanson, J.C. (2004) The compression of wood/thermoplastic fiber mats during consolidation. Compos. Part A. 35: 273-279.

Godbille, F.D. (2002) A simulation model for the hot pressing of particleboard. Ph. D. dissertation, University of New Brunswick, Fredericton, New Brunswick.

Jones, R.L. (1963) The effect of fiber structural properties on compression response of fiber beds. Tappi J. 43: 20-27.

Kallmes, O., Corte, H. (1960) The structure of paper. Part I: The statistical geometry of an ideal two dimensional network. Tappi J. 43: 737-752.

Kollmann, F.F.P., Kuenzi, E.W., Stamm, A.J. Principles of wood science and technology. Vol. II: Wood based materials. Springer-Verlag, New York, Heidlberg, Berlin, 1968.

Komori, T., Makishima, K. (1977) Numbers of fiber-to-fiber contacts in general fiber assemblies. Text. Res. J. 47: 13-17.

Kunesh, R.H. (1961) The inelastic behavior of wood: A new concept for improved panel forming process. Forest Prod. J. 11: 395-406.

Lang, E.M., Wolcott, M.P. (1996a) A model for viscoelastic consolidation of wood-strand mats. Part I. Structural characterization of the mat via Monte Carlo simulation. Wood Fiber Sci. 28: 100-109.

Lang, E.M., Wolcott, M.P. (1996b) A model for viscoelastic consolidation of wood-strand mats. Part II. Static stress-strain behavior of the mat. Wood Fiber Sci. 28: 369-379.

Lenth, C.A., Kamke, F.A. (1996a) Investigations of flakeboard mat consolidation. Part I. Characterizing the cellular structure. Wood Fiber Sci. 28: 153-167.

Lenth, C.A, Kamke, F.A. (1996b) Investigations of flakeboard mat consolidation. Part II. Modeling mat consolidation using theories of cellular materials. Wood Fiber Sci. 28: 309-319.

Lundquist, L., Willi, F., Leterrier, Y., Manson, J.-A.E. (2004) Compression behavior of pulp fiber networks. Polym. Eng. Sci. 44: 45-55.

Martin, C.L., Bouvard, D., Shima, S. (2003) Study of particle rearrangement during powder compaction by the Discrete Element Method. J. Mech. Phys. of Solids. 51: 667-693.

Neagu, R.C., Gamstedt, E.K., Berthold, F. (2006) Stiffness contribution of various wood fibers to composite materials. J. Compos. Mater. 40: 663-699.

Neagu, R.C., Gamstedt, E.K., Lindstrom, M. (2006) Characterization methods for elastic properties of wood fibers from mats for composite materials. Wood Fiber Sci. 38: 95-111.

Neckar, B. (1997) Compression and packing density of fibrous assemblies. Text. Res. J. 67: 123-130.

Oudjehane, A., Lam, F., Avramidis, S. (1998) A continuum model of the interaction between manufacturing variables and the consolidation of wood composite mats. Wood Sci. Technol. 32: 381-391.

Painter, G., Budman, H., Pritzker, M. (2006) Predictions of oriented strand board properties from mat formation and compression operating conditions. Part 1. Horizontal density distribution and vertical density profile. Wood Sci. Technol. 40:139-158.

Pan, N. (1993) A modified analysis of the microstructural characteristics of general fiber assemblies. Text. Res. J. 63: 336-345.

Pawlak, J.J., Keller, D.S. (2005) The compressive response of a stratified fibrous structure. Mech. Mater. 37: 1132-1142.

Poquillon, D., Lemaitre, J., Baco-Carles, V., Tailhades, Ph., Lacaze, J. (2002) Cold compaction of iron powders – relations between powder morphology and mechanical properties. Part I: Powder preparation and compaction. Powder Technol. 126: 65-74.

Robertson, G., Olson, J., Allen, P., Chan, B., Seth, R. (1999) Measurement of fiber length, coarseness, and shape with the fibre quality analyzer. Tappi J. 82: 93-98.

Schofield, J. (1938) Research on wool felting. J. Text. Inst. 29: T239-T252.

Suchsland, O. (1959) An analysis of the particleboard process. Michigan Quarterly Bulletin. 42: 350-372.

Suchsland, O. (1967) Behavior of a particleboard mat during the press cycle. Forest Prod. J. 17: 51-57.

Thoemen, H., Humphrey, P.E. (2003) Modeling the continuous pressing process for wood-based composites. Wood Fiber Sci. 35: 456-468.

Thoemen, H., Humphrey, P.E. (2006) Modeling the physical process relevant during hot pressing of wood-based composites. Part I. Heat and mass transfer. Holz Roh-Werkst. 64: 1-10.

Thoemen, H., Haselein, C.R., Humphrey, P.E. (2006) Modeling the physical process relevant during hot pressing of wood-based composites. Part II. Rheology. Holz Roh-Werkst. 64: 125-133.

Toll, S. (1998) Packing mechanics of fiber reinforcements. Polym. Eng. Sci. 38: 1337-1350.

Toll, S., Manson, J.-A.E. (1995) Elastic compression of a fiber network. J. Appl. Mech. 62: 223-226.

van Wyk, C.M (1946) Note on the compressibility of wool. J. Text. Inst. 37: T285-T292.

Wolcott, M.P., Kamke, F.A., Dillard, D.A. (1990) Fundamentals of flakeboard manufacture: Viscoelastic behavior of the wood composite. Wood Fiber Sci. 22: 345-361.

Wolcott, M.P., Kamke, F.A., Dillard, D.A. (1994) Fundamental aspects of wood deformation pertaining to manufacture of wood-based composites. Wood Fiber Sci. 26: 496-511.

Wood Handbook: Wood as an Engineering Material (1999) Gen. Tech. Rep. FPL-GTR-113 USDA Forest Prod. Lab., Madison, WI.

Zombori, B.G., Kamke, F.A., Watson, L.T. (2001) Simulation of the mat formation process. Wood Fiber Sci. 33: 564-580.

Zombori, B.G., Kamke, F.A., Watson, L.T. (2003) Simulation of the internal mat conditions during the hot-pressing process. Wood Fiber Sci. 35: 2-23.

CHAPTER 3 CHARACTERIZING HYDRO-THERMAL COMPRESSION OF ASPEN WOOD STRANDS[2]

3.1 Introduction

Hot-pressing is a critical operation in the manufacture of wood-based composites such as oriented strand board (OSB), particleboard, and medium-density fiberboard (MDF). During this process, mats of resinated strands, particles, or fibers are consolidated under heat and pressure, resulting in contact between the wood constituents and the formation of bonds. Once the press closes, simultaneous heat and mass transfer takes place, making the temperature and moisture content (MC) functions of position within the mat and time. As compression of the mat continues, void volume is reduced and deformation of wood constituents occurs. This densification changes the physical and mechanical properties of the wood components, the extent to which is strongly affected by the local temperature and MC. Like any other material, the properties of a wood composite will be determined by that of its constituent materials and the spatial arrangement of the wood elements. As such, characterizing the compressive behavior of individual wood constituents during hot pressing is critical to understanding how manufacturing processes affect final product properties.

During the pressing process, the wood elements are compressed primarily in the perpendicular-to-grain direction with the overall mat response being the average compression of the radial and tangential directions. A number of publications have

[2] A version of this chapter has been published. Zhou, C., Smith, G.D., Dai, C. (2009) Characterizing hydro-thermal compression of aspen wood strands. Holzforschung 63: 609-617.

reported the work on wood transverse compression. The mechanical properties of solid wood in perpendicular-to-grain compression were investigated at different temperatures and MCs by Youngs (1957) and Kunesh (1961). Bodig (1965) related the anatomy of the wood and the direction of loading to the transverse compression behavior and proposed the weak layer theory in radial compression as well as the spaced column theory in tangential compression. Kennedy (1968) found that ring orientation, specific gravity, ray volume, and earlywood-to-latewood ratio within a single growth ring could strongly affect the wood mechanical properties under perpendicular-to-grain compression.

Empirical models have been developed in the past to predict the effects of temperature and MC on the transverse compression behavior of solid wood (Palka 1973; Gerhards 1982). After testing small wood specimens in transverse compression, Wolcott et al. (1989) found that the results were influenced by specimen size and geometry as well as the test procedure. Furthermore, Wolcott et al. (1994) applied theories of cellular solids to model the nonlinear transverse compression behavior of small wood blocks and flakes. Dai and Steiner (1993) developed a model to predict the mat stress-strain relationship based on transverse compression behavior of wood flakes at room temperature. Tabarsa and Chui (1997, 2000) studied the effect of press temperature on the stress-strain relationship and the cell-wall collapse mechanism of white spruce under transverse compression. More recently, Ncube et al. (2004) investigated the behavior of wood particles compressed in the radial and tangential direction under conditions that simulated hot-pressing.

Although the above-mentioned reports covered a variety of wood species, specimen sizes and test conditions, little research was conducted on the transverse compression of aspen (*Populus tremuloides*) strands during hot-pressing, a common low-density material (specific gravity 0.38) for OSB panel manufacturing in Canada. Investigating the compression behavior of individual strands during hot-pressing is helpful for understanding how manufacturing variables affect the final panel properties. Furthermore, this investigation of the compression behavior of aspen strands at a variety of temperatures and MCs will provide valuable information for later model development of vertical density profile (VDP), which is an important panel characteristic strongly affecting the mechanical properties of the final product.

Therefore, the overall objective of this research is to provide a deeper and quantitative understanding of the effects of temperature and MC on the properties of aspen strands. The specific objectives are:

1) to experimentally measure the transverse compressive response of aspen strands for various combinations of temperature and MC;

2) to model the strand compression modulus as a function of temperature and MC; and

3) to present the predictive effects of temperature and MC on the stress-strain response of wood strands in transverse compression.

3.2 Literature Review: Dependence of Wood Softening on Temperature and MC

Wood can be treated as a polymeric composite material. For an amorphous polymer, it exhibits a typical response to heating – thermal softening or even transition from a glassy state to a rubbery state (Young and Lovell 1991). The temperature at which the transition occurs is commonly termed as glass transition temperature T_g. It is usually taken as the temperature at the midpoint of the temperature range over which transition occurs. The mobility of the constituent molecules changes significantly above this temperature and this manifests itself in a dramatic change in mechanical properties. For example, the elastic modulus of an amorphous polymer may decrease by a factor of over 1000 times as the temperature rises through this transition region (Nielsen 1974; Irvine 1985). While for a partially crystalline polymer such as cellulose, the modulus will fall off much less (Salmén and Back 1980).

The concept of free volume may be the most useful approach to analyze this transition phenomenon. The free volume is defined as the space in a solid or a liquid which is not occupied by polymer molecules. A rise in temperature will increase the thermal energy available for molecular motion, which increases the free volume and allows the molecules to move and so change their conformation (Young and Lovell 1991).

The addition of diluents to a polymer may shift its glass transition temperature to lower temperatures due to an increase in the free volume of the system. In plasticization of polymers by water, secondary interactions between water and the polymer such as

hydrogen bonding should be taken into account apart from the free volume (Irvine 1985; Kelly et al. 1987). Based on these considerations, the Kwei model (Eq. 1) was applied by several researchers (Kelly et al. 1987; Wolcott et al. 1990) to predict the effect of moisture content on the glass transition of amorphous components in wood as shown in Figure 3.1:

$$T_g = \frac{W_1 T_{g1} + kW_2 T_{g2}}{W_1 + kW_2} + qW_1 W_2 \tag{3.1}$$

where W and T_g represent the weight fraction and glass transition temperature of polymer (1) and moisture (2), and *k* and *q* are adjustable parameters accounting for free volume considerations and molecular interactions, respectively. The parameter values used in this model for lignin, hemicellulose, and water are listed in Table 3.1. This model was found to provide an excellent fit to the experimental data for both lignin and hemicellulose (Kelly et al 1987). In addition, for MCs less than 15%, which is usually encountered in the wood composites manufacturing, it is reasonable to assume the temperature and moisture only influence the amorphous hemicellulose and lignin rather than the partly crystalline cellulose in wood (Salmén et al. 1985; Wolcott et al. 1990).

Most of the investigations on the glass transition focused on the examination of isolated or *in situ* lignin and hemicellulose individually (Goring 1963; Cousins 1976, 1978; Back and Salmén 1982; Irvine 1984, 1985; Kelley et al. 1987; Salmén and Olsson 1998). Although these results are important and provided some insights, due to the unavoidable alteration of these components during their extraction or preparation, their applicability to intact, unadulterated wood is questionable. In addition, wood is not a random mixture of cellulose, hemicellulose and lignin and thus wood softening is affected by the

organization of its constituents and the interaction between them (Chow and Pickles 1971). Recognizing the limitation of those methods, several researchers directly investigated the thermal softening behavior of solid wood specimens at various moisture contents (Östmen 1985; Blechschmidt et al 1986; Lenth and Kamke 2001; Wolcott and Shutler 2003). These authors found that the thermal softening was largely dependent on wood moisture and wood species due to natural variation in cellulose, hemicellulose and lignin present in different species.

3.3 Model Development

Wood is a natural cellular material and thus exhibits unique mechanical behavior when compressed in the perpendicular-to-grain direction. Figure 3.2a shows a typical stress-strain relationship of wood in transverse compression where three distinct stages can be defined. The initial stage is in a linear elastic manner due to the uniform cell wall bending. When the cell walls start buckling or collapsing, the second stage is entered, in which the stress is almost constant while the strain continues to increase. At the end of the plastic region, the stress increases rapidly as a result of cell lumen collapse and cell wall contacts. Therefore, the last stage is termed cell wall densification, where strain only changes slightly with increasing stress. The length of each stage is strongly dependent on the cell wall material properties and the cellular structure.

Although Hooke's law cannot be used directly to describe the stress-strain behavior of wood strands under transverse compression, earlier researchers have applied a modified

Hooke's law (Wolcott 1990; Dai and Steiner 1993; Wolcott et al. 1994; Lenth and Kamke 1996; Lang and Wolcott 1996) based on the load-compression behavior of flexible foams (Rusch 1969) in the following form:

$$\sigma = E\varphi(\varepsilon)\varepsilon \tag{3.2}$$

where σ is the stress, E is the transverse compression modulus of wood, ε is the strain, and $\varphi(\varepsilon)$ is the dimensionless strain function. This strain function $\varphi(\varepsilon)$ is assumed to be independent of the properties of the cell wall and depends only on the cellular structure (Wolcott 1990; Dai and Steiner 1993; Wolcott et al. 1994). $\varphi(\varepsilon)$ can describe the full range of stress development during transverse compression for cellular materials. As shown in Figure 3.2b, $\varphi(\varepsilon)$ equals unity in the linear elastic range, starts to decrease and reaches a minimum during cell wall collapse, and finally increases rapidly and approaches infinity during cell wall densification.

The elastic modulus of wood not only depends on the cell wall material and the specific gravity of wood species (Gibson and Ashby 1988), but it also depends on the local temperature and MC as well as the loading rate (Kunesh 1961, 1968; Wolcott et al. 1989; Wolcott et al. 1990; Dai and Steiner 1993). In other words, the effect of temperature, moisture content and loading rate should not affect $\varphi(\varepsilon)$, but only E. Once the strain function is determined at a given condition (e. g., room temperature and oven-dried), one can predict the stress-strain relationship at any temperature and MC as long as the dependence of E on temperature and MC is known.

Consequently, Eq. (3.2) can be rewritten as follows:

$$\sigma = E(T, MC)\varphi(\varepsilon)\varepsilon \tag{3.3}$$

where T is the temperature, MC is moisture content. It is noted that wood density also has a great effect on the elastic modulus. In this case, aspen is a diffuse-porous hardwood and its density is relatively uniform throughout the stem cross section (Yanchuk et al. 1983). The loading direction, radial (LR) or tangential (LT), affects the transverse compression behavior of wood strands. During the stranding process, the predominant plane of the strand face will range from being purely LT to LR as the stranding knives move from the edge of the log to its center. Thus, the compressive response of a random collection of strands should be the average response of the strands in the LT to LR orientations. As a result, the effect of loading direction is not taken into account in this work.

3.4 Experimental

The experiment described below had two objectives: 1) to quantitatively investigate the effects of temperature and MC on the strand modulus of elasticity; and 2) to determine if the strain function for wood strand is independent of environmental conditions.

3.4.1 Materials

Thin sheets of sliced aspen veneer, 0.75 mm thick, were cut into 25 mm by 25 mm samples. To minimize the effect of density variations between individual samples, strands were randomly selected for the transverse compression test.

To reach the different target MCs, the specimens were conditioned in a glass desiccator over a selected saturated salt solution at 20°C until equilibrium was reached (typically three days) (Greenspan, 1977). According to Simpson's model (1973), the equilibrium moisture content (EMC) of these specimens can be predicted at a given relative humidity and temperature. The different MCs at 20°C for the saturated salt solutions are listed in Table 3.2. For the MC = 0% samples, the specimens were prepared by oven-drying them in a force-convection oven at a temperature of 103 ± 2°C for 3 hours. Dried samples were stored in a desiccator with fresh desiccant until they reached room temperature. For the MC = 9%, the specimens were conditioned in a chamber maintained at a relative humidity 50% and temperature 20°C. To investigate the compression behavior of strands during hot pressing, seven temperatures (20°C, 50°C, 80°C, 110°C, 140°C, 170°C, 200°C) were used for each MC. These temperatures and MCs were selected to simulate the parameters during panel manufacturing process.

3.4.2 Methods

The strand compression tests were conducted on a miniature hot press which was set up in an Instron load frame equipped with a 9.8 kN load cell. Preliminary tests with a thermocouple placed at the interface between two strands showed that the interface temperature reached the press temperature within 10 s. Based on this, it was decided that all compression tests would be done using two strands and no thermocouple.

All the specimens were stored over the saturated salt solutions and then transported to the load frame in sealed plastic bags where they remained until just prior to testing. To maintain MC and temperature during hot pressing, the specimens were wrapped in two layers of aluminum foil. Since the thickness of this foil, only 0.0017 mm, was much thinner than the strands and the elastic modulus of aluminum is much higher than wood, it was assumed that the foil had no effect on the strand compression behavior. Prior to compression, two thermocouples were placed on each surface of the press to monitor temperature. Once the temperature had stabilized, the thermocouples were removed, then the specimen was positioned in the center of the platen, and the test began.

The samples were compressed at a loading rate of 0.5 mm min^{-1} to a maximum load of 9 kN. This maximum load corresponded to a pressure within the cell-wall densification region (Dai and Steiner 1993). The deformation of the specimen during testing was measured by two displacement transducers mounted on two opposite sides of the platen. The schematic drawing of this test set-up is shown in Figure 3.3. Fifteen replicates were made for each combination of MC and temperature.

Stress-strain curves were computed from the load/displacement results. The compressive modulus of each strand pair was obtained from a linear least squares fit to the elastic portion of the curve. It should be noted that, due to the surface roughness of the specimen, usually there is an initial low stiffness region before the stress-strain curve enters the linear elastic region. This initial nonlinear region was ignored when the elastic modulus was estimated in this work.

The mass of each strand pair was also measured just before testing and after testing and then oven-dried to determine moisture loss during pressing. The method of wrapping strands in aluminum foils was found to be effective at minimizing moisture loss during testing. The temperature range over which the moisture loss was less than 1% was 20 to 200°C for the oven dry samples, 20 to 110°C for the 3, 6, and 9% MC samples, and 20 to 80°C for the 12 and 15% MC samples. Results from samples with a moisture loss of more than 1% were discarded.

3.5 Results and Discussion

3.5.1 Effects of Temperature and MC on Strain Function $\varphi(\varepsilon)$

For flexible polyurethane foams, the strain function is, in principle, dependent only on the geometric features of the matrix structure and independent of the modulus of the matrix polymer, i.e., the temperature is assumed to only influence the elastic modulus not the strain function (Rusch 1969). In a similar manner, moisture is also assumed to have no effect on its cellular structure but only affects its elastic modulus (Wolcott et al. 1990; Dai and Steiner 1993; Lang and Wolcott 1996; Lenth and Kamke 1996).

According to Eq. (3.3), if the stress σ, the strain ε and the elastic modulus E for a given temperature and MC are known, the strain function $\varphi(\varepsilon)$ can be computed. Although $\varphi(\varepsilon)$ can be obtained from the stress-strain response of each specimen, it is more useful

for the model development when it is expressed as a mathematical equation. For example, when T = 20°C and MC = 0%, the corresponding $\varphi(\varepsilon)$ is derived from the average responses of the replicates with a polynomial curve fitting technique:

$$\varphi(\varepsilon) = \begin{cases} 1 & \varepsilon \le 0.15 \\ -6.0768\varepsilon^3 + 11.282\varepsilon^2 - 6.485\varepsilon + 1.6179 & \varepsilon > 0.15 \end{cases} \quad (3.4)$$

It is noted that this estimation assumes $\varphi(\varepsilon)$ equal to unity in the linear range and ignores the slight nonlinearity at the beginning. It is suggested that this discrepancy has little impact on the prediction accuracy, especially for the high strain regions where it is negligible compared to the total predicted stress (Dai and Steiner 1993).

Following the same procedure, strain functions at typical combinations of T and MCs are plotted in Figure 3.4, in which each curve represents average response of the replicates in each group. For strains less than 0.5, the curves are similar in magnitude and shape; at higher strains the trajectories diverge and fall into two groups. The first group has relatively lower values for the strain function and consists of the oven dry samples at 20 and 110°C, the 6% MC samples at 20 and 80°C, and the 15% samples at 20°C. These results support the assumption made by earlier researchers (Wolcott et al. 1990; Dai and Steiner 1993; Lang and Wolcott 1996; Lenth and Kamke 1996) that the strain function is independent of temperature and MC. However, there is also a high strain function group for two conditions: the oven dry samples at 200°C and the 15% MC samples at 80°C. These results contradict the previously accepted assumption that these parameters have no effect on the strain function as the stain increases.

It is noted that this assumption is valid only when the change in temperature does not cause the cell wall material to become brittle or to degrade (Rusch 1969, 1970). According to LeVan (1989), thermal degradation reactions of some wood components occur around the temperature of 200°C, at which hemicelluloses and lignin are susceptible to pyrolysis and result in carbohydrate weight loss of wood. Although cellulose remains mostly unpyrolyzed, its thermal degradation can be accelerated in the presence of water, acids and oxygen. For the 200°C samples, the color of sample surface became much darker after compression indicating the presence of some degradation. As for the effect of moisture, Wolcott and Shutler (2003) suggested that the presence of bound water in wood at elevated temperatures may result in kinetic effects or altered wood polymer structures and thus influence the mechanical behavior of wood. These chemical reactions within the cell wall due to high temperature or moisture violate the assumptions made for describing the behavior of foams described earlier.

Furthermore, another reason this assumption becomes invalid can be attributed to the difference between flexible polyurethane foams and wood. Flexible foams exhibit 100% recovery after strain as high as 0.8 at 25°C (Rusch 1970). In contrast, wood deforms permanently for strains higher than 0.15 at room temperature. This permanent deformation may play an important role in the effects of temperature and moisture on the strain function as the structure of the wood material itself is changing. This is very different for the case of flexible foams where one has essentially the same configuration of molecules after a large deformation as existed before the deformation.

According to Eq. (3.3), the transverse stress-strain relationships of wood strands for typical temperatures and MCs are described in Figure 3.5, which were obtained using the same strain function, Eq. (3.4), derived from the reference temperature 20°C at MC = 0%. Figures 3.5a, 3.5b and 3.5c show that the model predictions agree well with the experimental results when the strain is lower than 0.6 at elevated temperatures. It is interesting to note that model predictions diverge from experimental results for strains of approximate 0.6 and above, which, from Figure 3.2, roughly corresponds to the transition from cell wall buckling to cell wall densification. This observation suggests that cell wall polymers may be altered due to high compressive stress and strain at elevated temperatures. On the other hand, Figures 3.5a, 3.5d, and 3.5e show that the effect of moisture on the strain function is not as significant as that of temperature, even when for strains larger than 0.6. Nevertheless, with the good agreement between model predictions and test data for strains below 0.6, this model, with some modifications to the strain functions, can be applied to high strain levels at elevated temperatures.

3.5.2 Effects of Temperature and MC on Compression Modulus *E*

The compression modulus of wood strands at different temperatures and MCs are listed in Table 3.3. As expected, the *E* decreases with increasing temperature or MC. Shown in Figure 3.6 are the results for oven dry samples which eliminate the influence of moisture. Obviously, the strands become softer and easier to compress when the temperature increases from room temperature to 200°C. This phenomenon can be explained from a molecular perspective. When a material is heated, thermal expansion increases the

molecular separation and the molecules effectively become a softer spring. In addition, the increased temperature also permits small molecular movements in the structure, further decreasing the elastic modulus (Gibson and Ashby 1988).

Figure 3.7 shows that the softening behavior is reflected in the compressive modulus reduction as temperature increases for all MCs examined. The normalized *E* values were calculated using the value of *E* at T = 20°C and MC = 0% as the reference. Examining the results at all MC levels shows that the effects of T_g values of hemicellulose and lignin on wood softening are not as significant as expected. For example, at MC = 0%, both T_g values of hemicellulose and lignin are assumed equal to 200°C, which means that the modulus will decrease sharply near this temperature. However, the largest decrease in normalized *E* occurs from 20 to 50°C. In addition, the modulus appears to level off with increasing temperature from 140 to 200°C, indicating that changes in modulus at MC = 0% from 20 to 200°C is nonlinear. Based on this result, the nonlinear relationship between modulus and temperature is assumed applicable to other moisture levels. Therefore, T_g values of hemicellulose and lignin themselves cannot adequately explain the trend in modulus reduction as a function of temperature. This may be ascribed to the complexity of wood as a composite material of cellulose, hemicellulose and lignin.

Figure 3.8 shows that, at room temperature, the influence of moisture on the strand transverse compression is similar to that of temperature, i.e., increasing MC reduces the stress required to achieve a given strain. This can be attributed to water acting as a plasticizer for the cellulosic components – reducing the effectiveness of hydrogen

bonding in the amorphous portion of cellulose and hemicellulose (Salmén and Back 1980). Lignin is also softened by water resulting from the replacement of intermolecular hydrogen bonds within the lignin with weaker lignin-water linkages (Irvine 1985).

This plasticization effect on wood strands is also interpreted as the drop in modulus as shown in Figure 3.9, which shows a similar trend to that of temperature. It appears that the moisture usually has a greater influence on modulus at higher temperature than at lower temperature. In addition, within the range of the completed experimental conditions, the moisture has a less pronounced effect on the wood strands in terms of modulus reduction than the temperature. Moreover, due to the existence of partially crystalline cellulose, the modulus of wood decreases slowly, remaining within a factor of 10 of its modulus at MC = 0% and T = 20°C whereas the modulus of an amorphous polymer would fall by a factor of 1000 or more (Nielsen 1974; Irvine 1985).

To model the effect of temperature on the modulus of the cell wall material for amorphous polymers, Gibson and Ashby (1988) established a linear relationship given by Eq. (3.5) when the temperature is between 0 and $0.9T_g$:

$$E_w = E_w^0(1-\alpha_m \frac{T}{T_g}) \tag{3.5}$$

where E_w is the modulus of cell wall material, E_w^0 is the modulus at 0°C, α_m is a parameter accounting for temperature effect, T is temperature, T_g is the glass transition temperature of cell wall material. However, when the temperature rises through the glass transition range, the modulus E_w cannot be described any more by a simple equation as a

function of temperature T, not to mention the effect of MC as the case in this study. Accordingly, for lack of a theoretical model for the temperature-moisture-dependent modulus, a regression model was established to quantitatively describe this relationship by means of Number Cruncher Statistical System™ (NCSS) 2000 (Jerry L. Hintze & Number Cruncher Statistical Systems, Kaysville, Utah, USA) to produce the following:

$$E(T, MC) = -16.29581 \ln T - 1.507311 MC + 103.4776 \quad (3.6)$$

where E(T, MC) is the strand modulus at a given temperature and moisture level. Although this model is far from perfect, as can be seen in Figure 3.10, it does provide a reasonable quantitative description of the effects of temperature and moisture on the compression modulus of wood strands. This will be useful for further model development of VDP.

3.6 Summary and Conclusions

The transverse compression behavior of aspen strands was investigated at different combinations of temperature and MC. Based on modified Hooke's law, the compressive stress can be modeled as the product of elastic modulus of strand, strain and the nonlinear strain function, which was assumed to be only dependent on the geometric structure of the strand and independent of temperature and moisture. Contrary to the assumption, it is found that high temperatures and moisture levels influence the strain function likely due to some chemical reactions within wood polymers. However, the model predictions agree well with the experiment results when the strain is lower than 0.6 for the temperatures and MCs examined. Consequently, the modified Hooke's law can still be applied to

predict the entire compression behavior by modifying the strain function at elevated temperatures. Quantitative relationships between the modulus and temperatures and MCs have been established by a regression model in the present study.

Table 3.1: The glass transition temperatures of wood components and water and the best fit values of *k* and *q* used for the Kwei model (Kelley et al. 1987)

Components	*k*	*q*	T_g (°C)
Lignin	10	585	200
Hemicellulose	13	355	200
Water	-	-	-137

Table 3.2: Relative humidity and EMC values for selected saturated salt solutions

Saturated salt solution	Temperature (°C)	Nominal RH (%)	Expected EMC* (%)	Measured MC (%)
LiCl	20	12	2.9	3.9
$MgCl_2$	20	33	6.7	6.8
NaBr	20	59	10.9	12.6
NaCl	20	75	14.5	15.1

* EMC predicted by Simpson (1973)

Table 3.3: Compression modulus *E* (MPa) of wood strands at various combinations of temperatures and MCs (Standard deviation in parentheses).

Temperature	Nominal MC (%)					
(°C)	0	3	6	9	12	15
20	55.5 (8.9)	46.5 (6.6)	42.5 (8.5)	39.2 (6.8)	37.3 (2.9)	31.4 (4.8)
50	39.7 (2.1)	37.5 (3.4)	33.6 (4.9)	30.2 (4.1)	21.5 (4.6)	15.9 (2.6)
80	34.8 (6.7)	32.7 (4.4)	25.1 (4.1)	17.2 (3.1)	12.7 (1.9)	10.1 (1.3)
110	29.9 (4.4)	22.7 (3.3)	18.6 (3.8)	12.3 (1.4)	-	-
140	18.5 (2.1)	-	-	-	-	-
170	15.3 (1.2)	-	-	-	-	-
200	14.8 (1.1)	-	-	-	-	-

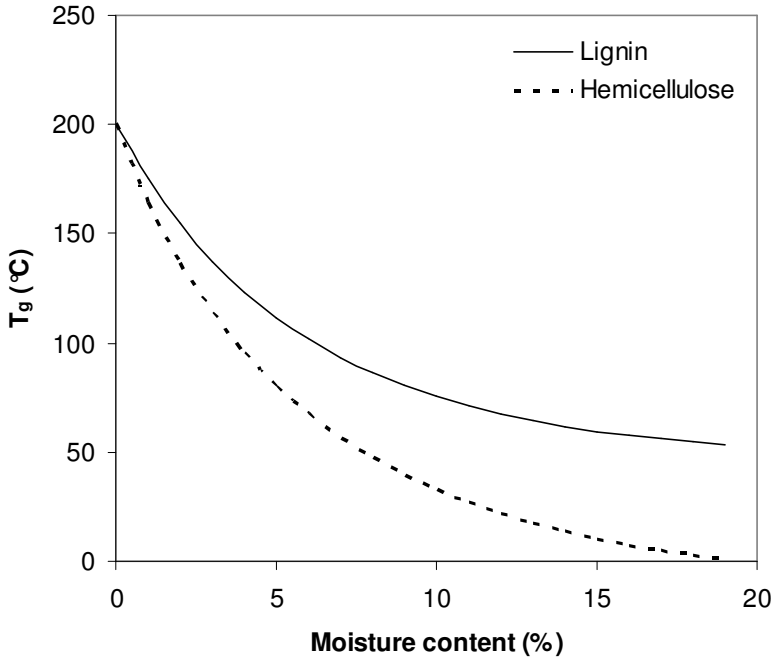

Figure 3.1 Predictive effects of moisture content on the glass transition temperature of lignin and hemicellulose from the Kwei model.

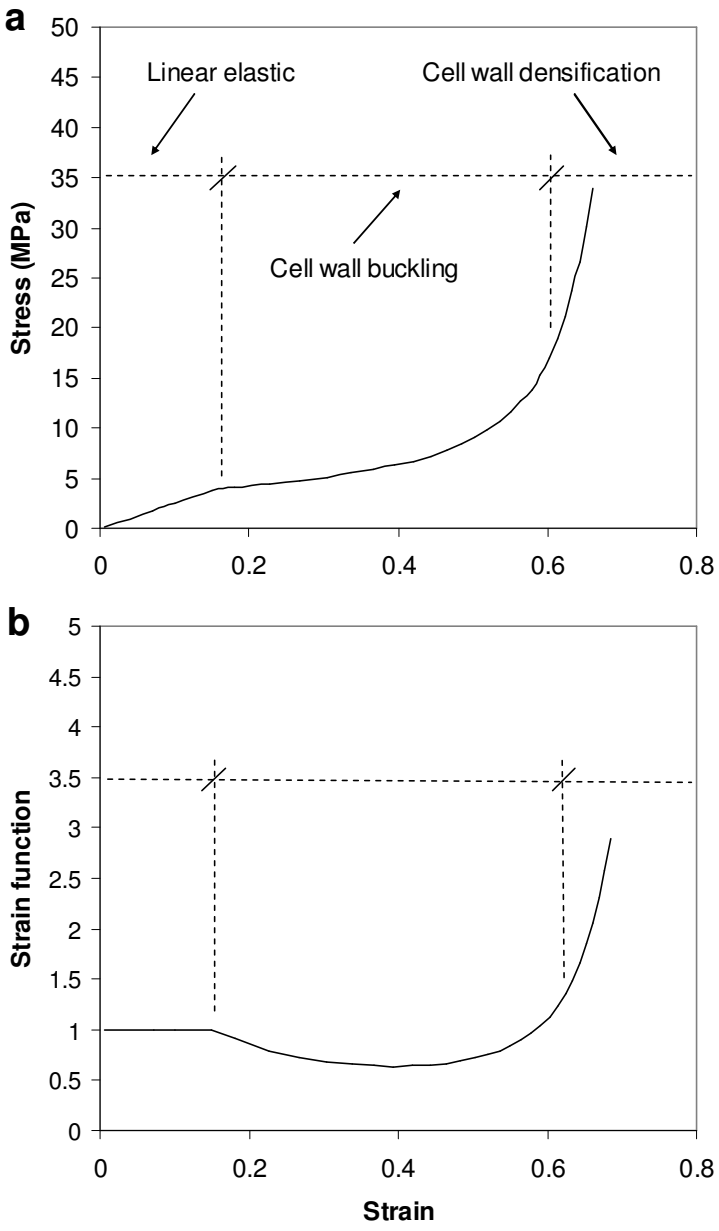

Figure 3.2 (a) An idealized stress-strain relationship of wood in transverse compression; (b) Strain function $\varphi(\varepsilon)$ corresponding to the stress-strain relationship in (a).

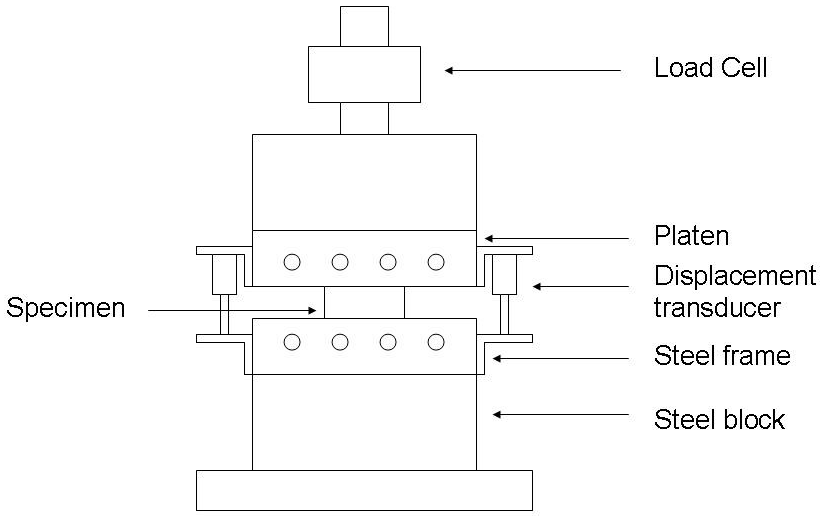

Figure 3.3 Schematic drawing of the test apparatus for strand compression.

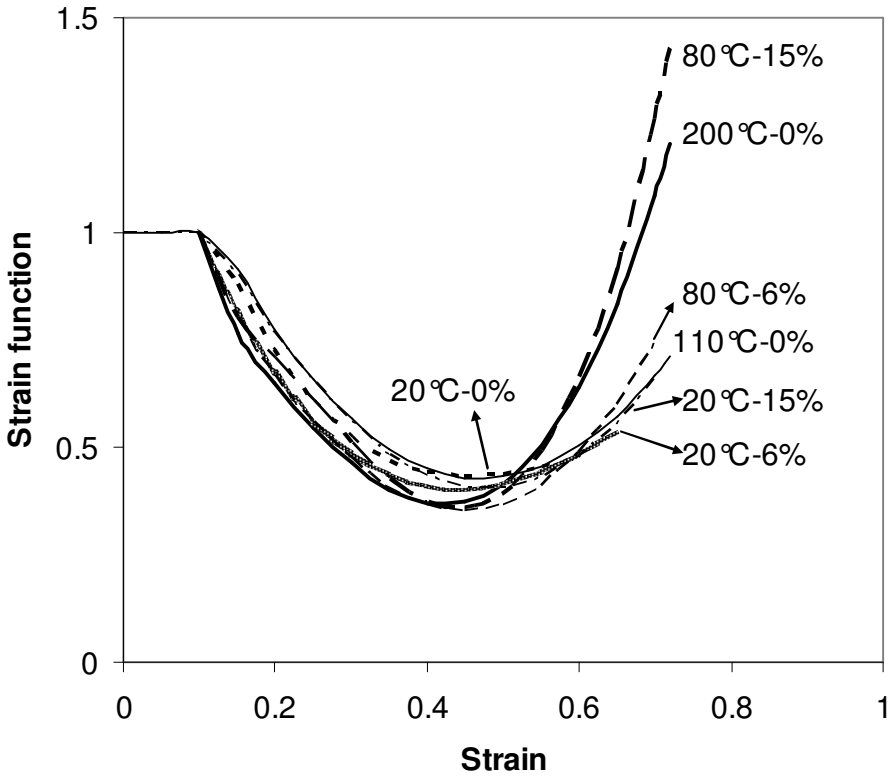

Figure 3.4 Strain function $\varphi(\varepsilon)$ at different temperatures and MCs.

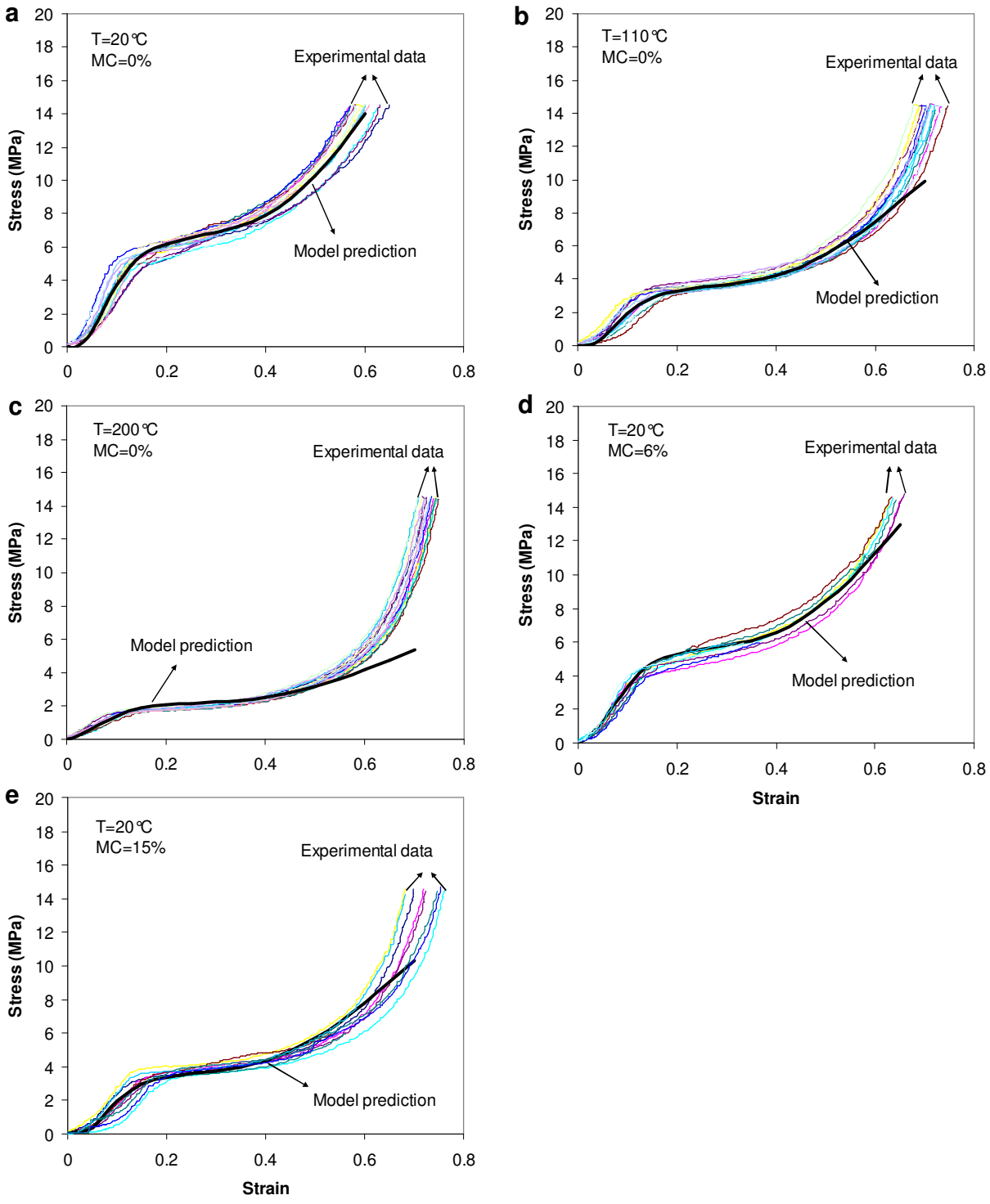

Figure 3.5 Typical comparisons between experimental results and model prediction of strand stress-strain relationship.

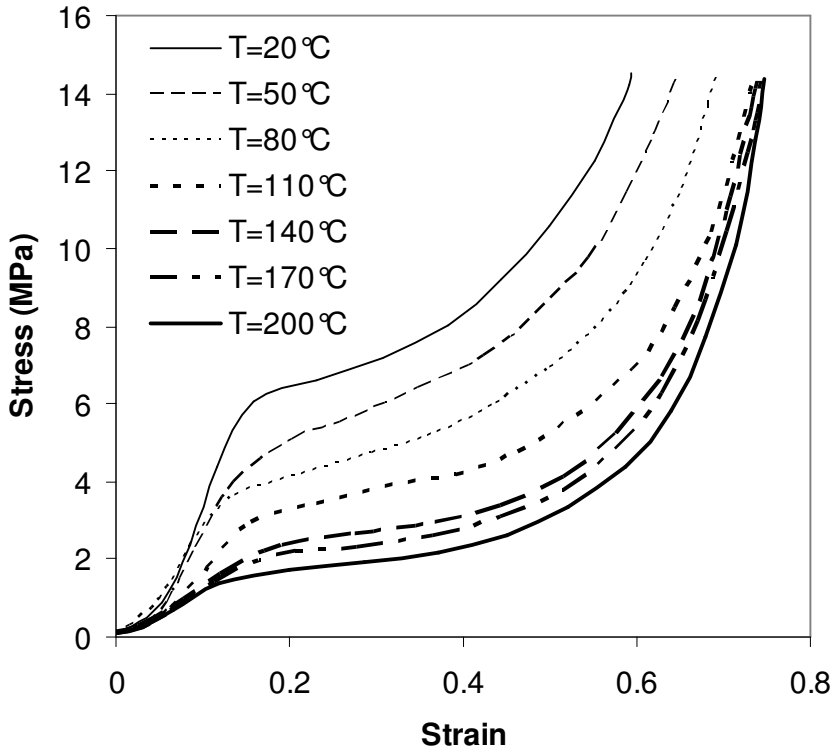

Figure 3.6 Compressive stress-strain relationship of wood strands at different temperatures (MC = 0%).

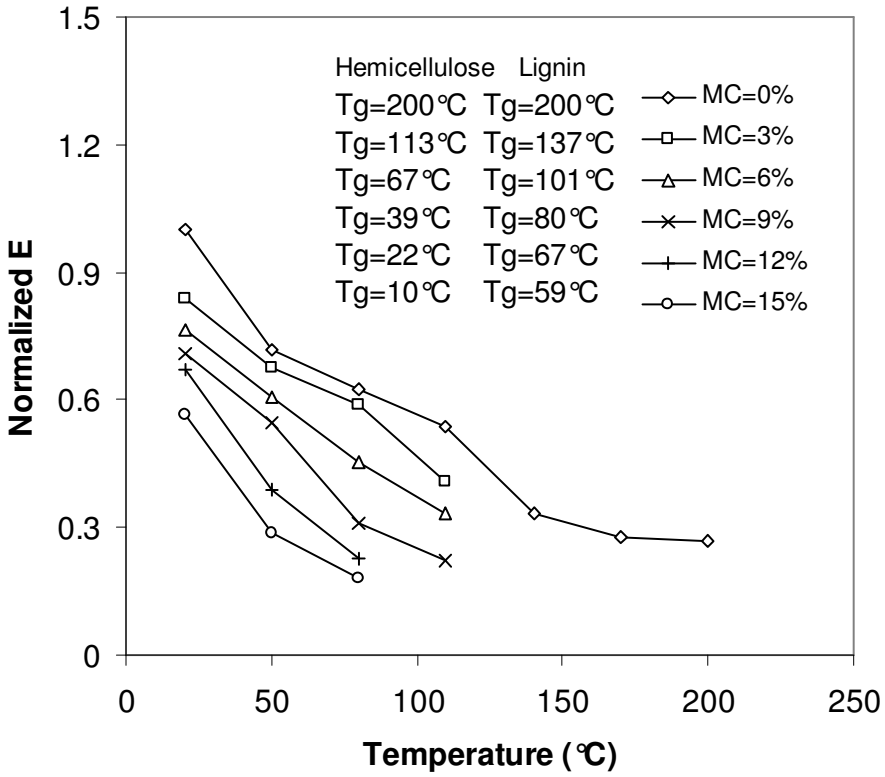

Figure 3.7 Effect of temperature on the normalized modulus *E* of wood strands (normalized using *E* at T = 20°C and MC = 0% as the reference point).

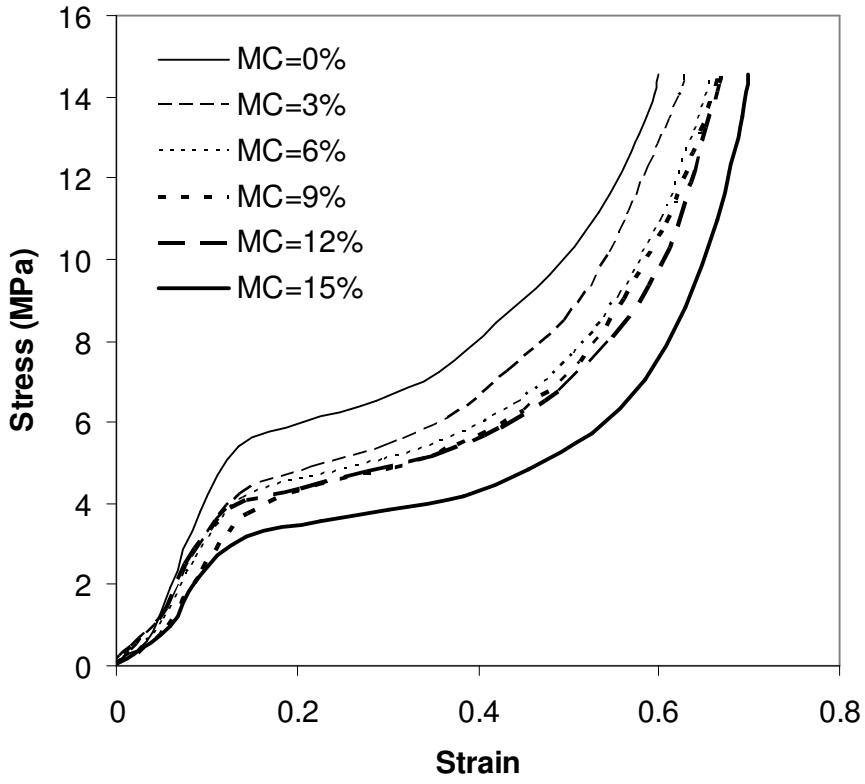

Figure 3.8 Compressive stress-strain relationship of wood strands at different MCs (T = 20°C).

.

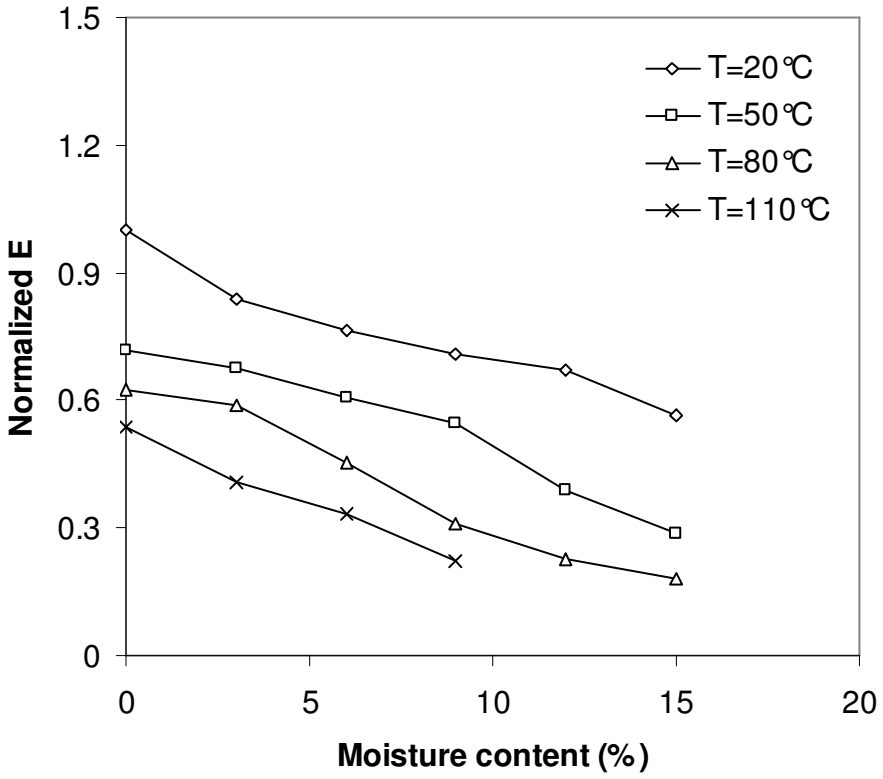

Figure 3.9 Effect of moisture content on the normalized modulus *E* of wood strands (normalized using *E* at T = 20°C and MC = 0% as the reference point).

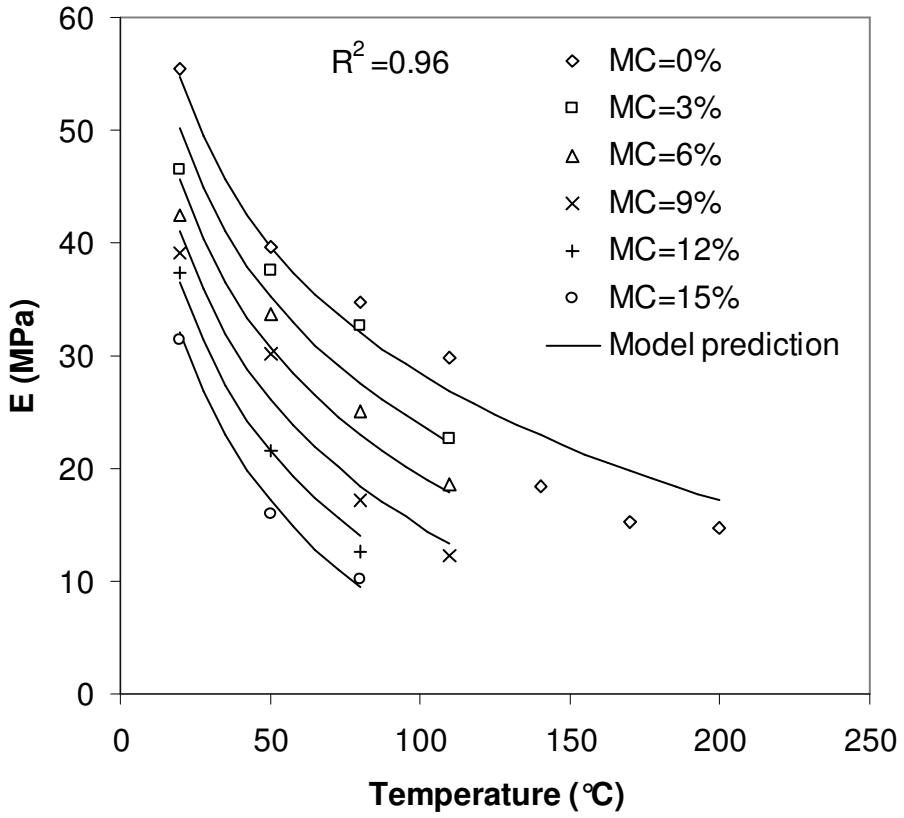

Figure 3.10 Comparison between experimental results and model prediction of *E* values.

3.7 Bibliography

Back, E.L., Salmén, N.L. (1982) Glass transition of wood components hold implications for molding and pulping processes. Tappi J. 65: 107-110.

Blechschmidt, J., Engert, P., Stephan, M. (1986) The glass transition of wood from the viewpoint of mechanical pulping. Wood Sci. Technol. 20: 263-272.

Bodig, J. (1965) The effect of anatomy on the initial stress-strain relationship in transverse compression. Forest Prod. J. 15: 197-202.

Chow, S.-Z., Pickles, K.J. (1971) Thermal softening and degradation of wood and bark. Wood Fiber. 3: 166-178.

Cousins, W.J. (1976) Elastic modulus of lignin as related to moisture content. Wood Sci. Technol. 10: 9-17.

Cousins, W.J. (1978) Young's modulus of hemicellulose as related to moisture content. Wood Sci. Technol. 12: 161-167.

Dai, C., Steiner, P.R. (1993) Compression behavior of randomly formed wood flake mats. Wood Fiber Sci. 25: 349-358.

Gerhards, C.C. (1982) Effect of moisture content and temperature on the mechanical properties of wood: An analysis of immediate effects. Wood Fiber Sci. 14: 4-36.

Gibson, L.J., Ashby, M.F. Cellular Solids: Structure and Properties. Pergamon Press, New York, USA, 1988.

Goring, D.A.I. (1963) Thermal softening of lignin, hemicellulose, and cellulose. Pulp Paper Mag. Can. 64: T517-527.

Greenspan, L. (1977) Humidity fixed points of binary saturated aqueous solutions. J. Res. Nat. Bur. Stand. 81A:89-96.

Irvine, G.M. (1984) The glass transitions of lignin and hemicellulose and their measurement by differential thermal analysis. Tappi J. 67: 118-121.

Irvine, G.M. (1985) The significance of the glass transition of lignin in the thermomechanical pulping. Wood Sci. Technol. 19: 139-149.

Kelley, S.S., Rials, T.G., Glasser, W.G. (1987) Relaxation behaviour of the amorphous components of wood. J. Mater. Sci. 22: 617-624.

Kennedy, R.W. (1968) Wood in transverse compression: Influence of some anatomical variables and density on behavior. Forest Prod. J. 18: 36-40.

Kunesh, R.H. (1961) The inelastic behavior of wood: A new concept for improved panel forming process. Forest Prod. J. 11: 395-406.

Kunesh, R.H. (1968) Strength and elastic properties of wood in transverse compression. Forest Prod. J. 18: 65-72.

Lang, E.M., Wolcott, M.P. (1996) A model for viscoelastic consolidation of wood-strand mats. Part II. Static stress-strain behavior of the mat. Wood Fiber Sci. 28: 369-379.

Lenth, C.A., Kamke, F.A. (1996) Investigations of flakeboard mat consolidation. Part II. Modeling mat consolidation using theories of cellular materials. Wood Fiber Sci. 28: 309-319.

Lenth, C.A., Kamke, F.A. (2001) Moisture dependent softening behavior of wood. Wood Fiber Sci. 33: 492-507.

LeVan, S.L. (1989) Thermal degradation. In: Concise Encyclopedia of Wood & Wood-Based Materials. Ed. Schniewind, A.P. Pergamon Press, Elmsford, New York. USA. pp.271-273.

Ncube, E., Irle, M., Mansfield-Williams, H. (2004) Behavior of particles compressed in the radial and tangential direction during hot-pressing. In proceedings of the 8th European Panel Products Symposium. Llandudno, UK. pp. T8-T19.

Nielsen, L.E. Mechanical properties of polymers and composites. Marcel Dekker Inc., New York, USA, 1974.

Östman, B.A.-L (1985) Wood tensile strength at temperatures and moisture contents simulating fire conditions. Wood Sci. Technol. 19: 103-116.

Palka, L.C. (1973) Predicting the effect of specific gravity, moisture content, temperature and strain rate on the elastic properties of softwoods. Wood Sci. Technol. 7:127-141.

Rusch, K.C. (1969) Load-compression behavior of flexible foams. J. Appl. Polym. Sci. 13:2297-2311.

Rusch, K.C. (1970) Load-compression behavior of brittle foams. J. Appl. Polym. Sci. 14:1263-1276.

Salmén, N.L., Back, E.L. (1980) Moisture-dependent thermal softening of paper, evaluated by its elastic modulus. Tappi J. 63: 117-120.

Salmén, N.L., Olsson, A.-M. (1998) Interaction between hemicelluloses, lignin and cellulose: Structure-property relations. J. Pulp Paper Sci. 24: 99-103.

Salmén, N.L., Kolseth, P., de Ruvo, A. (1985) Modeling the softening behaviour of wood fibers. J. Pulp Paper Sci. 11: J102-J107.

Simpson, W.T. (1973) Predicting equilibrium moisture content of wood by mathematical models. Wood Fiber 5: 41-49.

Tabarsa, T., Chui, Y.H. (1997). Effects of hot-pressing on properties of white spruce. Forest Prod. J. 47: 71-76.

Tabarsa, T., Chui, Y.H. (2000) Stress-strain response of wood under radial compression. Part I. Test method and influences of cellular properties. Wood Fiber Sci. 32: 144-152.

Wolcott, M.P. (1990) Modelling viscoelastic cellular materials for the pressing of wood composites. Ph.D. dissertation, Virginia Polytechnic Institute and State University, Blacksburg, VA.

Wolcott, M.P., Eugene, L.S., Jr. (2003) Temperature and moisture influence on compression-recovery behaviour of wood. Wood Fiber Sci. 35: 540-551.

Wolcott, M.P., Kamke, F.A., Dillard, D.A. (1990) Fundamentals of flakeboard manufacture: Viscoelastic behavior of the wood component. Wood Fiber Sci. 22: 345-361.

Wolcott, M.P., Kamke, F.A., Dillard, D.A. (1994) Fundamental aspects of wood deformation pertaining to manufacture of wood-based composites. Wood Fiber Sci. 26: 496-511.

Wolcott, M.P., Kasal, B., Kamke, F.A., Dillard, D. A. (1989) Testing small wood specimens in transverse compression. Wood Fiber Sci. 21: 320-329.

Yanchuk, A.D., Dancik, B.P., Micko, M.M. (1983) Intraclonal variation on wood density of trembling aspen in Alberta. Wood Fiber Sci. 15: 387-394.

Young, R.J., Lovell, P.A. Introduction to polymers. Chapman & Hall, New York, USA, 1991.

Youngs, R.L. (1957) Mechanical properties of red oak related to drying. Forest Prod. J. 9: 315-324.

CHAPTER 4 VISCOELASTICITY OF ASPEN WOOD STRANDS DURING HOT PRESSING[3]

4.1 Introduction

The viscoelasticity of wood is due to the large fraction of hemicellulose and lignin that surrounds the semi-crystalline cellulosic portion to produce classical viscoelastic behavior. The properties of wood are therefore time-dependent and they affect the performance of wood in service. For example, the structural members in a building system undergo creep under constant load, i.e., the deformation gradually increases with time (Bodig and Jayne 1982). Since the actual load levels of wood in use are within certain limits, wood can be adequately considered as a linear viscoelastic material from a practical point of view (Schniewind 1968; Schniewind and Barrett 1972). As a result, the theory of linear viscoelasticity (i.e., the use of spring-dashpot models to represent the actual material) has been applied by many researchers to characterize the creep behavior of timber (Schniewind 1968, 1982; Bodig and Jayne 1982; Bolton and Breese 1987; Holzer et al. 1989; Dinwoodie 2000). Another characteristic of viscoelastic materials is stress relaxation which refers to the continuous decrease in the magnitude of stress required to maintain a constant strain or displacement; little research has been done in this area due to its limited practical significance in wood engineering (Dinwoodie 2000). More recently, Penneru et al. (2005) conducted macro- and micro-level strain analyses to understand the mechanism of bulk forming of wood. In addition, they conducted stress

[3] A version of this chapter has been submitted for publication. Zhou, C., Dai, C., Smith, G.D. (2009) Viscoelasticity of aspen wood strands during hot pressing.

relaxation experiments on solid wood in transverse compression at high temperature and relative humidity (Penneru et al. 2006).

However, the resin content of wood composites is low and results in a discontinuous film of resin on the surface of the furnish particles and as a result the pressure required to achieve a high degree of contact and acceptable bonding between particles is relatively high – well above the linear elastic limit of the wood itself (Dai et al. 2007). This high pressure, together with the temperature and moisture content (MC) distributions inside the mat, results in a nonlinear compression behavior not only for composite mats but also for the wood elements (Dai and Steiner 1993; Dai 2001). In addition, the nonlinear viscoelastic behavior of these wood elements during hot pressing greatly influences the manufacturing variables as well as the final product properties such as internal bond strength and dimensional stability (Kelly 1977; Wolcott 1990; Geimer et al. 1998; Dai et al. 2000; van Houts et al. 2000; Wolcott and Shutler 2003).

In a typical pressing cycle, the press closes rapidly and compresses the mat to a target thickness and then maintains it to allow the resin to cure. During this stage, the thickness of the mat is held constant and the mat pressure gradually decreases due to the thermal softening and stress relaxation of the mat (Dai et al. 2000; van Houts et al. 2003; Yu et al. 2007). After that, the mat enters the decompression and venting stage, in which the press opens slowly and the mat pressure drops to zero. It should be noted that compared with stress relaxation, the creep behavior of the mat is not significant due to the short time period for which the mat remains in the press, typically in the order of 3 to 6 minutes,

depending on panel density and thickness (Bowyer et al. 2002). Furthermore, from a materials science perspective, the viscoelastic properties of wood composites will be determined by the viscoelasticity of their constituents and the structural organization of these elements (Dai 2001). Thus, the focus of this study was on the stress relaxation behavior of individual wood strands during hot pressing in order to obtain better understanding of the mechanism of composite mat consolidation. This investigation will also provide valuable information for further modeling of mat consolidation of wood composites during hot pressing.

4.2 Background

4.2.1 Stress Relaxation Behavior of Cellular Materials in Compression

Youngs (1957) and Kunesh (1961) were among the earliest researchers to investigate the nonlinear viscoelastic behavior of wood in transverse compression. They found that the stress relaxation and creep responses of wood were significantly affected by temperature, MC, and initial stress/strain levels. The experimental data for stress relaxation could be fitted by an expression of the following form:

$$\sigma = \sigma_0 (t+1)^b \tag{4.1}$$

where σ is the stress at time t, σ_0 is the initial stress, t is the relaxation time in minutes, b is the coefficient of relaxation, which is calculated as the slope of the straight line fitted to these relaxation data in a log-log plot. To some extent, b can be treated as the rate of relaxation response.

Meinecke and Clark (1973) experimentally investigated the viscoelastic responses of polymeric foams in compression. The relaxation modulus of a linear viscoelastic material could be described as follows:

$$E_r'(t) = \frac{\sigma(t)}{\varepsilon_0} \tag{4.2}$$

where $\sigma(t)$ is the stress at time t, ε_0 is the imposed initial strain, t is the time in seconds. It is noted that this modulus is strain-independent, but time-dependent. If the test data of relaxation modulus and time are expressed in a log-log plot, a straight or nearly straight line is obtained and it can be mathematically described by a power law, Eq. (4.3), of the following form:

$$E_r'(t) = Kt^{-\xi} \tag{4.3}$$

where K is the specific relaxation modulus given by the value of $E(t)$ at time t = 1 s, $-\xi$ is the slope of this straight line, which is indicative of the rate of stress relaxation.

For polymeric foams and other cellular materials such as wood, the nonlinearity of compression behavior was attributed to the geometric nonlinearities of cellular deformation (Rusch 1969, 1970; Gibson and Ashby 1988; Wolcott 1990; Dai and Steiner 1993; Lang and Wolcott 1996; Lenth and Kamke 1996). Rusch (1969) first proposed a modified Hooke's law to describe this nonlinear stress-strain relationship under compression (Eq. 4.4):

$$\sigma = E\varphi(\varepsilon)\varepsilon \tag{4.4}$$

where σ is the stress, E is the elastic modulus of foam, ε is the strain, and $\varphi(\varepsilon)$ is the nonlinear dimensionless strain function, which can describe the full range of cellular structure deformation in compression (i.e., cell wall bending, buckling, and densification). The significance of this method is to separate the responses of cell wall material from the cellular structure; in other words, E is only dependent on environmental conditions such as temperature and moisture while $\varphi(\varepsilon)$ is only strain-dependent.

Likewise, Meinecke and Clark (1973) defined the relaxation modulus of nonlinear viscoelastic material:

$$E_r(t) = \varphi(\varepsilon) E'_r(t) \tag{4.5}$$

where $E_r(t)$ is the relaxation modulus, $E_r'(t)$ is the linear response defined in Eq. (3) . Therefore, Eq. (4.5) can be rewritten as:

$$E_r(t) = \varphi(\varepsilon) K t^{-\xi} \tag{4.6}$$

where K is a constant which can be determined in the linear range. For most solid polymers, the relaxation rate ξ is only dependent on the cell-wall polymer and independent of strain level (Meinecke and Clark 1973) while for some polymeric foams, this rate is not only dependent on matrix material but also dependent on strain level (Meinecke and Clark 1973). This seems controversial for wood as some research has shown it to be strain-independent (Rosa and Fortes 1988; Wolcott 1990) whereas other researchers found it to be strain-dependent (Youngs 1957; Kunesh 1961; Dai 2001).

4.2.2 Extension of Boltzmann Superposition Principle

In the theory of linear viscoelasticity, the Boltzmann superposition principle describes the response of a material to different strain or stress histories. It states that the response of a material to a given deformation or load is independent of the response to any deformation or load already applied on the material (Nielsen 1974; Ferry 1980). It implies that the response of a material to successive deformation or loads could be obtained. For a material with a continuous varying strain history, the stress at time *t* can be given in the following integral form (Meinecke and Clark 1973):

$$\sigma(t) = E_r(t)\varepsilon_0 + \int_0^t E_r(t-t')\frac{d\varepsilon(t')}{dt'}dt' \tag{4.7}$$

where ε_0 is the initial applied strain, t' is the past time, and t is the current time. If the relaxation rate ξ is not too large, Meinecke and Clark (1973) pointed out that the Boltzmann integral (Eq. 4.7) can be empirically extended to a nonlinear material in a simplified form with sufficient accuracy as follows:

$$\sigma(t) = \varphi(\varepsilon)\int_0^t E_r(t-t')\frac{d\varepsilon(t')}{dt'}dt' \tag{4.8}$$

where $\varphi(\varepsilon)$ is the strain function. However, the validity of this simplification method has only been confirmed for the sample subjected to a constant strain rate (Meinecke and Clark 1973).

Following the same concept, Wolcott (1990) investigated the viscoelastic responses of wood in compression under various environmental conditions. With a time-temperature-moisture superposition method using temperature and moisture shift factors, master

curves for stress relaxation and creep under the linear behavior regime were obtained that covered a large range of times. Then by taking into account the cellular deformation, the nonlinear stress relaxation and creep behavior at a given condition could be predicted. It is noted that these linear viscoelastic properties were investigated based on the wood samples in tension perpendicular to the grain direction. This implied that the wood samples in tension would behave with the same viscoelastic properties as those in compression in the linear range provided that they are in the same grain orientation. More recently, Dai (2001) investigated the viscoelastic behavior of wood flakes in transverse compression at ambient condition. Based on the stress relaxation responses of flakes and random mat structure, a model for predicting the viscoelastic consolidation of wood composite mats was developed and compared with experimental data.

The present work aims at providing some input parameters for the further VDP formation model of strand-based wood composites, which is based on the wood strand properties and mat structure. In addition, from the point of view of practical operation, it is not necessary to investigate the stress relaxation of wood strands for long time scales as it lasts for only a few minutes during panel pressing. As such, the approach applied here is similar to the one used by Dai (2001).

The overall objective of this study is to quantitatively investigate how the environmental conditions and initial strain levels affect the stress relaxation of aspen (*Populus tremuloides*) strands, a common low-density (specific gravity 0.38) raw material for oriented strand board (OSB) manufacturing in Canada. The specific objectives are:

1) to experimentally study the stress relaxation of wood strands in transverse compression for various combinations of initial strain level, temperature and MC;

2) to model the stress relaxation rate as a function of strain level, temperature and MC and the modulus K as a function of temperature and MC; and

3) to predict the stress relaxation behavior of wood strands in transverse compression and compare predictions with experimental results.

4.3 A Model for Predicting Stress Relaxation of Wood Strands in Compression

In an idealized stress relaxation test, the target strain would be imposed on the material instantaneously. As the application of a strain involves the movement of a mechanical device, e.g., load-frame crosshead or press platen, the time required to reach the imposed strain cannot be infinitely small. When manufacturing composite panels, the strain rate is carefully controlled during the press cycle in order to achieve the desired VDP and the required panel properties. Therefore, to model the stress relaxation of wood samples in compression, the loading history must first be defined.

To model the press closing operation, a linear loading strain history is assumed. For a stacked strand column with i overlaps made up of strands of initial thickness τ, the initial column thickness is $i\tau$. The target column thickness after deformation is H then the resultant strain ε_i is given by:

$$\varepsilon_i = \frac{i\tau - H}{i\tau} \tag{4.9}$$

where τ and H are in mm. If the crosshead moves at a constant rate v, the time required for the column to reach the target thickness, t_i, is determined by:

$$t_i = \frac{i\tau - H}{v} \tag{4.10}$$

where t_i has units of seconds, and v is the velocity in mm s^{-1}. Then the strain history for this strand column is then defined as follows:

$$\varepsilon_i(t) = \begin{cases} \dfrac{t}{t_i}\varepsilon_i & (0 \le t < t_i) \\ \varepsilon_i & (t \ge t_i) \end{cases} \tag{4.11}$$

This strain history is described in Figure 4.1. Then the corresponding strain rate for the strand column can be obtained by taking derivative of Eq. (4.11) and substituting ε_i and t_i with Eqs. (4.9) and (4.10), respectively:

$$\frac{d\varepsilon_i(t)}{dt} = \begin{cases} \dfrac{v}{i\tau} & (0 \le t < t_i) \\ 0 & (t \ge t_i) \end{cases} \tag{4.12}$$

Then Eq. (4.8) together with Eqs. (4.6) and (4.12) yield:

$$\sigma_i(t) = \varphi(\varepsilon_i)\int_0^t K(t - t')^{-\xi_i} \frac{v}{i\tau} dt' \tag{4.13}$$

where $\sigma_i(t)$ is the stress for i-strand column at time t, and ξ_i is the relaxation rate for the strand column. For time $t < t_i$, Eq. (4.13) can be rewritten as:

$$\sigma_i(t) = \frac{\varphi(\varepsilon_i)Kv}{i\tau(1-\xi_i)} t^{1-\xi_i} \tag{4.14}$$

For time $t \ge t_i$, Eq. (4.13) can be expressed as:

$$\sigma_i(t) = \frac{\varphi(\varepsilon_i)Kv}{i\tau(1-\xi_i)} [t^{1-\xi_i} - (t-t_i)^{1-\xi_i}] \tag{4.15}$$

It is noted that the specific relaxation modulus K is a function of temperature and MC while the relaxation rate ξ_i is dependent on strain, temperature and MC of the material, both of which need to be determined experimentally. Consequently, Eqs. (4.14) and (4.15) can be written as the following expression:

$$\sigma_i(t) = \frac{\varphi(\varepsilon_i)K(T,MC)v}{i\tau[1-\xi_i(\varepsilon_i,T,MC)]}t^{1-\xi_i(\varepsilon_i,T,MC)} \qquad (t < t_i) \qquad (4.16)$$

$$\sigma_i(t) = \frac{\varphi(\varepsilon_i)K(T,MC)v}{i\tau[1-\xi_i(\varepsilon_i,T,MC)]}[t^{1-\xi_i(\varepsilon_i,T,MC)} - (t-t_i)^{1-\xi_i(\varepsilon_i,T,MC)}] \qquad (t \geq t_i) \qquad (4.17)$$

Thus, a model for predicting the stress relaxation response of columns of strands in compression is established. Furthermore, the global mat stress relaxation behavior can be predicted based on the viscoelastic properties of local strand columns and initial mat structure (Dai 2001).

4.4 Experimental

The experiment described below investigated the effects of strain level, temperature and MC on the stress relaxation of strands under transverse compression and compared the test data with model prediction.

4.4.1 Materials

Thin sheets of sliced aspen veneer with nominal thickness 0.75 mm were cut into 25 mm by 25 mm samples. Aspen is a diffuse-porous hardwood and its density is relatively uniform throughout the stem cross section, as mentioned above (Yanchuk et al. 1983).

Nevertheless, to minimize the effect of density variations between individual specimens, strands were selected randomly for the test. These strands were of the same batch previously used in the study of hydro-thermal compression behavior of aspen strands in the perpendicular-to-grain direction (Chapter III).

To reach the different moisture levels, the samples were conditioned in a glass desiccator over a selected saturated salt solution at 20°C until equilibrium was reached (Greenspan, 1977). According to Simpson's model (1973), the equilibrium moisture content (EMC) of these specimens can be predicted at a given relative humidity and temperature. The measured strand MCs at 20°C are compared with model prediction in Table 4.1. A more detailed description of specimen preparation was presented in Chapter III. Six moisture levels (0%, 3%, 6%, 9%, 12%, and 15%) were used in this test. To investigate the stress relaxation behavior of strands during hot pressing, seven temperatures (20°C, 50°C, 80°C, 110°C, 140°C, 170°C, and 200°C) were used for each moisture level. These temperatures and MCs were selected to simulate the conditions that strands are exposed to during panel manufacture.

4.4.2 Methods

The stress relaxation tests for wood strands were conducted on a miniature hot press, which was set up on a universal servo-hydraulic MTS machine equipped with a 222.5 kN load cell. To simulate the strands under compression inside a mat during panel manufacture, a number of strands were stacked together as a sample for testing.

Preliminary experiments showed that it was very difficult to obtain a uniform temperature distribution within the strand stack within a few seconds for more than two strands. As such, all tests were done by stacking two strands together as one sample, where the grain orientation of one strand was perpendicular to that of the other one. Note that the stacked strands cannot be rigorously treated as a continuum as there is no bonding between strands. As a result, stacking two strands together could create a slightly different behavior from one solid sample due to the interface effect.

All the specimens were stored over the saturated salt solutions and then transported to the load frame in sealed plastic bags where they remained until just prior to testing. To maintain MC and temperature during hot pressing, the samples were wrapped in two layers of aluminum foil. The thickness of this foil (0.0017 mm) was much smaller than the strands. At temperatures far below the melting point (660°C), viscoelastic effects in metals are usually much smaller than those in polymers (Lakes 1999). Therefore, it was assumed that the foil had no effect on the stress relaxation behavior of wood strands. It should be noted that the samples were loosely wrapped with foil and it did not significantly affect the deformation pattern of the samples. The foil used here minimized the moisture loss of samples during hot pressing and did not constrain the samples during pressing. Prior to compression, two thermocouples were placed on each surface of the press to monitor temperature. Once the temperature had stabilized, the thermocouples were removed, then the specimen was positioned in the center of the platen, and the test began.

The stress relaxation tests were conducted by imposing a step strain on the samples and then maintaining this strain for 1 min. This step strain is defined as the crosshead displacement divided by the initial thickness of a specimen. Then the load and the crosshead displacement were recorded as a function of time. As shown in Figure 4.2a, six strain levels (0.1, 0.2, 0.3, 0.4, 0.6, and 0.7) were selected to represent different regions of compression curve to cover the range of different deformation mechanisms (linear elastic stage, cell wall buckling, and cell wall densification). These selected strain levels also represented the strains that individual strands may undergo during the panel manufacturing process. Five replicates were made for each combination of strain level, MC and temperature.

It should be noted that strain rate, which affects the viscoelastic properties of wood strands, was not taken into account in the present work. Strain rate as shown in Eq. (4.12) is dependent on the crosshead speed and the sample thickness. In the panel manufacturing process, usually only one loading speed is used although it may vary according to the desired panel properties. However, at a constant loading speed, for local strand columns within the mat, the corresponding strain rates are different due to the number of strands in those columns. As the strand column thickness in the mat varies significantly depending on the location, it is too complicated to cover the full range of strain rate for all strand columns, not mention that three factors with several levels have already been considered in the test. In addition, loading speed has a direct effect on the heat and mass transfer which indeed determines the mat consolidation behavior and thus the panel properties. Since temperature, MC and initial strain level are more important and relatively easy to

control during testing, these factors were chosen for this study. The effect of strain rate on stress relaxation of wood could be investigated in future.

The mass of each strand pair was measured just before testing and after testing. The specimen was then oven-dried and reweighed to determine moisture loss during pressing. Results from samples with a moisture loss more than 1% were discarded. As such, not all the results obtained from the test groups were used for data analysis. Hence, this was not a full factorial experimental design as initially expected.

4.5 Results and Discussion

The stress relaxation data at different strain levels were obtained from the corresponding load/time results, in which the nominal stress is defined as the load divided by the initial specimen area. It was assumed that the stress was uniformly distributed in the cross-sectional area which remained constant during deformation. This definition is accurate for small deformations but less accurate for large deformations and cross-sectional area changes. However, preliminary compression tests on two strands showed that the expansion of the sample size after the test varied from 1 to 3% at the strain level of 0.7, which meant that the sample area did not change significantly. As such, to simplify the test and computational procedures, it was decided that the nominal stress should be used for all test groups.

Figure 4.2b shows that, at a given environmental condition, e.g., T = 20°C, MC = 9%, the initial stress required to reach the target strain increases with increasing strain level. All the stress relaxation curves are similar in shape and are arranged in ascending order of strain level from bottom to top. In addition, the stress at all strain levels decreases monotonically with time. It was noted that most of the stress reduction occurred within 20 seconds and after which the stress leveled off.

4.5.1 Effects of Strain Level on Stress Relaxation

The logarithm of stress relaxation modulus *E(t)*, defined as the stress at a particular time divided by the strain level, at different strain levels is plotted as a function of log time in Figure 4.2c and shows a nearly linear relationship. This double logarithmic linear relationship agrees well with earlier studies conducted by others (Youngs 1957; Kunesh 1961; Meinecke and Clark 1973; Rosa and Fortes 1988; Wolcott 1990; Dai 2001).

Figure 4.2c shows that the relaxation modulus *E(t)* at a given time decreases with increasing strain levels before the strain enters the densification region. After that, *E(t)* increases as the strain level increases. Although the modulus at the selected highest strain of 0.7 (Figure 4.2a, point F) is smaller than that corresponding to the linear region 0.1 (Figure 4.2a, point A) in this test, it could be predicted that, at some higher strain level, its relaxation modulus would be greater than that in the linear range (Dai 2001). In addition, the strain corresponding to the minimum relaxation modulus appears to be close to the beginning of the densification stage, which is consistent with that reported by

Wolcott (1990). It is interesting to find that the tendency of relaxation modulus related to strain levels follows a similar nonlinear manner to the strain function derived from the strand compression test (Zhou et al. 2009).

The slope of each line, which is the stress relaxation rate, was obtained from a linear least squares fit to the test data. Figure 4.2d shows that these relaxation rates vary with the strain levels. This finding is consistent with the results reported by Youngs (1957), Kunesh (1961), and Dai (2001). Similar results were found with some solid polymers such as cellulose monofilament (Nielsen 1974), but differs from the findings of Rosa and Fortes (1988) and Wolcott (1990), where the slopes were found to be independent of the strain levels.

As shown in Figure 4.2d, the stress relaxes relatively slowly when the strain level is in the linear elastic range. When the strain increases to the yield point, which is nearly at the beginning of the stress plateau region, the stress relaxes much more rapidly. After that, the stress relaxation rate seems to increase slightly with strain as long as the strain is within the stress plateau region. However, this relaxation rate tends to decrease significantly with increasing strain level when the strain enters the densification region.

The dependence of the stress relaxation rate on strain level may be associated with the free volume change (Ferry 1980) and the behavior of chemical bonds in the wood cell wall (Kauman 1966; Kwei, 1984; Kelley et al. 1987; Bolton and Breese 1987). The free volume can be defined as the space in a solid or a liquid which is not actually occupied

by the molecules themselves. The higher the free volume, the more room the molecules will have in which to move around (Young and Lovell 1991). According to the concept proposed by Ferry (1980) that the mobility of the molecules at any temperature depends primarily on the free volume remaining, the rate of relaxation can be expressed in terms of free volume as the independent variable. As such, the higher the free volume, the greater the stress relaxation rate will become.

In the case of wood, free volume exists in the wood cell wall (Dai 2001). The formation of additional free volume and the breakage of chemical bonds breakage are dependent on the imposed stress in both mode and magnitude. The tensile and shear stresses due to bending tend to promote formation of free volume, whereas the compressive stress may decrease free volume (Ferry 1980; Dai 2001). Buckling is a fracture mechanism that occurs when a system exhibits instability, which could also lead to the formation of free volume. As shown in Figure 4.2a, when the wood specimen is under transverse compression, the cell wall subsequently undergoes three different stages: bending, buckling, and densification (Gibson and Ashby 1988). Therefore, it is perhaps for this reason that the stress relaxation rate increases with strain during cell wall bending and buckling and decreases during cell wall densification (Dai 2001).

4.5.2 Effects of Temperature on Stress Relaxation

Figure 4.3 presents the stress relaxation curves over the temperature range from 20 to 200°C at MC = 0% with an initial strain of 0.2. Stress levels decrease noticeably with

increasing temperature. For example, the initial stress needed to reach the target strain reduced from 4.9 to 1.8 MPa when the temperature increased from 20 to 200°C. This thermal softening effect can be explained from a molecular perspective. When a material is heated, thermal expansion increases the molecular separation and the elevated temperature permits small molecular movements in the structure, thus softening the material and making it easier to compress (Gibson and Ashby 1988).

The effects of temperature on the stress relaxation rate at various moisture levels are shown in Figure 4.4. For the same moisture level, the stress relaxation of the specimen occurs faster as the temperature increases. This is because a rise in temperature will increase the thermal energy for molecular motion, which increases the free volume, thus enabling the polymer to relax more rapidly.

Moreover, it appears that the temperature has a greater effect on the relaxation rate at high MCs than at low MCs. For example, at MC = 0%, when temperature increases from 20 to 80°C, the relaxation rate at all strain levels approximately varies in a range from 0.04 to 0.06 in Figure 4.4a. Whereas, at MC = 15% in Figure 4.4f, in the same temperature range, the corresponding relaxation rate varies from 0.06 to 0.15, which is much broader than that of oven dry samples. This can be interpreted that moisture has an effect on free volume as temperature is raised, thus an increase in moisture leads to more free volume formation and higher relaxation rates of wood strands.

In addition, the stress relaxation rates at high strain levels converge, indicating that the environmental conditions have less significant effects on the relaxation rate in the densification stage. This can be interpreted that the viscoelasticity of wood may be partially lost when the cell walls buckle and create permanent deformation in that stage (Penneru et al. 2006). This provides a partial explanation, although the mechanism for this phenomenon is not clearly understood.

4.5.3 Effects of MC on Stress Relaxation

Stress relaxation curves for the specimens in the MC range from 0 to 15% at T = 20°C with an initial strain of 0.2 are presented in Figure 4.5. Close inspection of the initial stress for each MC shows a similar effect to temperature in that the stress required to produce a given strain decreases with increasing MC. For example, the initial stress decreased from 4.9 to 3.0 MPa as the MC increased from 0 to 15%. This softening effect can be attributed to water acting as a plasticizer and reducing the effectiveness of secondary bonds in the amorphous portion of cellulose, hemicellulose, and lignin (Salmén and Back 1980; Irvine 1985).

Note that the amount of stress reduction when MC increases from 0 to 15% is less than that for temperature increasing from 20 to 200°C. It shows that moisture has a less significant effect on stress relaxation than temperature at a given strain level. It also shows that the stress tends to level off after the initial rapid drop for all relaxation curves.

Figure 4.6 shows the effects of MC on the stress relaxation rate of wood specimens in compression at different temperatures. Again, similar to the effect of temperature, the rate of relaxation generally increases with increasing moisture levels at a given temperature. This can be also explained in terms of free volume. When a diluent of low molecular weight (e.g., water) is added to an undiluted polymer, additional free volume is introduced by the diluent molecules (Ferry 1980). As a result, the magnitude of relaxation rate highly depends on the amount of water added into the polymer; the higher the MC in the wood, the higher the relaxation rate.

The moisture level also has a more pronounced effect on the relaxation rate at high temperatures than at low temperatures. For example, when MC increases from 0 to 9%, the relaxation rate varies approximately from 0.03 to 0.07 at T = 20°C in Figure 4.6a whereas it varies from 0.06 to 0.16 at T = 110°C in Figure 4.6d. Interestingly, it seems that the moisture level does not influence the relaxation rate significantly when MC increases from 6 to 12% at T = 20°C (Figure 4.6a) and from 6 to 9% at 50°C (Figure 4.6b). It may imply that there are no significant interactive effects of low temperature and moderate moisture levels on stress relaxation.

4.5.4 Model Validation

There are very complicated interactions between time, temperature, moisture, loading mode and level, and material properties in determining the stress relaxation behavior of polymers. These complexities make it very difficult to develop a truly predictive

quantitative model for the viscoelastic response of polymer under various test conditions. Therefore, the best that can be done at this time is to apply an empirical approach to quantitatively describe how environmental conditions influence the relaxation rate ξ_i and the specific modulus K. Forx example, in the log-log plot as shown in Fig. 4.2(c), ξ_i is the slope of the straight line while log$K$ is the intercept on the vertical axis. In the linear range, there is one particular value of log$K$ corresponding to a given temperature and MC. Based on the experimental data analysis with Number Cruncher Statistical System™ (NCSS) 2000 (Jerry L. Hintze & Number Cruncher Statistical Systems, Kaysville, Utah, USA), the regression models for ξ_i and log$K$ are expressed in Eqs. (4.18) and (4.19), respectively:

$$\xi_i(\varepsilon, T, MC) = -1.65357\times10^{-3} + 5.734314\times10^{-4}T + 3.561552\times10^{-3}MC + 0.213291\varepsilon - 0.3063129\varepsilon^2 \quad (4.18)$$

where $\xi_i(\varepsilon$, T, MC) is the relaxation rate at a given temperature and moisture level with an initial applied strain ε; and

$$\log K(T, MC) = 1.344561 - 2.406084\times10^{-3}T - 6.826339\times10^{-3}MC - 6.064806\times10^{-4}MC^2 \quad (4.19)$$

where K(T, MC) is the specific relaxation modulus at a given temperature and moisture level within linear range. Consequently, K as a function of temperature and MC can be estimated from Eq.(4.19). Although these models are far from perfect, as can be seen in Figures 4.7 and 4.8, they do provide reasonable quantitative descriptions of the effects of temperature and MC on ξ_i and K.

The measured stresses as a function of time under typical test conditions are compared with the predictions from Eqs. (4.17-19) in Figure 4.9. The model follows a similar trend to the experimental observations although the discrepancies between model predictions

and test data appear to become larger as strain level increases. Note that both stress relaxation rate ξ_i and specific relaxation modulus K were estimated from the limited experimental data in this work. The heterogeneity of wood specimens, the surface roughness of the specimens, the loading conditions, and the variation of environmental conditions during testing make it very difficult to obtain accurate input parameters. In addition, the strain function used here was based on experimental data from the previous study (Chapter III), in which there may be additional inaccuracies. All these factors are believed to contribute to the discrepancies between model predictions and test data.

Figure 4.10 describes the predictive effects of loading rate on the stress relaxation behavior of wood strands. At the same environmental conditions (T = 20°C, MC = 9%), a faster loading rate $2v$ results in higher maximum stress to reach the same target strain. When MC increases to 15% for the same strain level, a faster loading rate $2v$ still results in higher stress. But this maximum stress is lower than the one at MC = 9% with the same loading rate $2v$ due to the softening effect of MC on wood. Conversely, at 110°C, a loading rate $2v$ results in a maximum stress which is even lower than the one at T = 20°C for loading rate v. The result is that the strands exhibit more stress relaxation at elevated temperature or MC and could be attributed to the reduced modulus K and the higher relaxation rate ξ due to the softening effect on wood.

The complexities of the wood structure and associated test conditions make it difficult to obtain models that predict its behavior with great accuracy. This model provides predictions that are in reasonable agreement with the experimental results. But more

importantly, it qualitatively reveals the way in which the stress relaxation behavior of wood in transverse compression depends on environmental and loading conditions, giving some insight into the link between the viscoelastic behavior of wood strands and that of strand-based wood composites.

4.6 Summary and Conclusions

The stress relaxation behavior of wood strands in transverse compression was investigated at different combinations of strain level, temperature, and MC. The experimental results were consistent with the previous studies in that the log-log relationship between stress and time was linear (Meinecke and Clark 1973; Rosa and Fortes 1988; Wolcott 1990; Dai 2001). It was found that the relaxation rate varies with strain levels and the environmental conditions, which was quantitatively described by a regression model. A model was developed to predict the stress relaxation of wood strands during compression. Model predictions agreed reasonably well with the experimental data although there were some discrepancies. It is significant that this model can describe the time-dependent stress behavior in terms of material properties such as strand specific relaxation modulus, stress relaxation rate, strand thickness, and the loading rate. By combining this model with the mat structure, it can be further developed to predict the viscoelastic behavior of strand-based wood composites during hot pressing.

Table 4.1: Relative humidity and EMC values for selected saturated salt solutions

Saturated salt solution	Temperature (°C)	Nominal RH (%)	Expected EMC* (%)	Measured MC (%)
LiCl	20	12	2.9	3.6
$MgCl_2$	20	33	6.7	6.4
NaBr	20	59	10.9	11.5
NaCl	20	75	14.5	15.3

* EMC predicted by Simpson (1973)

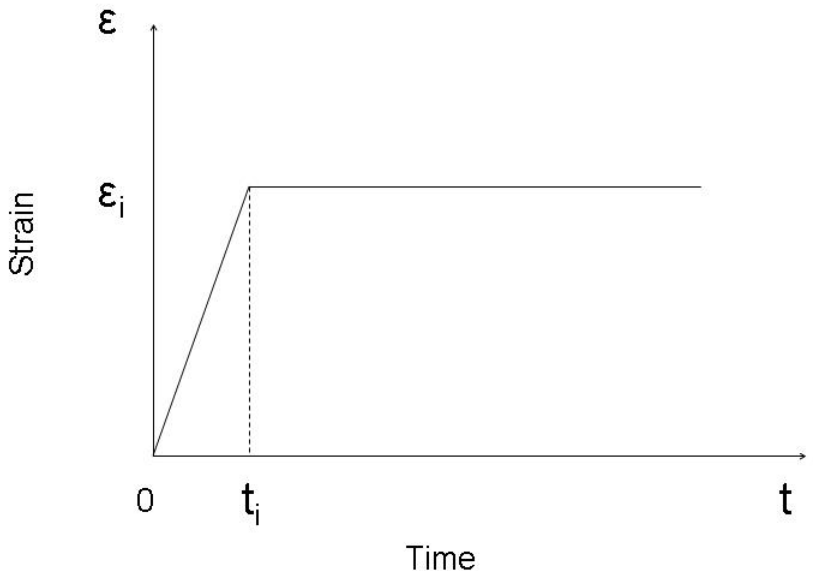

Figure 4.1 A linear loading strain history for strand columns in compression. t_i is the time needed for the i-strand column to reach the target strain ε_i.

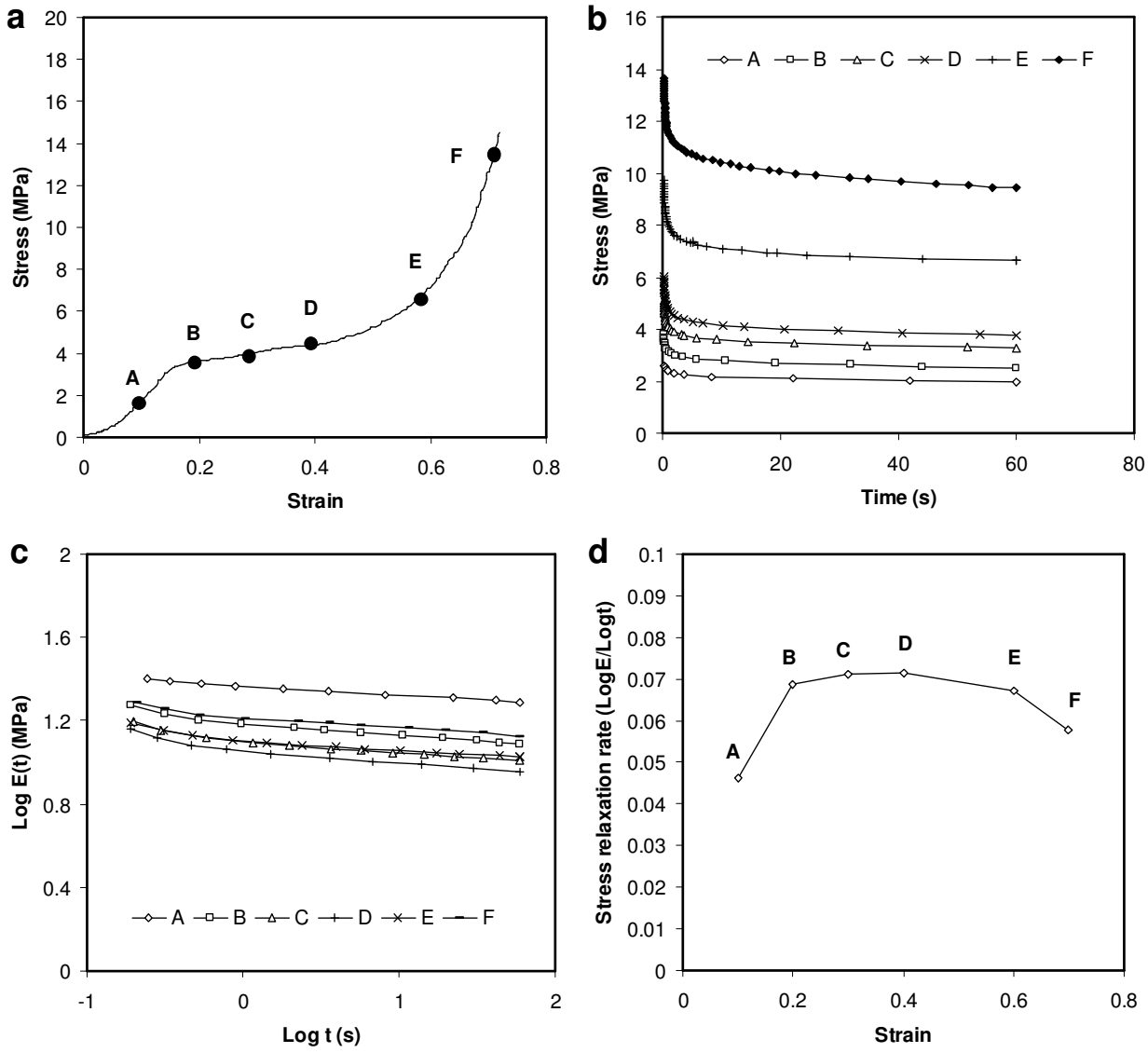

Figure 4.2 (a) The selected strain levels for strand stress relaxation tests as indicated in a typical stress-strain curve. (b) The stress relaxation vs. time at selected strain levels in (a). (c) Double logarithm plots of stress relaxation modulus vs. time corresponding to (b). (d) The stress relaxation rate at selected strain levels obtained from (c). Test condition: T = 20°C, MC = 9%.

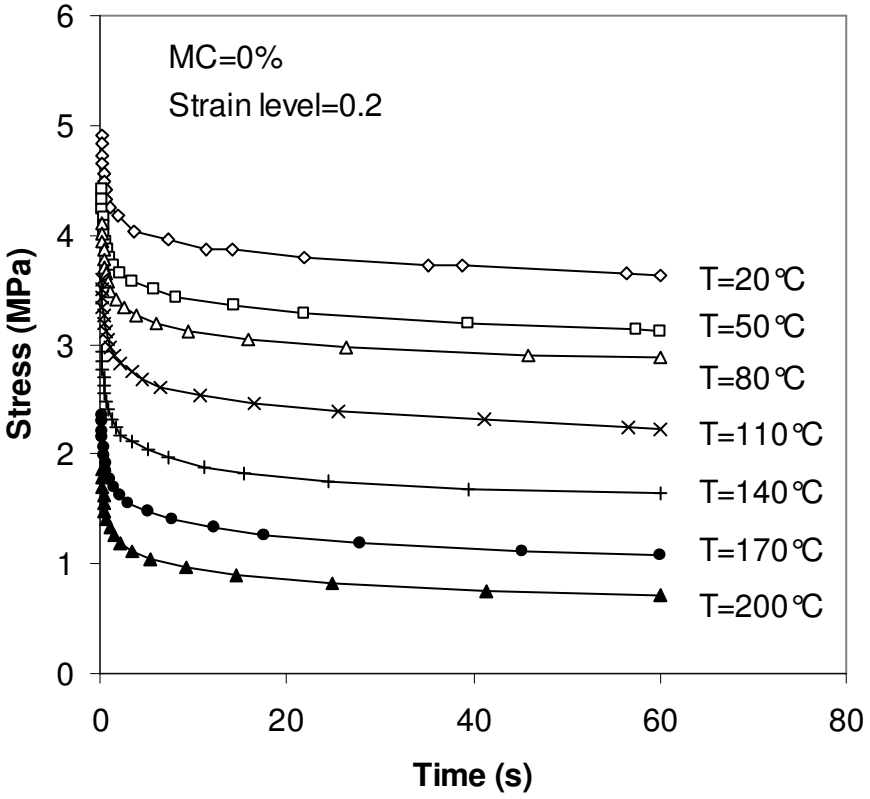

Figure 4.3 Effect of temperature on the stress relaxation of wood strands under transverse compression for ovendry samples.

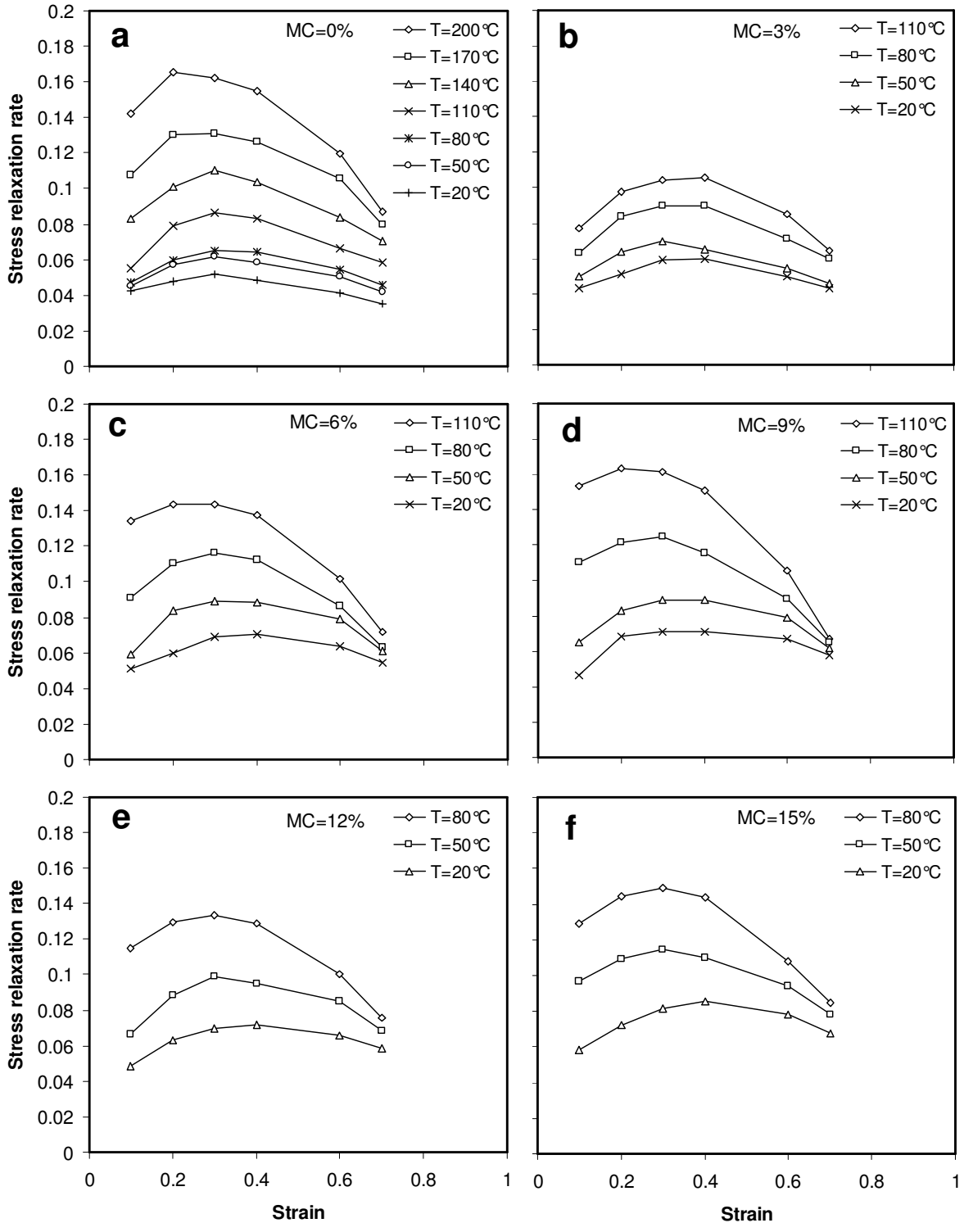

Figure 4.4 Effect of temperature on the stress relaxation rate of wood strands under transverse compression at different MCs.

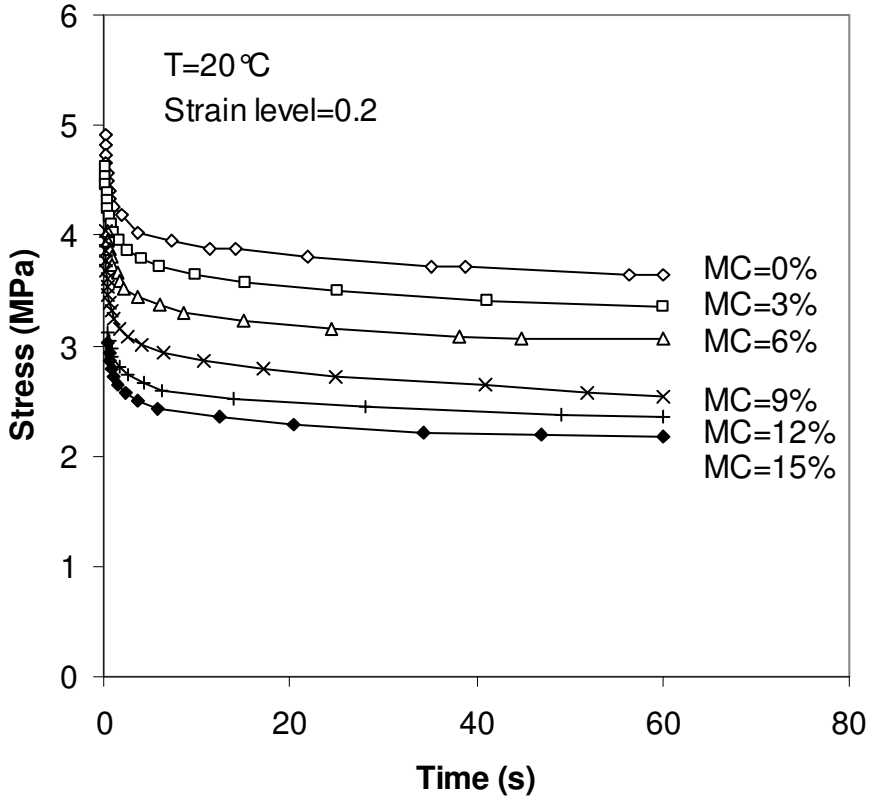

Figure 4.5 Effect of MC on the stress relaxation of wood strands under transverse compression.

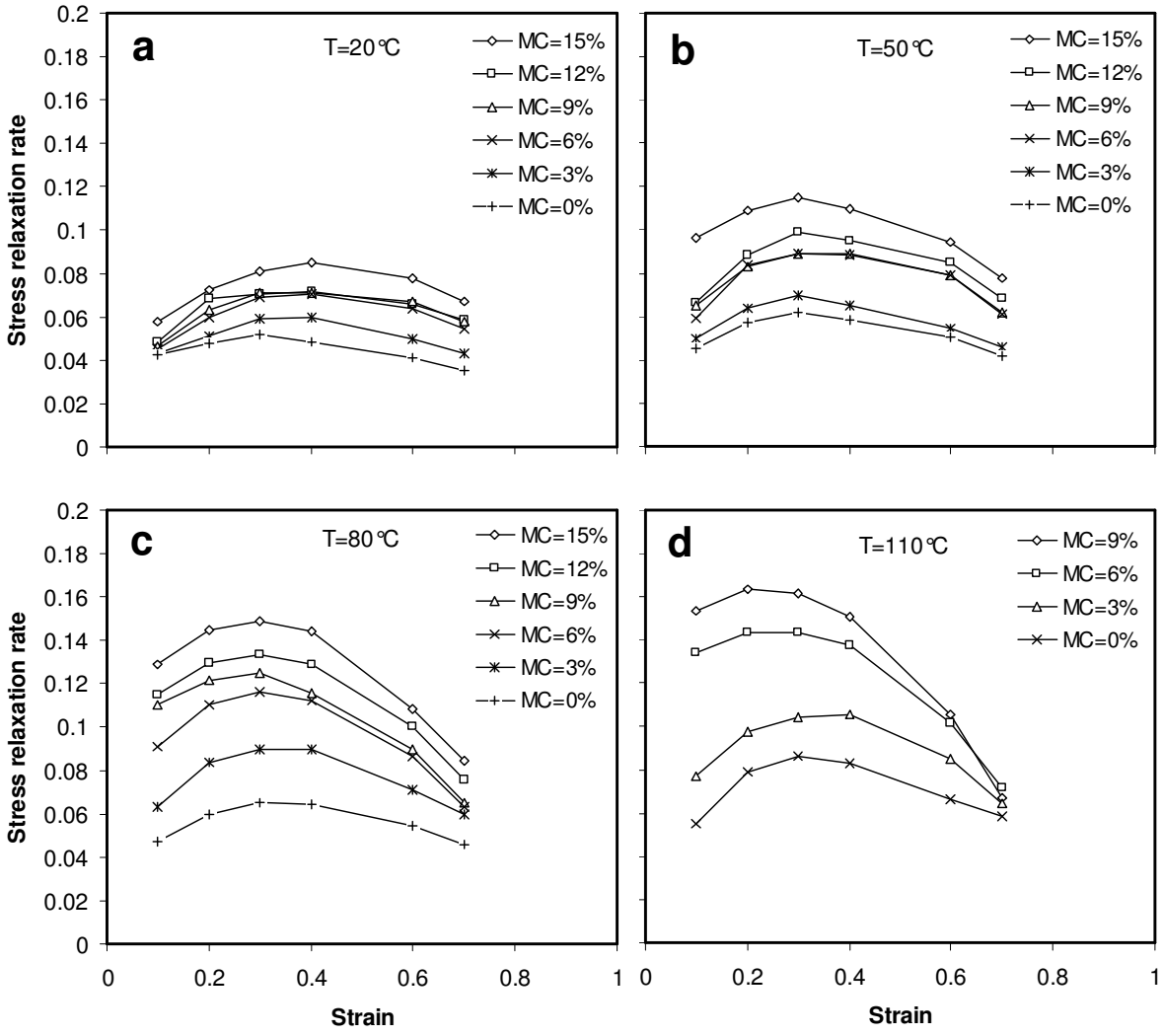

Figure 4.6 Effect of MC on the stress relaxation rate of wood strands under transverse compression at different temperatures.

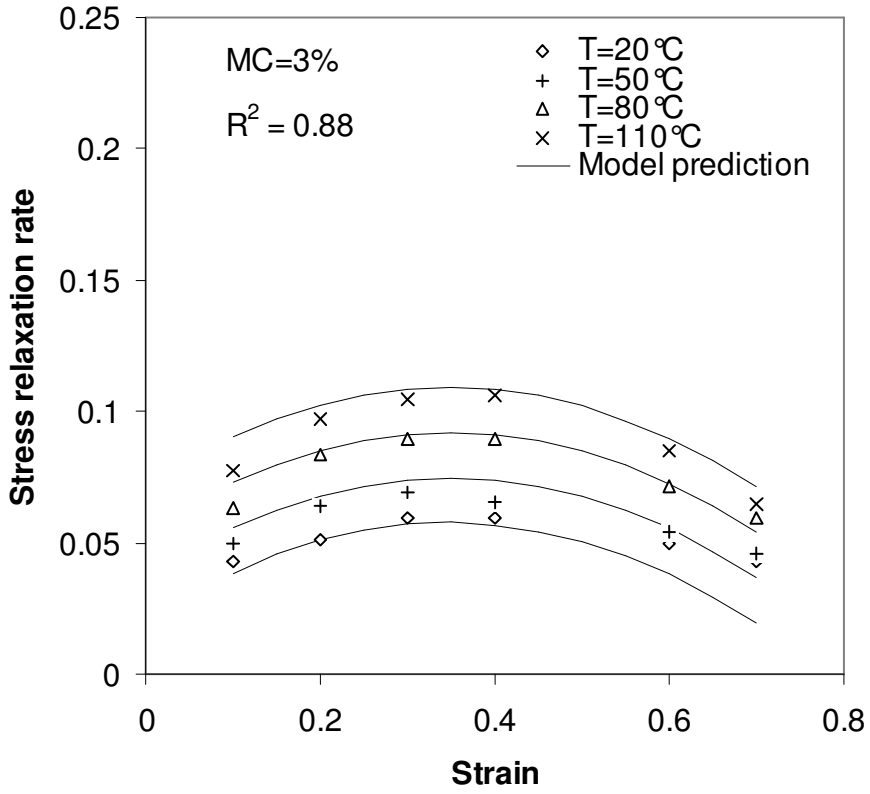

Figure 4.7 Comparison between experimental results and model prediction of stress relaxation rate ξ.

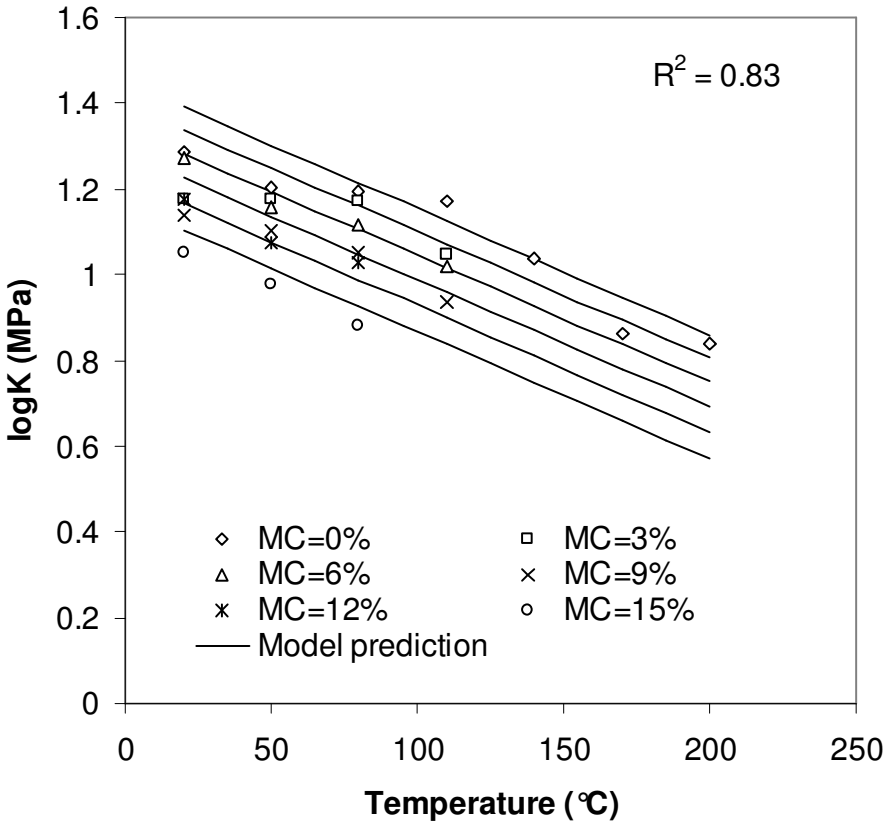

Figure 4.8 Comparison between experimental results and model prediction of *logK* values.

.

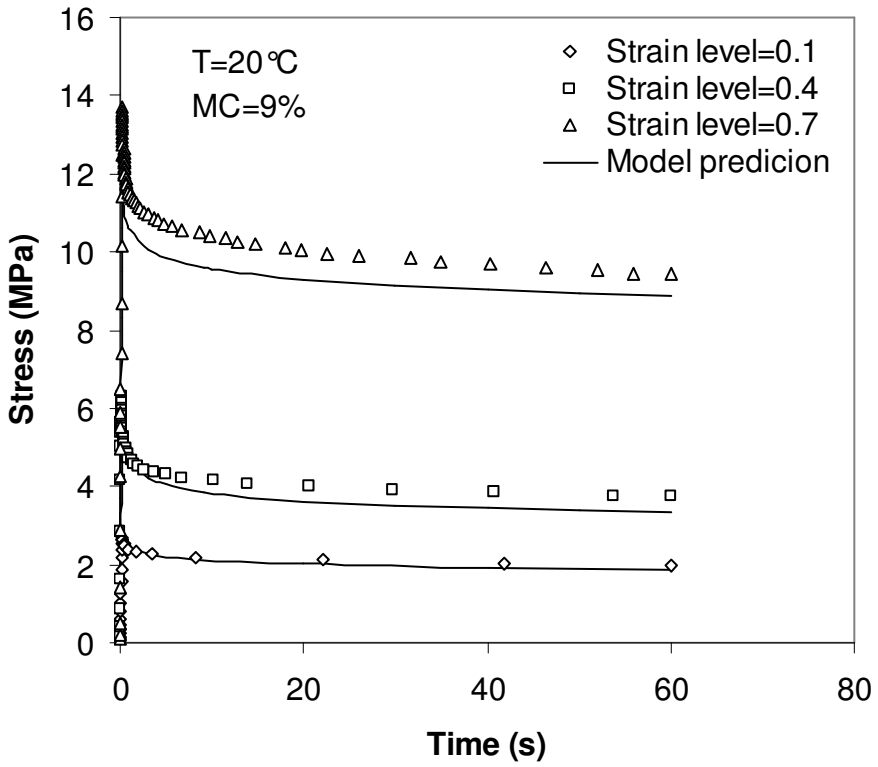

Figure 4.9 Comparison between experimental results and model prediction of stress relaxation response at various strain levels.

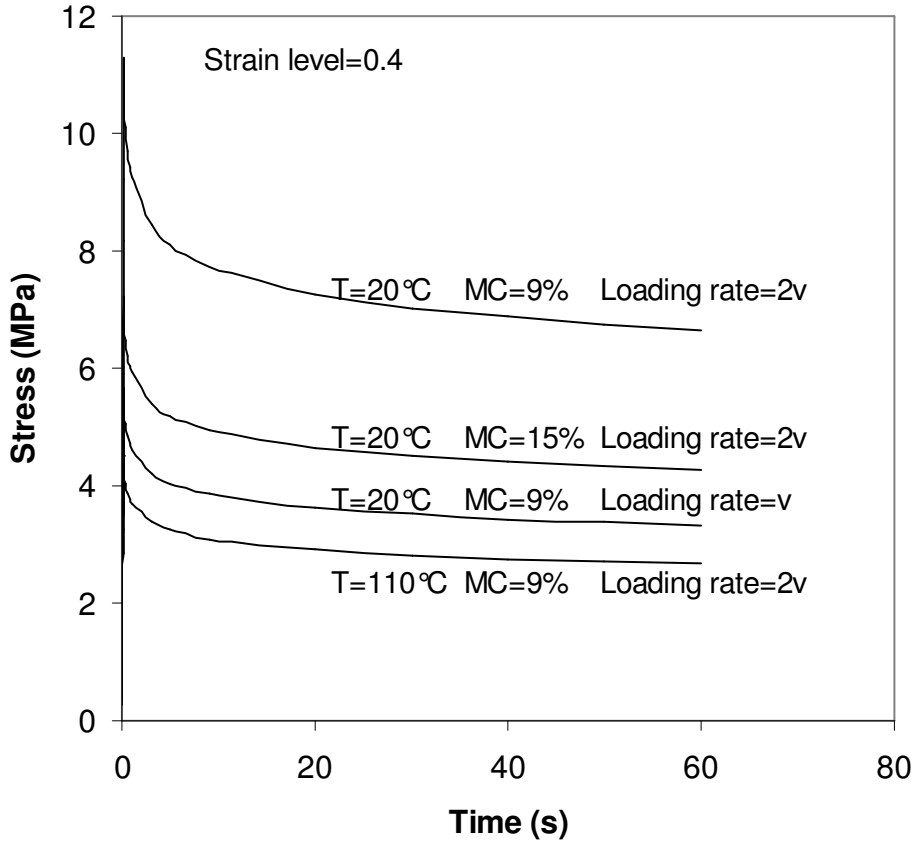

Figure 4.10 Effect of loading rate *v* on the stress relaxation for different combinations of temperatures and MCs.

4.7 Bibliography

Bowyer, J.L., Shmulsky, R., Haygreen, J.G. Forest products and wood science: An introduction. Iowa State Press, Ames, IA. 2002.

Bodig, J., Jayne, B.A. Mechanics of Wood and Wood Composites. Van Nostrand Reinhold, New York, NY, 1982.

Bolton, A.J., Breese, M.C. (1987) Time dependent strain development of wood loaded at right angles to the strain. In: Wood and Cellulosics: Industrial Utilisation, Biotechnology, Structure and Properties. Eds. Kennedy, J.F., Phillips, G.O., Williams, P.A. John Wiley & Sons, New York, NY. pp. 553-564.

Dai, C. (2001) Viscoelasticity of wood composite mats during consolidation. Wood Fiber Sci. 33:353-363.

Dai, C., Steiner, P.R. (1993) Compression behavior of randomly formed wood flake mats. Wood Fiber Sci. 25: 349-358.

Dai, C., Yu., C., Hubert, P. (2000) Modeling vertical density profile in wood composites during hot-pressing. In: Proceedings of the 5th Pacific Rim Bio-based Composites Symposium. Canberra, Australia. pp. 220-226.

Dai, C., Yu, C., Zhou, C. (2007) Theoretical modeling of bonding characteristics and performance of wood composites. Part 1. Inter-element contact. Wood Fiber Sci. 39: 48-55.

Dinwoodie, J.M. Timber: Its Nature and Behaviour. 2nd ed. E & FN Spon, London, 2000.

Ferry, J.D. Viscoelastic Properties of Polymers. 3rd ed. John Wiley & Sons, Inc., New York, NY, 1980.

Geimer, R.L., Kwon, J.H., Bolton, J. (1998) Flakeboard thickness swelling. Part I. Stress relaxation in a flakeboard mat. Wood Fiber Sci. 30:326-338.

Gibson, L.J., Ashby, M.F. Cellular Solids: Structure and Properties. Pergamon Press, New York, NY, 1988.

Greenspan, L. (1977) Humidity fixed points of binary saturated aqueous solutions. J. Res. Nat. Bur. Stand. 81A:89-96.

Holzer, S.M., Loferski, J.R., Dillard, D.A. (1989) A review of creep in wood: Concepts relevant to develop long-term behaviour predictions for wood structures. Wood Fiber Sci. 21:376-392.

Irvine, G.M. (1985) The significance of the glass transition of lignin in the thermomechanical pulping. Wood Sci. Technol. 19: 139-149.

Kauman, W.G. (1966) On the deformation and setting of the wood cell wall. Holz Roh-Werkst. 24: 551-556.

Kelley, S.S., Rials, T.G., Glasser, W.G. (1987) Relaxation behaviour of the amorphous components of wood. J. Mater. Sci. 22: 617-624.

Kelly, M. (1977) Critical review of relationships between processing parameters and physical properties of particleboard. Gen. Tech. Rep. FPL-10 USDA Forest Prod. Lab., Madison, WI.

Kunesh, R.H. (1961) The inelastic behavior of wood: A new concept for improved panel forming process. Forest Prod. J. 11: 395-406.

Kwei, T.K. (1984) The effect of hydrogen bonding on the glass transition temperatures of polymer mixtures. J. Polym. Sci. 22: 307-313.

Lakes, R.S. Viscoelastic Solids. CRC Press LLC, Baca Raton, FL, 1999

Lang, E.M., Wolcott, M.P. (1996) A model for viscoelastic consolidation of wood-strand mats. Part II. Static stress-strain behavior of the mat. Wood Fiber Sci. 28: 369-379.

Lenth, C.A., Kamke, F.A. (1996) Investigations of flakeboard mat consolidation. Part II. Modeling mat consolidation using theories of cellular materials. Wood Fiber Sci. 28: 309-319.

Meinecke, E.A., Clark, R.C. Mechanical properties of polymeric foams. Technomic, Westport, CT, 1973.

Nielsen, L.E. Mechanical properties of polymers and composites. Marcel Dekker Inc., New York, NY, 1974.

Penneru, A.P., Jayaraman, K., Bhattacharyya, D. (2005) Strain analysis in bulk forming of wood. Holzforschung 59:456-458.

Penneru, A.P., Jayaraman, K., Bhattacharyya, D. (2006) Viscoelastic behaviour of solid wood under compressive loading. Holzforschung 60:294-298.

Rosa, M.E., Fortes, M.A. (1988) Stress relaxation and creep of cork. J. Mater. Sci. 23:35-42.

Rusch, K.C. (1969) Load-compression behavior of flexible foams. J. Appl. Polym. Sci. 13:2297-2311.

Rusch, K.C. (1970) Load-compression behavior of brittle foams. J. Appl. Polym. Sci. 14:1263-1276.

Salmén, N.L., Back, E.L. (1980) Moisture-dependent thermal softening of paper, evaluated by its elastic modulus. Tappi J. 63: 117-120.

Schniewind, A.P. (1968) Recent progress in the study of the rheology of wood. Wood Sci. Technol. 2:188-206.

Schniewind, A.P. (1982) Mechanical behaviour and properties of wood. In: Wood as a Structural Material. Volume II. Clarke C. Heritage Memorial Series on Wood. Eds. Dietz, A.G.H., Schaffer, E.L., Gromala, D.S. Pennsylvania State University, University Park, PA. pp. 55-94.

Schniewind, A.P., Barrett, J.D. (1972) Wood as a linear orthotropic viscoelastic material. Wood Sci. Technol. 6:43-57.

Simpson, W.T. (1973) Predicting equilibrium moisture content of wood by mathematical models. Wood Fiber 5: 41-49.

van Houts, J., Bhattacharyya, D., Jayaraman, K. (2000) Determination of residual stresses in medium density fibreboard. Holzforschung 54:176-182.

van Houts, J., Bhattacharyya, D., Jayaraman, K. (2003) Viscoelastic behaviour of wood fibres during the hot pressing of medium density fibreboard. Holzforschung 57:391-399.

Wolcott, M.P. (1990) Modelling viscoelastic cellular materials for the pressing of wood composites. Ph.D. dissertation, Virginia Polytechnic Institute and State University, Blacksburg, VA.

Wolcott, M.P., Shutler, E.L., Jr. (2003) Temperature and moisture influence on compression-recovery behaviour of wood. Wood Fiber Sci. 35: 540-551.

Young, R.J., Lovell, P.A. Introduction to polymers. Chapman & Hall, New York, NY, 1991.

Youngs, R.L. (1957) Mechanical properties of red oak related to drying. Forest Prod. J. 9: 315-324.

Yu, C., Dai, C., Wang, B.J. (2007) Heat and mass transfer in wood composite panels during hot pressing: Part 3. Predicted variations and interactions of the pressing variables. Holzforschung 61:74-82.

Zhou, C., Smith, G.D., Dai, C. (2009) Characterizing hydro-thermal compression behavior of aspen wood strands. Holzforschung 63:609-617.

CHAPTER 5 MODELING VERTICAL DENSITY PROFILE FORMATION OF STRAND-BASED WOOD COMPOSITES DURING HOT PRESSING[4]

5.1 Introduction

Hot pressing is a key operation in wood composite manufacture as it not only affects the final product properties but also determines the production efficiency and cost. The consolidation of a composite mat is a complicated process as it involves physical, mechanical and chemical interactions during hot pressing. When the press closes, heat and mass transfer takes place between the platens and the mat, which softens the mat and makes it easier to consolidate. However, the mat deformation is not uniform through the mat thickness due to the temperature and moisture content (MC) differences between the surface and core layers. After the resin is cured, the bonds between woody constituents become permanent and hold the board together as the press opens. This leads to the formation of vertical density profile (VDP) in wood composite panels usually with high-density surface layers and low-density core layers.

The VDP of oriented strandboard (OSB), particleboard, and medium-density fiberboard (MDF) are typically M-shaped. This density variation through the thickness of board greatly affects the physical and mechanical properties (e.g., bending strength, dimensional stability, internal bond strength, and fastener holding ability) of the final product (Strickler 1959; Suchsland 1967; Kelly 1977; Schulte and Frühwald 1996a,

[4] A version of this chapter will be submitted for publication. Zhou, C, Dai, C., Smith, G.D. (2010) Modeling vertical density profile formation of strand-based wood compostites during hot pressing.

1996b; Wong et al. 1998, 1999; Wang et al. 2000; Wang et al. 2001a, 2001b; Wang et al. 2004). As such, investigating changes in the development of the VDP under different processing conditions is necessary in order to optimize the VDP, and hence the panel performance for different applications.

Harless et al. (1987) were among the first to develop a model for the VDP formation of particleboard which simulated the hot pressing operation using input data of manufacturing parameters (i.e., target panel density, platen temperature, and press closing rate etc.). However, in their model neither convective heat transfer nor viscoelastic effects after the press had reached its final thickness were taken into account thus limiting the usefulness of the model. Suo and Bowyer (1994) proposed a VDP model by simulating a particleboard mat as a system of thin and uniform layers, in which the temperature and MC profiles during pressing were predicted from one-dimensional (1D) heat and moisture diffusion models respectively. However, the effects of temperature, MC, and layer density on mat consolidation were considered independently and the interactions between these variables were ignored.

Wolcott et al. (1990) applied viscoelastic theories of amorphous polymers to predict the glass transition temperature (T_g) of wood flakes within a mat. The difference between the flake temperature and the predicted T_g was regarded as an indicator of the amount of flake deformation, which could be used to qualitatively describe the density gradient formation. Utilizing the same concept and a two-dimensional (2D) heat and mass transfer model, Zombori (2001) presented a nonlinear viscoelastic compression model to simulate

the VDP formation for OSB panels, in which the effects of temperature and MC on mat compression were predicted by the time-temperature-moisture superposition method.

Winistorfer et al. (1996) modeled and compared the VDP of OSB panels using nonparametric regression technique. They fitted a mathematical expression to describe the relationship between density and panel thickness. Winistorfer et al. (2000) also designed a radiation-based system to measure *in-situ* density of wood-based composites during hot pressing. In addition, Wang and Winistorfer (2000a) proposed a methodology to describe the VDP formation with two periods and five stages. Although they did not present a model to predict VDP formation, their experimental studies are very valuable for further model development by other researchers. Similarly, Dai et al. (2000) conceptualized the VDP formation of wood composite during hot pressing into two stages. The primary VDP, which was formed before the mat reached the target thickness, could be modeled based on the compression stress-strain relationships of mat layers. The secondary VDP, which was developed after the mat reached the target thickness, was governed by mat viscoelasticity and elastoplasticity.

To describe the VDP development for MDF in continuous pressing, a comprehensive model was developed by Thoemen and Humphrey (2003, 2006) and Thoemen et al. (2006), which included heat and mass transfer, adhesion kinetics, and hygro-thermo-rheological behavior of fiber mat. Their model viewed the fiber mat as a homogenous material and ignored the variations in mat structure and physical properties. More

recently, Thoemen and Ruf (2008) applied this model to investigate the effects of pressing schedule on the VDP development in MDF.

Painter et al. (2006) developed a model to predict the VDP for commercial OSB panels, which was based on the compression behavior of cellular materials in combination with temperature and moisture profiles from a heat and mass transport model (Fenton et al. 2003). Drawing on the experimental results from von Hass and Frühwald (2000, 2001), they used an empirical approach to examine the effects of temperature and MC on mat compression. To predict the VDP for a multi-layered strand mat Lee et al. (2007) developed a mathematical model to simulate the hot-pressing process in combination with a heat and mass transfer model (García 2002). They used empirical models in an approach similar to that of Thoemen et al. (2006) to describe the viscoelastic compression behavior of the mat. Likewise, this model required many parameters either from the empirical relationships or from the experimental results of other researchers (Thoemen 2000; Zombori 2001; Hood et al. 2005).

Most of the above-mentioned models for VDP formation of wood composites were developed based on the analogs of the spring and dashpot. The basic concept used in these models was to treat the entire mat as one viscoelastic material during consolidation. This assumption seems reasonable for fiber mats where the fiber dimensions are much smaller than the mat size and for most purposes they can be considered as a homogeneous material. In the case of strand-based composites, such an assumption is very questionable. The width of the strands is often the same or larger than the final

thickness of the board and the orientation of the strands varies significantly; both lead to mats that are very in-homogeneous in the horizontal and vertical density distributions (Suchsland 1962; Suchsland and Xu 1989, 1991; Dai and Steiner 1997). In other words, from a structural standpoint, the strand mat cannot realistically be modeled as a homogenous material. Moreover, this horizontal density distribution has a great impact on the local heat and mass transfer process within the mat, which further influences the VDP formation of the local mat area. As such, it is an interesting issue to investigate the relationship between the local mat density and the corresponding local mat VDP. Unfortunately, none of the existing VDP models are able to investigate this relationship.

As an important panel characteristic, VDP is determined not only by the heat and mass transfer processes but also by the mechanical response of wood constituents in the mat. As a result, it is necessary to incorporate the fundamental properties of wood strands and their structure-property relationships into the development of the VDP model. Unlike those models based on mat properties that require many empirical parameters, this proposed model would be established on the basis of strand properties during hot pressing and the random mat structure. As such, the overall objective of this study is to improve the fundamental understanding of the mat consolidation during hot pressing. The specific objectives are:

1) to develop a simulation model for VDP formation in strand-based wood composites based on strand properties and the mat structure;

2) to validate this model through laboratory panel manufacture and VDP measurement; and

3) to present the predictive effects of some pressing variables on VDP formation.

5.2 Literature Review: Modeling of Heat and Mass Transfer during Hot Pressing

The VDP formation in wood composites mainly results from the interactions between mat pressure, temperature, and MC distributions within the mat during hot pressing. As a result, to model the VDP formation during hot pressing, a heat and mass transfer model must be established. Because of their importance heat and mass transfer during hot pressing has been extensively investigated not only with experimental approaches as reviewed by Bolton and Humphrey (1988) but also with a number of different modeling approaches as follows.

Humphrey and Bolton (1989) were among the first to model the heat and moisture transfer for particleboard during hot pressing. After analyzing the mechanisms of heat and mass transfer, they proposed a 2D cylindrical model to predict the environmental conditions inside the mat during hot pressing. However, this model assumed a constant mat structure and thus did not take into account the effect of press closing on the heat and mass transfer process. Nevertheless, their model significantly improved the understanding of the hot pressing process at that time. Haselein (1998) later extended this model to simulate the hot pressing of wood-fiber composites by taking into account the press closure and the rheological behavior of fiber mats with no resin applied.

Carvalho and Costa (1998) developed a three-dimensional (3D) heat and mass transfer model for MDF hot pressing. Similar to Humphrey and Bolton's model, this model also neglected the effect of press closing on mat structure and thus on the physical properties of the mat. More recently, using this model, Carvalho et al. (2001, 2003) developed a mechanical model to describe the viscoelastic behavior of fiber mats and incorporated the resin curing mechanism into a global model for MDF hot pressing.

Following the approach presented by Humphrey and Bolton (1989), Thoemen (2000) proposed a 3D model to simulate the heat and mass transfer during hot pressing of fiber composites. His model included the rheological mechanism and bond strength development that occur in mat during densification. The predicted temperature and MC distributions were compared with the experimental results (Thoemen and Humphrey 2003, 2006; Thoemen et al. 2006; Thoemen and Ruf 2008).

Zombori (2001) developed a 2D heat and mass transfer model for strand mat hot pressing that included the resin curing in addition to the physical and gas transport properties of the mat He used this model to perform a sensitivity analysis and identified the key parameters as initial mat MC, final panel density, press platen temperature, and press closing time. It was found that the thermal conductivity and gas permeability of the mat had the greatest influences on the model results (Zombori et al. 2003, 2004). Based on the similar principles of energy and mass conservation, a 3D heat and mass transfer model was developed by García (2002) for OSB hot pressing. A novel feature of this model was the inclusion of flake alignment and its effect on mat permeability and consequently on

heat and mass transfer. It was found that flake alignment increased lateral permeability, and decreased transverse thermal convection of the mat, which contributed to the lower temperatures and gas pressures in the alignment direction (García et al. 2001, 2003).

Fenton et al. (2003) developed a 2D model of heat and mass transport within an OSB mat during hot pressing. This model was unique in that it considered the velocity of press platen and treated the platen-mat interface as a moving boundary, which was believed to contribute to the movement of gases during pressing. In addition, the fines were considered in their model and they found that the distribution of fines affected the horizontal density distribution. Based on the theories of cellular materials, a compression model was developed to predict the final panel VDP, which agreed well with the measurements from a commercial OSB panel.

Utilizing the principles of thermodynamics and resin curing kinetics, Dai and Yu (2004) developed a comprehensive 3D heat and mass transfer model for the hot pressing of a strand mat. Dai et al. (2005) proposed a theoretical model for the first time to mathematically characterize the porosity and permeability of strand-based wood composites. It took into account the various relationships between the strand dimensions, the mat density, and the mat permeability, which determined the rate of heat and mass transfer within the mat during pressing. Their model was later validated by the experimental work (Yu et al. 2007; Dai et al. 2007); this model was used to predict the temperature and MC distributions for modeling VDP in the present work.

5.3 Model Development

The idealized typical press cycle for OSB panels can be divided into four stages as shown in Figure 5.1. In Stage I, the press closes at a given speed and compresses the mat to a given thickness which is slightly higher than the target thickness. In Stage II the mat pressure is held constant and the mat is slowly compressed to the target thickness. The mat deformation is the result of creep and thermal softening. In Stage III, the mat thickness is held constant and resin cures. Mat pressure gradually continues to decrease as a result of thermal softening and stress relaxation (Dai et al. 2000). In Stage IV, which is often referred to as the degas stage, the press is opened very slowly to permit the mat pressure to drop to zero and minimize the likelihood of a delamination or *blow* occurring. During this stage, the mat thickness increases slightly due to the springback of the woody material. It should be noted that creep does not play a significant role during pressing due to the short time span over which pressing occurs. Moreover, it is very difficult to maintain constant mat pressure in a practical operation, which means the mat behavior in Stage II does not conform to the constant load requirement typically associated with creep. As a result, it was decided that Stage II of the press cycle would be neglected and it was assumed that the mat thickness decreased from initial thickness to target thickness as in Stage I. As such the focus of the model development was on mat formation, mat consolidation, and mat stress relaxation.

5.3.1 Mat Formation

The approach used here to simulate the mat formation followed the stochastic model proposed by Dai and Steiner (1994a, b). All the strands were assumed to be rectangular in shape and of λ mm in length, ω mm in width, and τ mm in thickness. The dry strand density ρ_{ds} was also assumed to be uniform for all strands. A designated mat forming area of length L_m by width W_m set in a Cartesian coordinate system xy was discretized into a grid system with resolution unit of 1 × 1 mm.

The strands were then randomly deposited over the forming area, where the grids covered by strands were labeled with the corresponding overlap number and the void area was labeled zero. During the formation process, each strand was assumed to lie parallel to the horizontal plane and in close contact with the neighboring strands. The location of kth strand was represented by the center position (x_k, y_k) and the orientation φ_k as shown in Figure 5.2. Variables $x_{k,}$, y_k, and φ_k were generated from a uniform random distribution in the range of [0, L_m], [0, W_m], and [0, π], respectively. The term uniform random distribution refers to the fact that each strand has an equal chance of being placed at any point or oriented at any angle in the mat area. The total number of strands in the mat, N_s, was obtained on the basis of dry wood mass in the final product with target panel density ρ_m and thickness H_m.

After all the strands were deposited on the forming area, a 3D mat structure was constructed in the coordinate system xyz. It consisted of L_m × W_m imaginary strand

columns with different column heights which depended on the number *i* of overlapping strands in the column (Figure 5.3). The probability of a point in the mat covered by *i* strands, *p(i)*, follows the Poisson distribution (Dai and Steiner 1993):

$$p(i) = \frac{a_i}{A} = \frac{e^{-n} n^i}{i!} \tag{5.1}$$

where a_i is the total area of columns with *i* strands, *A* is the mat area, and *n* is the average strand number of all columns, which is determined by:

$$n = \frac{\lambda \omega N_s}{A} \tag{5.2}$$

The initial mat thickness H_0 was assumed as the height of strand column with maximum strand number i_m, i.e., $H_0 = i_m \tau$. Then the mat was divided into N_z layers and each layer was assumed to have the same dry wood mass for each column (Figure 5.4). The dry wood mass of the *j*th layer m_{dj} in the column with *i* strands is determined by:

$$m_{dj} = \frac{i \tau \rho_{ds}}{N_z} \qquad i = 1, 2, ..., i_m \qquad j = 1, 2, ..., N_z \tag{5.3}$$

where ρ_{ds} is the dry strand density. It was assumed that the dry wood mass of each layer remained constant during hot pressing.

5.3.2 Heat and Mass Transfer

The heat and mass transfer process begins when the press platen contacts the mat surface. For example, the heat is transferred from the platen to the surface layer by conduction, which also evaporates the bound water of the strands in face layers. As the water vapor is driven into the inner mat, the heat is transferred from face layers to core layers by

convection. This heat and mass transfer process softens the mat and makes the compressibility of mat layers as a function of temperature and MC. According to Dai and Yu's model (2004), once the pressing parameters and the initial mat conditions are determined, the inside environmental conditions at a given position within the mat could be predicted at any given time, which makes it possible to describe the compression behavior of strand columns during hot pressing.

To make the model predictions more consistent and accurate, the mat structure constructed during the formation process was used as an input for the heat and mass transfer model. Aside from the same layer number N_z in the thickness direction (the z-axis), the mat was divided into N_x and N_y mesh elements in the length (the x-axis) and width direction (the y-axis), respectively. Temperature and MC were assumed to be uniformly distributed within each mesh element. Note that the smaller the mesh elements, the more accurate the model prediction. However, due to the time limit of the computer program execution, the number of mesh elements N_x and N_y for the heat and mass transfer model were not necessarily to be the same as the number of 1 mm by 1mm mesh elements used for the mat formation model, respectively (Figure 5.5). In addition, as the mat structure was completely random and the boundary conditions of the mat were assumed to be symmetrical about the mid-plane and as such the predicted inside environmental conditions such as temperature and MC would also be symmetric.

5.3.3 Mat Consolidation and VDP Formation

At the early stage of strand mat compression, strand bending is the dominant mechanism in mat consolidation when the mat density is low (Dai and Steiner 1993; Lang and Wolcott 1996; Zhou et al. 2008). At higher stresses, the strands in the mat are mainly subjected to transverse compression (Dai and Steiner 1993; Wolcott et al. 1994; Lenth and Kamke 1996; Zhou et al. 2008). In wood composite manufacture, the pressure applied to the mat is usually highly dependent on target panel density. In order to reduce the complexity of the modeling task, bending and shear stresses were neglected and the whole strand mat was treated as a system of compression elements, i.e., the strand columns in each grid.

Time was assumed to be zero at the moment the top platen contacts the highest strand column. At a given time t during the press closing stage, the platen applied a force $P(t)$ on the mat and it compressed the mat to thickness $H(t)$ at a loading speed v in the following expression:

$$H(t) = H_0 - vt \tag{5.4}$$

where H_0 and $H(t)$ are in mm, t has units of seconds, and v is in mm s^{-1}. It is noted that $P(t)$ can only be supported by those strand columns with strand number i greater than $H(t)/\tau$, which can be written as follows:

$$P(t) = \sum_{i=H(t)/\tau}^{i_m} \sigma_i(t) a_i \tag{5.5}$$

where $\sigma_i(t)$ is the stress in columns with i strands in units of MPa, a_i is the total area of columns with i strands in units of mm^2, and i_m is the maximum strand number in columns.

For those columns under compression with i strands, the stress-strain relationship can be modeled by a modified Hooke's law (Dai and Steiner 1993; Wolcott et al. 1994):

$$\sigma_i = E\varphi(\varepsilon_i)\varepsilon_i \tag{5.6}$$

where E is the compression modulus of strand columns at the given temperature and MC, ε_i is the strand strain in columns, and $\varphi(\varepsilon_i)$ is a dimensionless nonlinear strain function, which is determined experimentally. The strain function was assumed to be independent of wood cell wall material and only depended on the cellular structure (Dai and Steiner 1993; Wolcott et al. 1994; Lang and Wolcott 1996; Lenth and Kamke 1996). More recently, Zhou et al. (2009) found that the strain function is affected by elevated temperature and MC at high strain levels due to changes in cell wall material. Nevertheless, this stress-strain relationship was used to model the VDP formation in the present work.

It should be noted that Eq. (5.6) implies the strain ε_i is uniformly distributed over all strands in the column at ambient conditions. However, for a multi-layered strand column under hot pressing, the temperature and MC are different for each layer due to the heat and mass transfer process. As the compression modulus of wood depends on environmental conditions, the layers in the column will not have the same strain at a given stress. Thus the stress-strain relationship for the strand column can no longer be described by Eq. (5.6).

To obtain the strain of each layer in the column with *i* strands, an iterative approach was applied as follows. At a given time t_0, an initial trial stress $\sigma_i(t_0)$ was applied on the column. This stress was believed to be uniformly transferred to each layer. In other words, the stress should be the same for all layers at any given time during pressing. For the *j*th layer in the column, the stress-strain behavior could be described as follows:

$$\sigma_i(t_0) = E_j(T_j, MC_j)\varphi(\varepsilon_j(t_0))\varepsilon_j(t_0) \qquad j = 1, 2, ..., N_z \tag{5.7}$$

where T_j is the temperature, MC_j is the moisture content, $\varepsilon_j(t_0)$ is the strain, and E_j is the compression modulus of the *j*th layer, respectively.

According to the research work reported in Chapter III, E_j and $\varphi(\varepsilon_i)$ could be expressed in the following empirical equations:

$$E_j(T_j, MC_j) = -16.29581 \ln T_j - 1.507311 MC_j + 103.4776 \tag{5.8}$$

and

$$\varphi(\varepsilon_j) = \begin{cases} 1 & \varepsilon \le 0.15 \\ -6.0768\varepsilon_j^{\,3} + 11.282\varepsilon_j^{\,2} - 6.485\varepsilon_j + 1.6179 & \varepsilon > 0.15 \end{cases} \tag{5.9}$$

As the heat and mass transfer model (Dai and Yu 2004) provided the predictions of T_j and MC_j at time t_0, the layer modulus E_j could be determined by Eq. (5.8). In addition, the stress $\sigma_i(t_0)$ was predetermined and $\varphi(\varepsilon_i)$ is a polynomial function of strain, which made the strain $\varepsilon_j(t_0)$ the only unknown variable in Eq. (5.7). Thus this strain $\varepsilon_j(t_0)$ could be solved by the Newton-Raphson iteration method. One can expect that the layers with higher temperature and MC would have lower compression moduli and thus have more deformation than those of lower temperature and MC in the same column.

Once the strain $\varepsilon_j(t_0)$ for each layer was obtained, $H_i(t_0)$, the thickness of strand column with i strands at time t_0 could be determined by:

$$H_i(t_0) = \sum_{j=1}^{N_z} (1 - \varepsilon_j(t_0)) H_{l0} \tag{5.10}$$

where H_{l0} is the initial layer thickness which is given by:

$$H_{l0} = \frac{i\tau}{N_z} \tag{5.11}$$

Note that the column thickness $H_i(t_0)$ must be the same as the overall mat thickness $H(t_0)$ which was obtained by Eq. (5.4). As a result, if $H_i(t_0)$ was not equal to $H(t_0)$, then the initial stress $\sigma(t_0)$ would be adjusted iteratively according to the difference between $H_i(t_0)$ and $H(t_0)$. At each iterative step, a new trial stress would result in a new strain for each layer based on Eqs. (5.7)-(5.9). This iterative process would not be terminated until an appropriate column stress $\sigma_i'(t_0)$ was obtained at which the column thickness matched the mat thickness.

So far, the anticipated column stress $\sigma_i'(t_0)$ and layer strain $\varepsilon_j'(t_0)$ in the column with i strands at $t = t_0$ have been determined. Based on the obtained layer strain, the corresponding layer density is given by:

$$\rho_j(t_0) = \frac{m_{dj}(1 + MC_j)}{(1 - \varepsilon_j'(t_0)) H_{l0}} \tag{5.12}$$

where $\rho_j(t_0)$ is the layer density, m_{dj} is the dry wood mass, which is determined by Eq. (5.3), and $(1 - \varepsilon_j'(t_0))H_{l0}$ is the layer thickness at time t_0, respectively. If the layer density is plotted as a function of the layer position in the z-axis, then the VDP for a column at $t = t_0$ is determined. Meanwhile, the same iterative procedures for layer strain

and density were applied to all the columns in compression where the strand number is greater than $H(t_0)/\tau$. For those columns that are uncompressed due to the strand number being less than $H(t_0)/\tau$, the density is still the same for all layers, which is determined by:

$$\rho_j(t_0) = \frac{m_{dj}(1+MC_j)}{H(t_0)/N_z} \tag{5.13}$$

where $H(t_0)/N_z$ is the layer thickness. Consequently, after the VDP for all strand columns have been obtained, then the average layer density of all columns is considered as the VDP for the entire mat at a given time. Likewise, at a new time step, the above-mentioned procedures will be applied to determine the resultant VDP for all strand columns and the mat. As shown in Figure 5.6, this process will be repeated at each time increment until the mat reaches the target thickness at $t = t_m$, and the mat VDP can be obtained at any given time during press closing.

5.3.4 Mat Stress Relaxation

After the mat is compressed to the target thickness, it will be held under this fixed deformation for resin curing. Heat is continually transferred from the press platens to the mat, which makes it softer and easier to deform. As wood is a viscoelastic material, stress relaxation will occur at this constant strain level. It is believed that both of these factors contribute to the drop in mat pressure at this stage.

Based on the work conducted by earlier researchers (Meinecke and Clark 1973; Wolcott 1990; Dai 2001), the stress relaxation behavior of the column with *i* strands during hot pressing can be described by the following equation:

$$\sigma_{ri}(t) = \varphi(\varepsilon_i)\int_0^t K(t-t')^{-\xi_i}\frac{d\varepsilon(t')}{dt'}dt' \tag{5.14}$$

where $\sigma_{ri}(t)$ is the column stress in relaxation, K is the relaxation modulus of the strand column, ξ is the rate of stress relaxation, which are determined by the following empirical relationships, respectively (Zhou et al. 2009):

$$\xi_i(\varepsilon,T,MC) = -1.65357\times10^{-3} + 5.734314\times10^{-4}T + 3.561552\times10^{-3}MC + 0.213291\varepsilon - 0.306312\varepsilon^2 \tag{5.15}$$

and

$$\log K(T,MC) = 1.344561 - 2.406084\times10^{-3}T - 6.826339\times10^{-3}MC - 6.064806\times10^{-4}MC^2 \tag{5.16}$$

If the press platen closed at a constant rate v, then the loading strain history of strand columns could be assumed to be linear as shown in Figure 5.7 (adapted from Dai 2001). The time t_m, which is needed for all supporting strand columns to reach the target mat thickness H_m, is determined by:

$$t_m = \frac{i_m\tau - H_m}{v} \tag{5.17}$$

The time from the moment at which the load is applied on the mat to the moment at which the i-strand columns start compression, t_1, is obtained by:

$$t_1 = \frac{i_m\tau - i\tau}{v} \tag{5.18}$$

The time required for i-strand columns to reach the target mat thickness, t_2, is given by:

$$t_2 = \frac{i\tau - H_m}{v} \tag{5.19}$$

In addition, the maximum strain in i-strand columns, ε_i, is determined by:

$$\varepsilon_i = \frac{i\tau - H_m}{i\tau} \tag{5.20}$$

Therefore, the strain history in *i*-strand columns can be obtained:

$$\varepsilon_i(t)=\begin{cases}0 & (t<t_1)\\ \dfrac{t-t_1}{t_2}\varepsilon_i & (t_1\le t<t_m)\\ \varepsilon_i & (t\ge t_m)\end{cases} \tag{5.21}$$

Taking the derivative of Eq. (21) with respect to t and substituting it into Eq. (5.14) for $t < t_m$ produces:

$$\sigma_{ri}(t)=\frac{Kv\varphi(\varepsilon_i)}{i\tau(1-\xi_i)}(t-t_1)^{1-\xi_i} \tag{5.22}$$

And for $t \ge t_m$, this becomes:

$$\sigma_{ri}(t)=\frac{Kv\varphi(\varepsilon_i)}{i\tau(1-\xi_i)}[(t-t_1)^{1-\xi_i}-(t-t_m)^{1-\xi_i}] \tag{5.23}$$

where ξ_i and K are determined by Eqs. (5.15) and (5.16), respectively. It should be noted that, to simplify the calculation process, the temperature and MC used in Eqs. (5.15) and (5.16) were the average values of all layers in strand columns. Moreover, according to Eq. (5.2), the overall mat stress σ_m at any given time t was determined by:

$$\sigma_m(t)=\sum_{i=H(t)/\tau}^{i_m}\frac{\sigma_{ri}(t)a_i}{A} \tag{5.24}$$

It is interesting to note that Eq. (5.24) is another means of stating press cycle; a plot of the overall mat pressure as a function of time should be identical to the press cycle.

5.3.5 Mat Elastoplasticity

If a material deforms in a manner proportional to the applied load within some limit, and it returns exactly to its original size when the load is removed, this material's deformation

behavior is deemed to be elastic; if the deformation is irreversible, it is plastic. During hot pressing, although most of the mat deformation is permanent, the mat still exhibits some strain recovery when the press opens. It means that the mat is neither perfectly plastic nor perfectly elastic. Thus, this type of material property is denoted elastoplastic, which was proposed by Dai et al. (2000) for wood composite mats. Like other mat properties, this property can be significantly affected by the temperature and MC distributions inside the mat during hot pressing. In fact, it has an impact on the redistribution of density between layers and hence VDP formation after the mat reaches the target thickness. During the thickness holding, the mat pressure starts to drop and this can be viewed as a type of unloading, which leads to the springback in certain layers and further densification in other layers. However, this elastoplastic behavior of mat has not been fully investigated. As a result, it is necessary to experimentally study this mat property and develop the quantitative relationship between the mat springback and the environmental conditions within the mat (e.g., temperature and MC).

5.4 Experimental

5.4.1 Panel Manufacture

The objective of the following experimental work was to validate the predictions of the VDP model. The aspen (*Populus tremuloides*) strands used in this study were obtained from a local OSB mill and these strands were initially screened to remove fines. Approximately 700 strands were randomly selected from the screened strands for size

measurement. The average length and width of the strands were obtained by an image analysis system (OSBVIEW, FPInnovations – Forintek Division) and found to be 110.3 mm and 23.4 mm, respectively; the average thickness was measured by hand using a digital caliper and found to be 0.7 mm.

In this experimental work, panels were manufactured with two furnish MCs. One moisture level was 6%, a common MC used in OSB panel manufacture. The other was oven dry, which aimed at minimizing the effect of moisture on strand properties during pressing. Oven-dried strands were obtained by drying the materials in a force-convection oven at a temperature of 103°C. The strands were removed from the oven and stored in sealed plastic bags prior to blending. For MC = 6%, the strands were first dried to an approximate MC of 2% at a temperature of 80°C. Then after the application of resin and wax, if needed, extra water was sprayed onto the strands in a rotary drum blender to bring the final MC of the strands up to 6%.

A commercial liquid phenol-formaldehyde resin (Hexion Specialty Chemicals Inc, Springfield, OR, USA) with a solid content of 55% was used for the 6% MC furnish, while a commercial powder phenol-formaldehyde resin from the same company was used for the ovendry furnish. In addition, a commercial liquid wax with a solid content of 58% was also applied in panel making for both type of furnish.

Strands at 6% MC were blended with resin in three board batches in a laboratory drum blender. The resin solids were 3% and wax application rate was 1.2% based on the

ovendry strand weight. Both resin and wax were atomized through a spray head via a pressurized air stream with a pumping system. For the batch of three-board ovendry furnish, the powder resin of 3% solids based on the ovendry strand weight was sprayed onto the strands by hand, and then the strands were blended to make the resin distribute as uniformly as possible on the strand surface. The wax application rate and procedure for ovendry furnish were the same as those for 6% MC furnish. Resin and wax were applied to the strands at room temperature and resin was applied before wax. Each type of furnish was sealed in a plastic bag to maintain moisture level immediately after the resin and wax application.

The materials for each panel were weighed and the strands were randomly oriented by hand in a 711 × 711 mm forming box. In the meantime, a small amount of strands was taken from each type of furnish and oven dried to obtain the MC just prior to pressing, which was used for the input mat MC in the model. Mats were then pressed to a nominal thickness of 11.1 mm in a hydraulic hot press with a target panel density of approximately 670 kg m^{-3}. The press platen temperature was maintained at 200°C. The total press cycle was 300 s, including the press closing time of 60 s, and a decompression stage of 60 s. To collect the data of the temperature and gas pressure during pressing, two PressMAN probes were inserted into the mat before the press closed. One was placed in the middle plane of the mat and the other was near the surface. Developed by the Alberta Research Council (Edmonton, AB), the probe has a single hole at its tip, where there exists a thermocouple and a pressure transducer.

5.4.2 VDP Measurement

After pressing, individual panels was trimmed to 610 × 610 mm to minimize the edge effect during the forming process. Then each panel was cut into 50 × 50 mm specimens for VDP measuring. In addition, the specimens were labeled to indicate the panel type and their position within the panel. Prior to VDP scanning, all these specimens were conditioned under laboratory conditions of approximately 20°C and 55% relative humidity for three days.

The VDP of each specimen was measured using a commercial x-ray density profiler (QMS Density Profiler, Quintek Measurement Systems, Knoxville, TN, USA). Density data were measured at 0.06 mm increments by an x-ray beam passing through the specimen thickness. Each specimen represented the local VDP within a panel while the total specimens per panel were averaged to represent the entire panel VDP.

5.4.3 Elastoplasticity of Strand Mat

The following test was conducted to investigate the elastoplastic properties of strand mat during a loading-unloading cycle. Aspen strands of small size (approximately 50 mm long) were obtained from an OSB plant in Ontario, Canada. Three types of furnish with MCs of 0%, 6% and 15% were prepared for testing in order to study the full possible range of MC encountered in panel manufacture. The strands with a MC of 6 and 15% were prepared by placing them in controlled temperature and humidity rooms until

constant strand mass were achieved. The 0% MC strands were oven-dried at a temperature of 103°C for 24 hours and then stored in a desiccator. After conditioning, each type of furnish was transported to the load frame in sealed plastic bags where they remained until just prior to mat forming.

All mats were made by hand in a 152 × 152 mm forming box with a target mat density of 670 kg m^{-3} based on the mat thickness of 11 mm. Efforts were made to ensure the randomness of mat structure during each forming process. The mat loading-unloading tests were conducted on an MTS machine with a 222.5 kN load cell at an ambient temperature of approximately 20°C. To minimize the variability in initial mat thickness, all mats were pre-compressed to a thickness of 40 mm prior to testing. Very low stresses (approximately 5 kPa) were detected when the mat was compressed from initial thickness to the pre-compressed thickness indicating that the forces presented during mat pre-compression could be neglected compared with the much larger forces encountered during the later mat compression.

The mats were compressed at a loading rate of 25 mm min^{-1} until the compressive force reached 210 kN. Then the mats were unloaded at the same rate as loading until the mat pressure dropped to zero. Three replicates were conducted for each mat at a given MC. Stress-strain relationships for loading and unloading stage were obtained from the load-displacement results. In addition, the mass of each mat was measured just before testing and after testing and then oven-dried in order to determine moisture loss during testing.

5.5 Results and Discussion

The input parameters for the mat formation model, such as strand geometry, mat size, and target mat density and thickness, are listed in Table 5.1. The generated mat structure as a system of strand columns is used for the heat and mass transfer model. Table 5.2 lists the number of mesh elements in three dimensions of strand mat, the pressing parameters, and boundary conditions during hot pressing, which are representative of the experimental conditions. Note that the MC of ovendry furnish for the model input is 2% according to the measured strand MC prior to pressing. This could be attributed to the wax which was applied in a water emulsion.

5.5.1 Predicted Temperatures and MCs inside the Mat

The comparisons of mat temperature predicted by the model and the experimental results are shown in Figure 5.8a and b, respectively, in which the predicted temperatures generally follow a similar trend to the measured results. Both surface temperature and core temperature changes nonlinearly with time and the temperatures are generally higher in the surface layers. After the platens contact the mat, a temperature gradient is established from the mat surface to the core. During the press closing stage, higher pressure results in more intimate contact between strands and thus enhances heat conduction. This heat conduction contributes to the rapid surface temperature increase while the core temperature does not change much during the first 40 s of the press cycle. When the mat reaches the target thickness and maintains it for resin curing, the mat

surface temperature increases at a relatively slow rate due to the decreasing temperature difference between press plates and mat surfaces.

The moisture contents of the mat layers change in a different manner. Due to the rapid increase of temperature, the moisture in surface strands is evaporated and the vapor pressure in face layer rises quickly and produces a large pressure gradient between the face and core layers. In response steam flows from the face to the core and heats the strands it flows past by convection. Heating by convection becomes the main factor that makes the core temperature increase at a moderate rate approximately after the press closing stage ends. When the cycle enters the venting stage and the press opens, both mat surface and core temperatures drop as the vapor escapes from the mat which takes away the thermal energy.

It is noted that, although the predicted temperatures show reasonable agreement with the measured ones, there are still some discrepancies between model predictions and test data, especially for the mat surface temperature during the press closing stage. One of the causes could be attributed to the inaccurate input mat properties such as thermal conductivity, permeability and compressibility, which were obtained by the experimental work. In addition, the predicted surface temperature from the model is the average value of the face layer while the measured one is the temperature at a specific position in the outer layer. Moreover, the temperature is highly sensitive to the vertical position of the sensors. However, in reality, it is very difficult to place the probes at the expected positions just before the press closes, especially for the positions in face layer. This could

be the reason that there is less deviation between predicted and measured data for the core temperature than the surface temperature in Figure 5.8.

The predicted changes in MC within the various layers during hot pressing are shown in Figure 5.9. It appears that the predicted MCs show a similar trend for the mats with furnish MC of 6% and 2%. When the press platens contact the mat, the surface temperature increases rapidly and this makes the corresponding surface MC decrease rapidly. After the press closes, the surface MC does not change much due to the relatively constant surface temperature. The vapor from the surface is driven into the inner layers by the vapor pressure gradient, where the temperature is relatively lower and then the vapor condenses and leads to an increase in MC in these inner layers. This evaporation and condensation process results in the sequential MC gain and loss within the intermediate and core layer, which makes the predicted MC in these layers appear to be lagging. When the press opens, the MCs in the surface and sub-surface layers increase due to the moisture gained from the ambient environment. Deeper in the panel, the MCs in the inner layers continue to decrease as the vapor escapes from the panel edges.

Figure 5.10 shows the predicted temperature gradients in the thickness direction at different stages during the press cycle. It appears that there exists the maximum temperature gradient in V shape when the mat reaches the target thickness. During the mat thickness holding stage, the core temperature increases at a faster rate than the surface temperature as was seen in Figure 5.8. Note that the magnitude of the temperature gradient will diminish as the core temperature rises. The predicted MC distributions in

the vertical positions at various pressing stages are shown in Figure 5.11. Similarly, the maximum MCs occur at 60 seconds and have a characteristic M-shape. Before the press cycle enters the degas stage at t = 250 s, the migration of moisture to the core is complete and the M-shaped profile has been replaced by an upside-down V shape (which is exactly the reverse of the temperature gradient at the same time). At the end of the press cycle, the core layer still has the highest MC inside the mat and the surface layers gain some moisture mainly from the ambient environment as the press opens.

5.5.2 VDP Model Validation

Based on the predicted temperature and MC distributions from the heat and mass transfer model, the strand compression modulus at a given time during the press cycle can be determined by Eq. (5.8). Then according to the stress-strain relationship for strand columns in compression (Eq. 5.7), the layer deformation and hence the layer density can be obtained with the above-mentioned iterative method. Figure 5.12 shows the typical predicted density profiles at various stages during press closing. Mat density is assumed to be uniform for all layers prior to pressing. After the press platens contact the mat, all layer densities increase with time as the mat thickness decreases. However, the outer layer densities increase at higher rates than inner layer densities because of the lower compression modulus due to the higher temperatures in the outer layers.

It is noted that the density peak occurs in inner surface layer although the surface layer has the highest temperature at t = 60 s. This is because the thermal softening effect in

surface layer due to high temperature could be partially offset by the hardening effect of rapid moisture loss. In the mean time, the temperatures in inner surface layers are relatively high (Figure 5.10) and their MCs are much higher than those in surface layer (Figure 5.11). It is the coupled thermal-hydro-softening effect that leaves the highest density in the inner surface layer. When the mat reaches the target thickness, the most significant VDP has been formed although after that VDP could experience some slight changes due to the mat elastoplascity (Dai et al. 2000) and moisture migration between layers (Winistorfer et al. 2000).

One capability of the proposed VDP model is to predict the local VDP in a designated area within the mat. Figure 5.13 shows the horizontal density distributions in the panel made of 6% MC furnish, where three 50 × 50 mm areas a, b, and c are selected to represent low, medium, and high local densities, respectively. The predicted and measured VDP data for these local areas and the overall mat area are presented in Figures 5.14a-d. It shows that the VDP of low-density area appears to be flatter than that of high-density area. In other words, there are greater density variations between layers within an area of higher local density. This is because there is a greater mass of material in that area, which gives more intimate contact between strands and enhances the heat conduction and diminishes the heat convection due to moisture migration from surface to core. Therefore, increasing gradients of temperature and MC are established, thus making the layer densities vary more significantly. As expected, the overall panel VDP appears to be much smoother than the individual samples due to the average effect. Figure 5.15 compares the VDP of a panel with dry strands between the model predictions and

experimental results. The density variations between outer layers and core layers inside the panel with dry strands are less significant than those of the panel with 6% MC. This is because more moisture in a mat will increase the heat transfer and hence increase the plasticization of the furnish, which results in the higher peak densities.

Each predicted VDP generally shows a similar shape to the measured one, both of which are in the shape of letter M. However, there are still some discrepancies between model predictions and measured data. Particularly, the predicted surface densities are much higher than the measurements and the model underestimates the densities of the inner layers. This could be attributed to the inaccurate characterization of material properties. For example, an important variable in the model – the strand compression modulus is highly dependent on the local temperature and MC within the mat, which are both predicted from the heat and mass transfer model. Unfortunately, some discrepancies are found between the predicted values and measured ones for temperatures and MCs, which will lead to the inaccuracy in the predicted modulus.

On the other hand, the function (Eq. 5.7) for compression modulus itself was empirically determined by experimental work, which also could introduce some uncertainties to the VDP model. If the surface layer densities are overestimated in the model, at a given target panel density, this will unavoidably result in the underestimated core layer densities. Furthermore, the predicted VDP is still in the press cycle while the measured data were obtained from the samples after conditioning. Thus how the moisture

distributes within the samples could also contribute to the discrepancies between model predictions and measured data.

In fact, the measured surface density is significantly low, which is even lower than the core density. This is believed to be associated with the precure or dryout of the resin in surface layers (Maloney 1993). When hot platens first come in contact with the mat, due to the high temperature (usually more than 150°C), resin curing occurs almost instantaneously in the surface layer. This causes the face strands to be hold in a set position of low density, thus causing the surface layers to be harder to further densify during the reminder of press cycle. After the press opens, the surface density could decrease further due to the springback of the face layers (Dai 2000).

The positions of the predicted peak densities are more inward than those of the measured ones. One of the possible causes could be attributed to the limited number of mesh elements in the thickness direction. For the model development, the mat is evenly divided into 12 layers in the vertical direction prior to pressing. In other words, only these 12 layer densities are used to represent the predicted VDP curve while the measured VDP curve consists of more than 180 density data. It is quite certain that the latter should be more accurate especially for the position of peak density. In addition, the predicted surface density is the average value of one layer while the measured one is relatively specific for one location. One could expect that the accuracy of the model predictions would be improved if more layers are divided in the thickness direction.

5.5.3 Predicted Effects of Pressing Variables on VDP Formation

Press closing time is one of the most significant factors in determining panel properties. By manipulating this factor, a number of density profiles can be developed to achieve the desired panel properties. Figure 5.16 presents the effect of closing time on the VDP formation in which the other pressing parameters are held constant in Table 5.2. As expected, the closing time significantly changes the VDP curves; the shorter the closing time, the higher the peak density and the lower the core density. In other words, the VDP appears to be more uniform as the closing time increases. For the shorter closing time, there is less heat transferred from the platen to the core when the mat reaches the target thickness. This results in a sharper temperature gradient between face layers and core layers. Thus there exists a more significant difference between the compressibility of face layers and core layers. At slower press closing times, the temperature gradient in the thickness direction is less pronounced at the target panel thickness, which leads to the more uniform density profiles. In addition, the position of peak density moves outward to the surface when the press closes faster, which makes the VDP more U shaped than M shaped. It implies that both the value and the position of peak density are sensitive to the press closing rate. This leads to the conclusion that faster pressing closing rates can improve the panel properties such as bending and stiffness but are detrimental to internal bond strength due to the low core density.

Another factor in altering VDP is initial mat temperature. In fact, preheating the mat before it enters the press can reduce both pressing time and required maximum pressure

and thus improve the productivity. The effect of initial mat temperature on the VDP formation is shown in Figure 5.17, and likewise, the other conditions are the same as in Table 5.2. Higher initial mat temperature increases the core density while decreasing the face density because of the less significant temperature gradient between the face and core layers, which produces more uniform density profiles. To some extent, preheating the mat is similar to closing press slowly, both of which result in lower peak densities and more inward peak density positions.

5.5.4 Sensitivity Analysis of VDP Model

The predicted core densities, shown in Figure 5.14, are consistently lower than the measured results. Some input parameters for the VDP model, i.e., the temperature and MC distributions within the mat, are based on the predictions from an existing heat and mass transfer model (Dai and Yu 2004) and may not correspond to the actual conditions within the mat. The magnitude of these predicted temperatures and MCs within the mat may have a very large effect on the predicted VDP of the panel. As such, a sensitivity analysis of these input parameters on the predicted VDP is needed in order to assess the likelihood that the discrepancy between the model predictions and the experimental results are due to these differences.

Inaccuracy in the heat and mass transfer model will manifest itself mostly in the core of the panel as it is farther away from the platens, i.e., the boundaries. In order to simulate this, the temperatures and MCs of the middle six layers of the panel were adjusted by

±20% for temperature and ±30% for MC. The value of 20% is somewhat arbitrary but it is thought to represent the most extreme difference between model and actual temperatures. The value of 30% for MC was chosen as it is representative of the range of MC values one typically encounters in a plant, i.e., the MC in the strands ranges between 4 to 6% and this range corresponds to a change of approximately 30%. As the VDP of panel is formed when the mat reaches its target thickness (i.e., t = 60 s) and thereafter experiences only minor changes (section 5.5.2), this was chosen as the time at which the VDP distributions for these different conditions were compared.

The input parameters for the base case are those listed in Table 5.2 except that the initial MC was set at 6%. The new panel VDP for each condition was determined by changing the temperature or MC in the six core layers by the appropriate amounts, which changes the local E value for each layer, and then computing the new equilibrium thickness of each layer subject to the overall panel thickness being constant.

The predicted VDP curves for the ±20% temperature difference are compared in Figure 5.18. As expected, compared to the base case, the +20% core temperatures made wood elements softer and more compressed , which resulted in thinner layers in the core and thicker layers on the faces. In the reverse case, the core layers were cooler and therefore stiffer, resulting in less deformation of the core layers with the correspondingly denser face layers compared to the base case as a result.

The sensitivity of the core layer densities to changes in MC are compared in Figure 5.19. As was the case for temperature, increasing MC produced core layers that were again softer than those in base case and therefore the core layer densities increased with the reverse being true for a decrease in MC. Comparing these outcomes with the under-prediction of the measured VDP in Figure 5.14 strongly suggests that the heat and mass transfer model predict temperatures and MCs that are in fact lower than those actually experienced by the mats during pressing. Further work is needed to improve the accuracy of the heat and mass transfer model, which will in turn help the VDP model.

5.5.5 Mat Stress Relaxation

Figure 5.20a and b show the stress relaxation behavior of the mat during hot pressing from experimental results and model predictions, respectively. In general, the model predictions display the similar trend to the test data except that there is no pressure holding stage in the model according to the model assumptions. The stress required to reach the target thickness for the mat with 2% MC is higher than that for the mat with 6% MC due to its higher compression modulus. It seems that the predicted maximum stresses are lower than the measure ones. This could be attributed to the inaccurate material properties such as relaxation modulus and relaxation rate, which were empirically obtained at elevated temperature and moisture levels. For the experimental results, an increase in MC results in a faster relaxation rate and a lower plateau stress. Based on the viscoelastic behavior of wood strands during hot pressing (Chapter IV), the proposed

model for predicting the viscoelastic response of strand mat well captures this important characteristic as shown in Figure 5.20b.

As reported by Dai et al. (2000), the drop in mat pressure during the holding stage is a coupled response of mat softening due to the decrease of compression modulus and stress relaxation due to the viscoelastic properties of wood. Consequently, the curves in Figure 5.20b are then broken down into the more specific ones as shown in Figure 5.21, which imply that the softening effect is more significant than the viscoelastic effect for the drop in mat pressure. Another possible explanation for the lower pressure could be attributed to resin, which is already cured and holding the strands in their set position (Maloney 1993).

5.5.6 Mat Elastoplasticity and Springback

The experimental results of mat elastoplasticity at various moisture levels are presented in Figure 5.22, in which the stress-strain curves go through different paths during loading and unloading. Take the mat with 15% MC for example; the loading curve starts from point O to point A while the unloading curve goes from point A to point C. If the mat is perfectly elastic, the unloading curve would exactly follow the loading curve from A to O. If the mat is perfectly plastic, there would be no change in strain when the stress drops to zero, which means the unloading curve would be the vertical line AB. In fact, the unloading curve AC lies between AO and AB, which means the mat exhibits elastoplastic characteristics.

The loading and unloading curves generally follow similar trends for different moisture levels. However, at a given stress during loading, the mat with a higher MC undergoes a larger strain due to its lower compression modulus. Similarly, at a given stress during unloading, the mat with a higher MC also exhibits a larger irreversible deformation due to the plastic properties. For the purpose of modeling, the stress-strain relationship during unloading is expressed in a mathematical equation using a curve fitting technique:

$$\frac{\varepsilon - \varepsilon_0}{\varepsilon_0} = c_p \ln \frac{\sigma}{\sigma_0} \tag{5.25}$$

where ε is mat strain, ε_0 is the initial strain at which the mat stress starts to drop, σ is mat stress, σ_0 is the stress corresponding to ε_0, c_p is a coefficient for characterizing the mat plasticity.

Based on the stress and strain obtained from the unloading curve, c_p is 0.025 for the dry mat, 0.022 for the 6% MC mat, and 0.019 for the 15% MC mat. Figure 5.23 compares the results from Eq. (5.25) and the experiment, which appears that the model predictions agree well with the test data. According to this equation, at a given stress of 1.1 MPa, the corresponding mat strain and springback are listed in Table 5.3. It shows that the mat with a higher MC undergoes less springback because it exhibits more plasticity. Thus, the coefficient c_p can be viewed as a characteristic for mat plasticity; the smaller the coefficient, the less the mat springback. In addition, the mat springback will become more significant when the mat pressure finally drops to zero.

This is just a preliminary study as only the effect of MC on mat elastoplasticity were investigated, and the temperature and resin curing were not taken into account. One would expect that the mat springback would reduce with an increase in pressing temperature and degree of resin curing. Moreover, such effects have an impact on the formation of VDP, particularly surface mat density after pressing. For example, it is thought that resin curing causes the surface panel density to decrease after the panel is released from the press. Due to the relatively low temperature and MC, the inner layers would exhibit more springback. As a result, at the fixed target mat thickness, the springback in the inner layers will inevitably lead to the further densification in the layers close to the surface.

5.6 Summary and Conclusions

Combining a 3D heat and mass transfer model for hot pressing (Dai and Yu 2004) and a mat formation model (Dai and Steiner 1994a, b), a comprehensive model was developed to simulate the VDP formation for strand-based wood composites. The model takes into account both mat forming and pressing variables, and therefore can predict both vertical and horizontal density variations. The strand deformation was explicitly modeled in terms of localized temperature, MC and compression modulus. The VDP model predictions were validated by comparing with the measured results. Localized VDP formation was found to be highly dependent on the corresponding local panel density, where the vertical density variations in high-density area were greater than those in low-density area. Also, increasing mat MC resulted in higher density values in VDP. As well

the predictive effects of key pressing variables on VDP formation were presented. Preheating was predicted to reduce the VDP, whereas the faster press closing can increased the VDP. Compressive viscoelasticity and elastoplasticity of a strand mat were also modeled. For the drop in mat pressure at the holding stage, thermal softening was found to be a much more significant factor than viscoelasticity. In addition, increasing mat MC was found to reduce the degree of mat springback.

Table 5.1 Parameters for mat formation model

Parameter	Input value
Strand length λ (mm)	110.3
Strand width ω (mm)	23.4
Strand thickness τ (mm)	0.7
Strand dry density ρ_{ds} (kg m^{-3})	380
Mat length L_m (mm)	710
Mat width W_m (mm)	710
Target panel thickness H_m (mm)	11.1
Target panel density ρ_m (kg m^{-3})	670

Table 5.2 Parameters for heat and mass transfer model

Parameter	Input value
Number of elements in mat length direction N_x	14
Number of elements in mat width direction N_y	14
Number of layers in mat thickness direction N_z	12
Initial mat MC (%)	6 or 2
Initial mat temperature (°C)	25
Press platen temperature (°C)	205
Ambient temperature (°C)	25
Press closing time (s)	60

Table 5.3 Mat strain and springback at σ = 1.1 MPa during unloading

MC (%)	Maximum mat strain ε_0	Mat strain ε	Springback (%)	Coefficient c_p
0	0.716	0.679	5.2	0.025
6	0.733	0.701	4.4	0.022
15	0.773	0.742	3.9	0.019

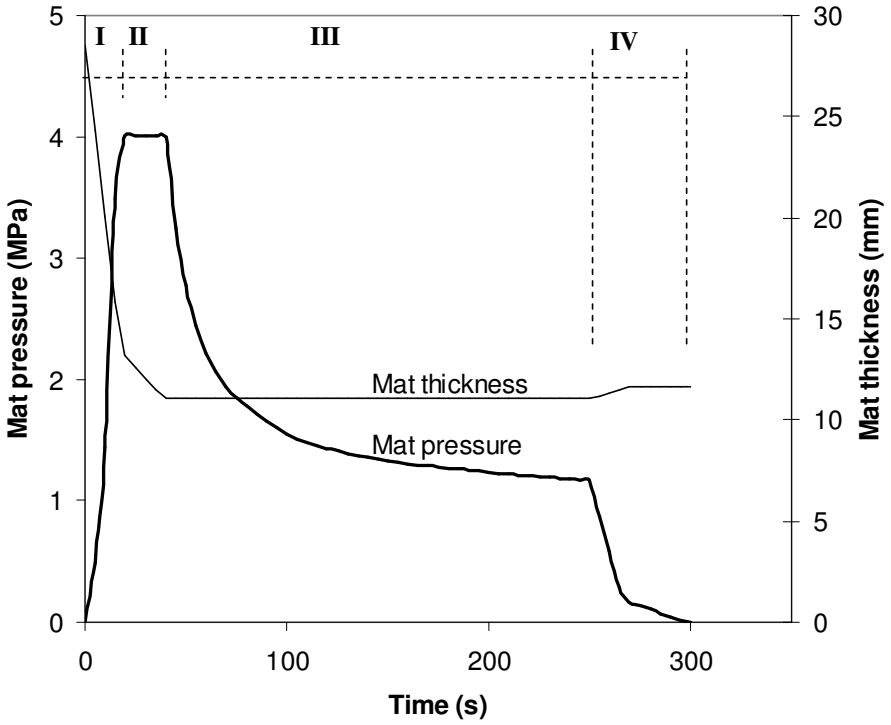

Figure 5.1 An idealized press cycle for OSB hot pressing.

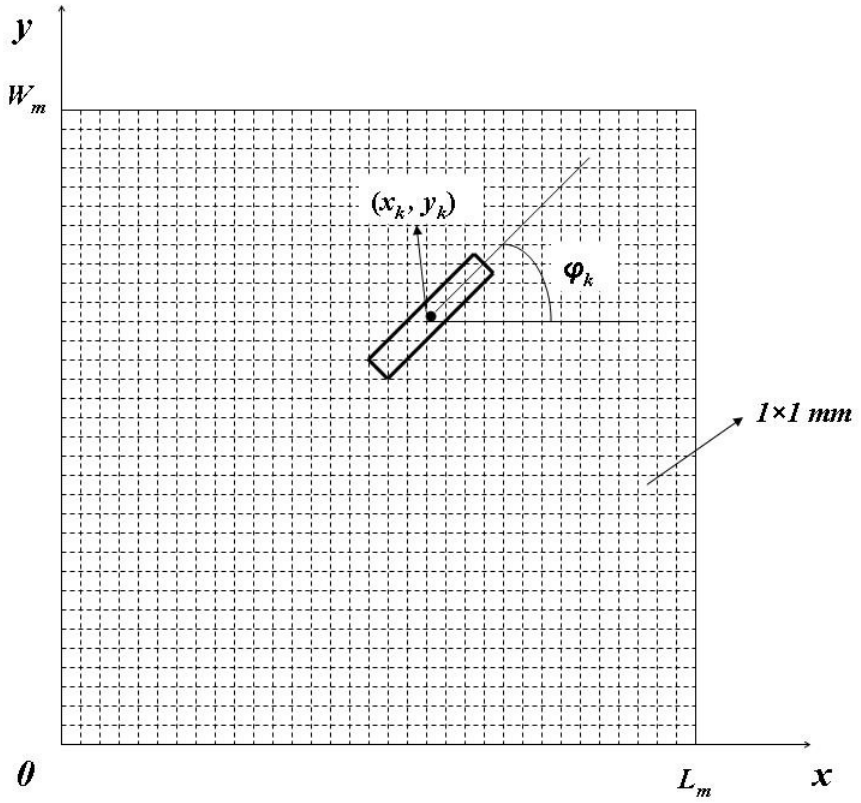

Figure 5.2 Schematic of a strand positioned in a mat forming area viewed as a grid system.

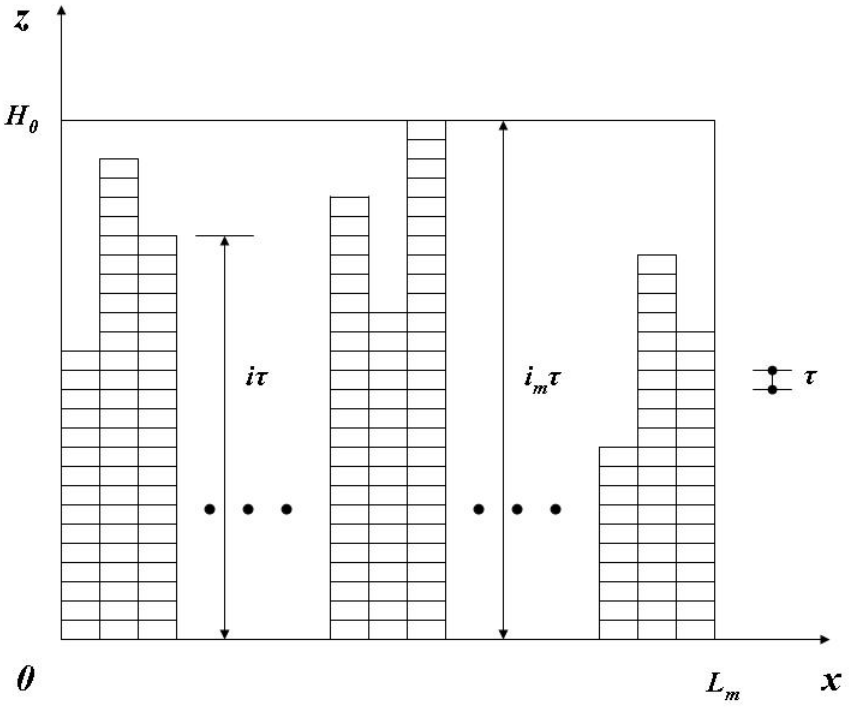

Figure 5.3 Schematic of a mat consisting of strand columns with different overlap number.

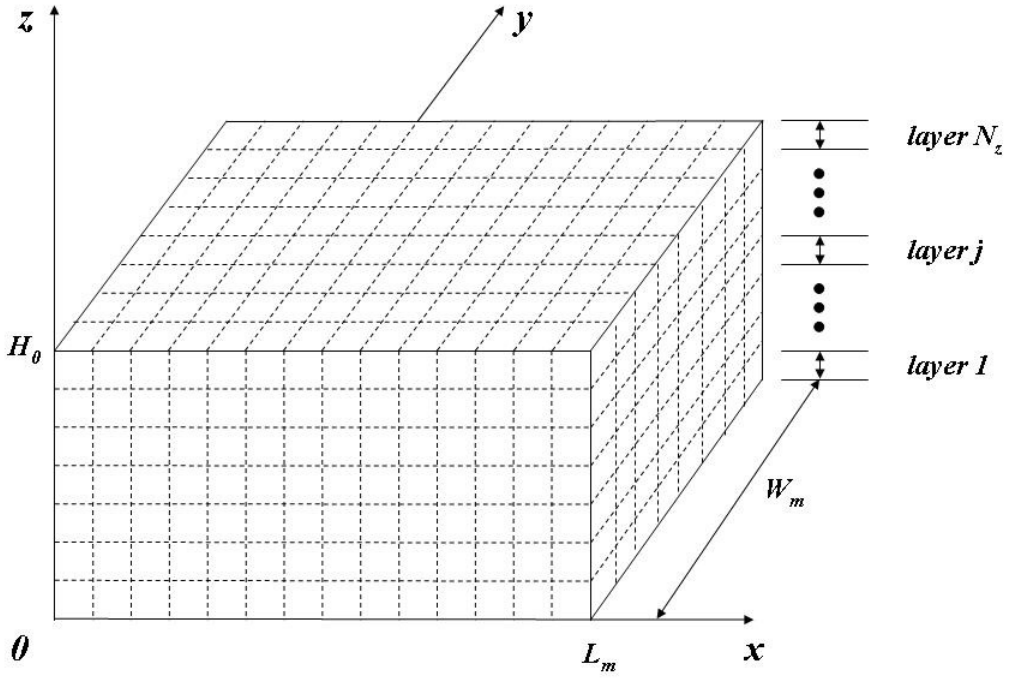

Figure 5.4 Schematic of a mat consisting of strand columns with N_z layers.

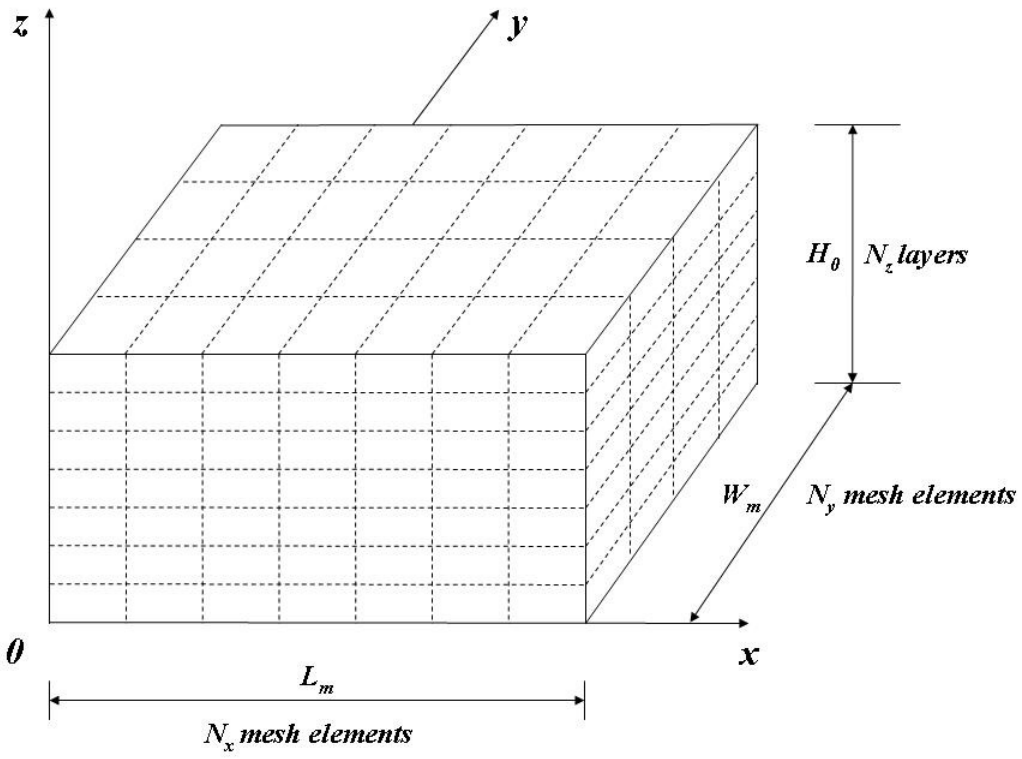

Figure 5.5 Schematic of a strand mat structure for heat and mass transfer model.

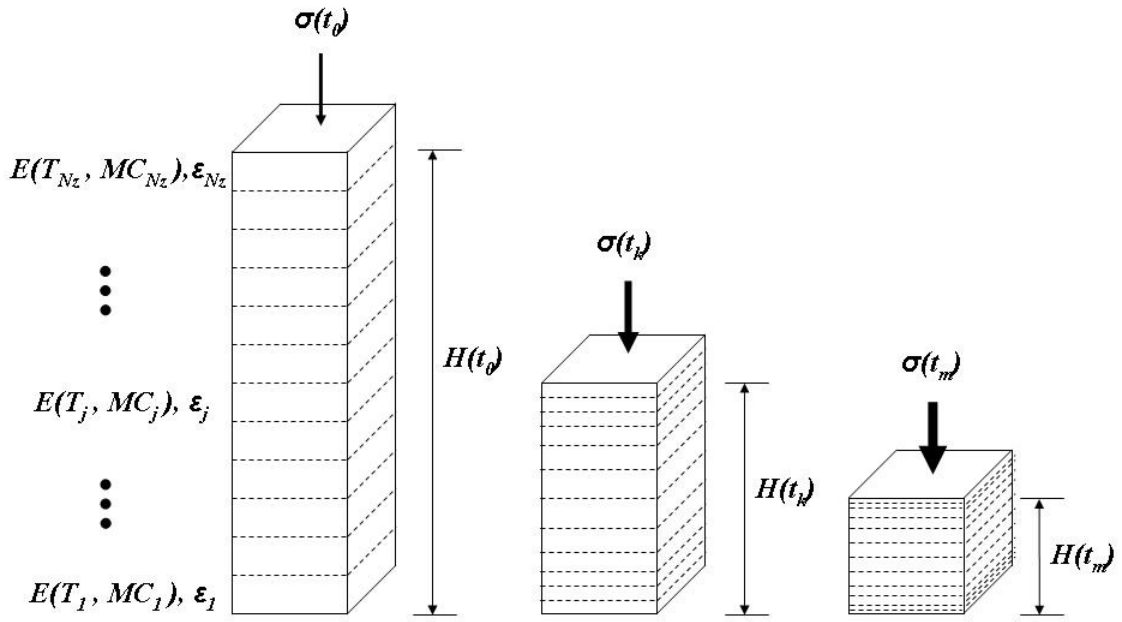

Figure 5.6 Schematics of a strand column in compression at different time steps during press closing.

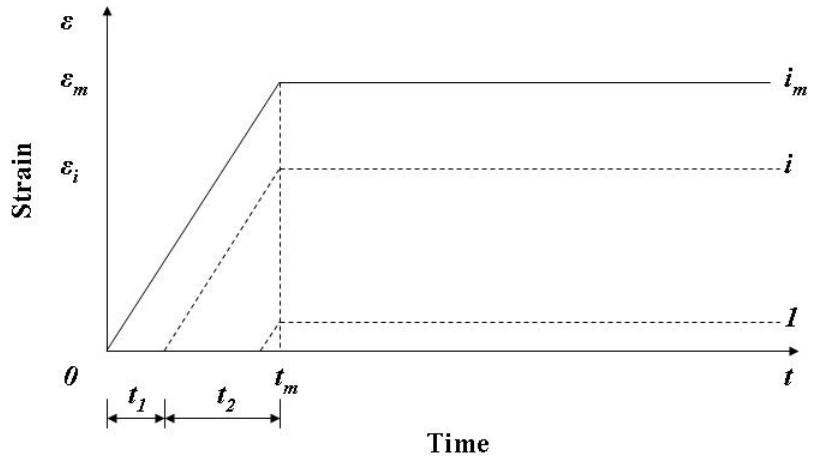

Figure 5.7 Schematic of linear loading strain histories for strand columns in compression.

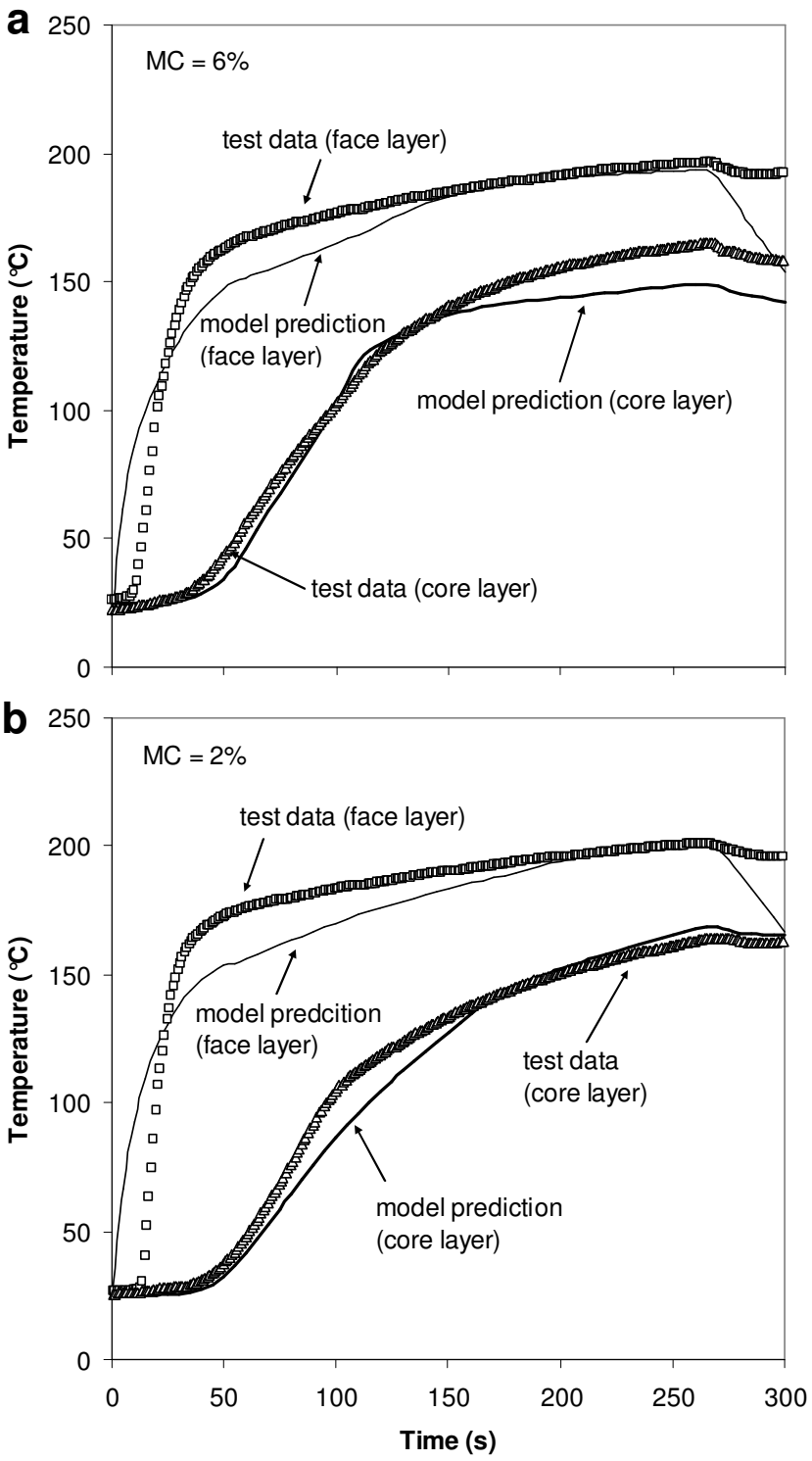

Figure 5.8 Comparison of predicted temperatures in face and core layers of a stand mat with experimental results.

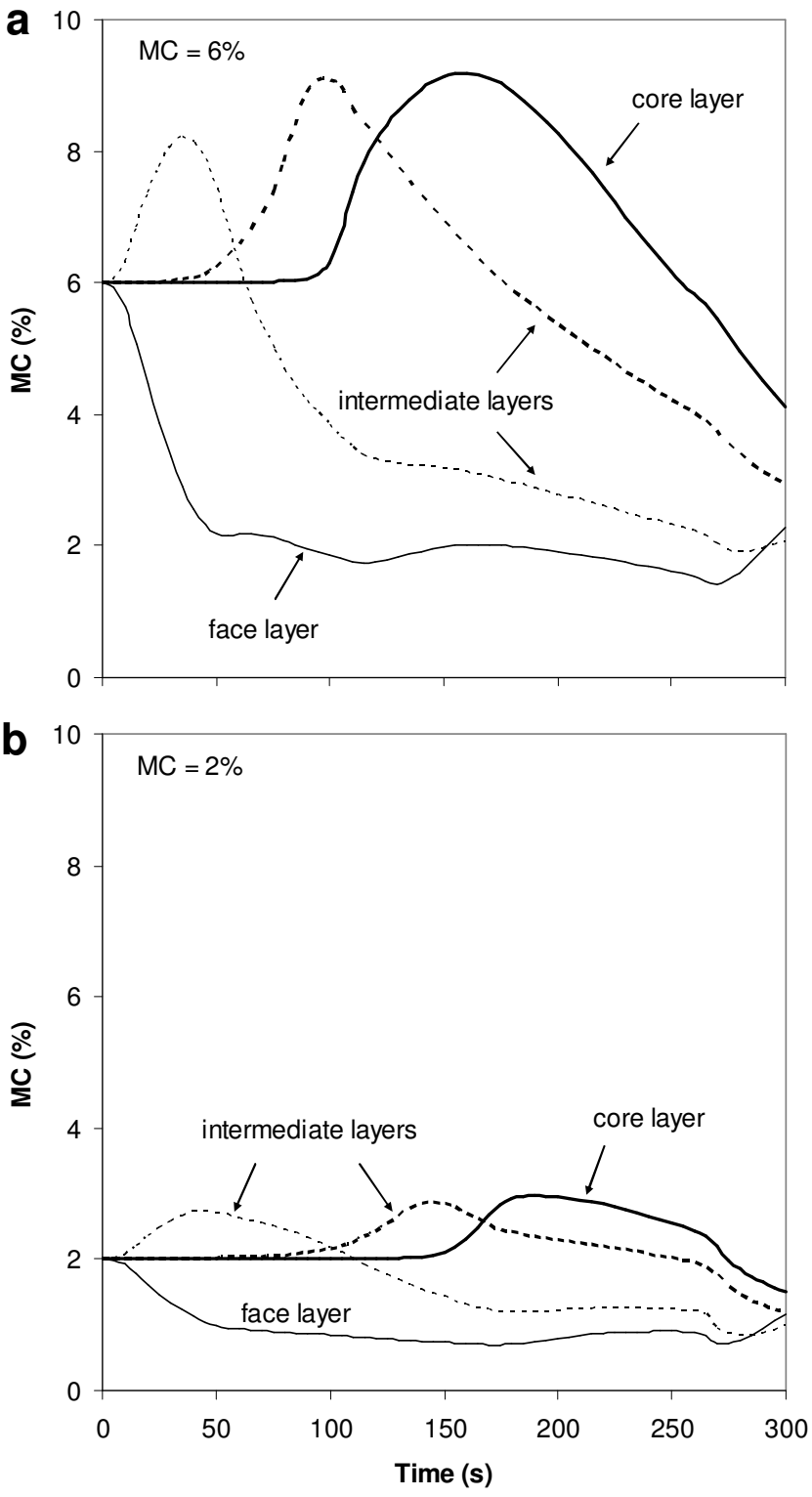

Figure 5.9 Predicted MC changes in different layers during hot pressing.

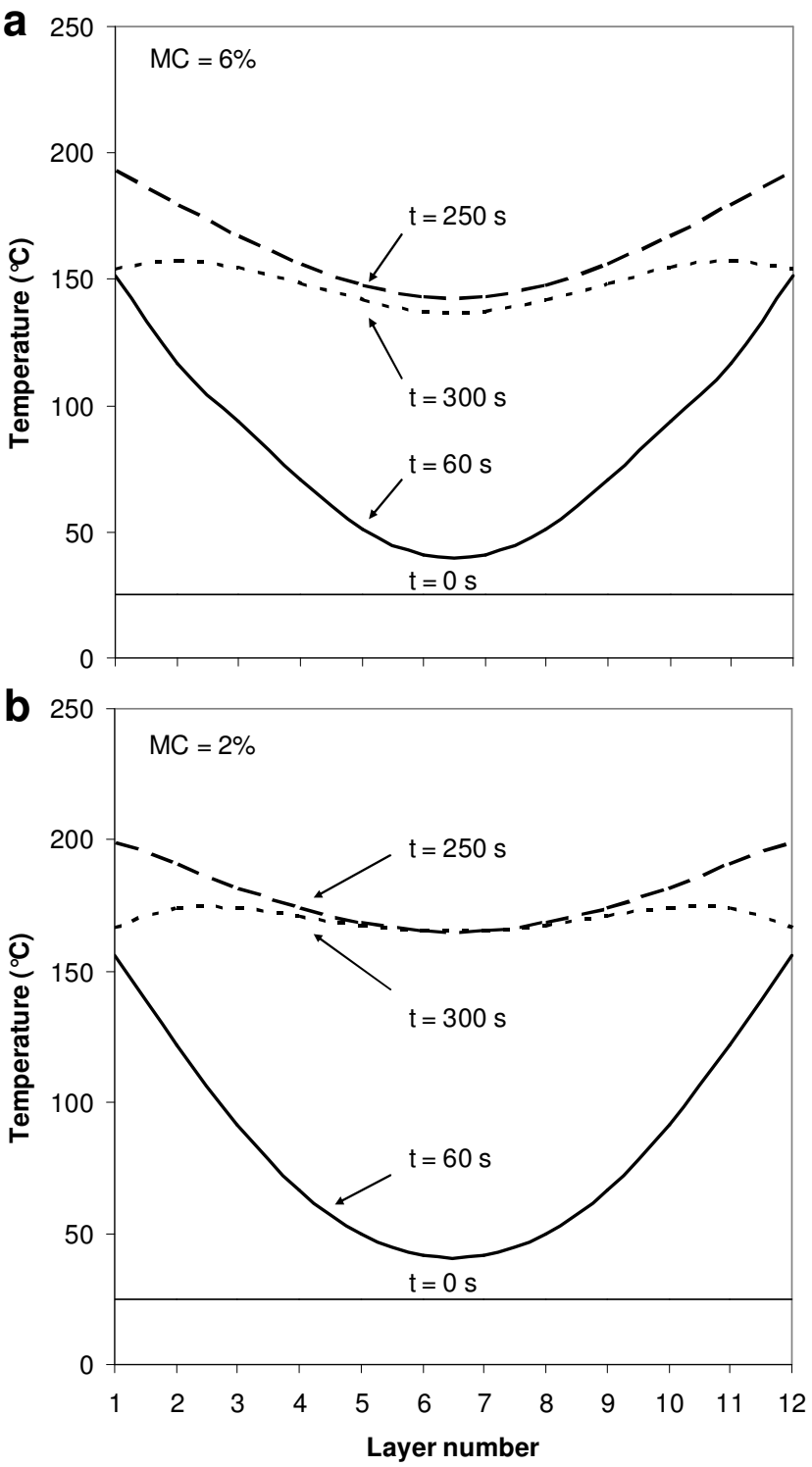

Figure 5.10 Predicted temperature distributions inside the mat at various stages during hot pressing.

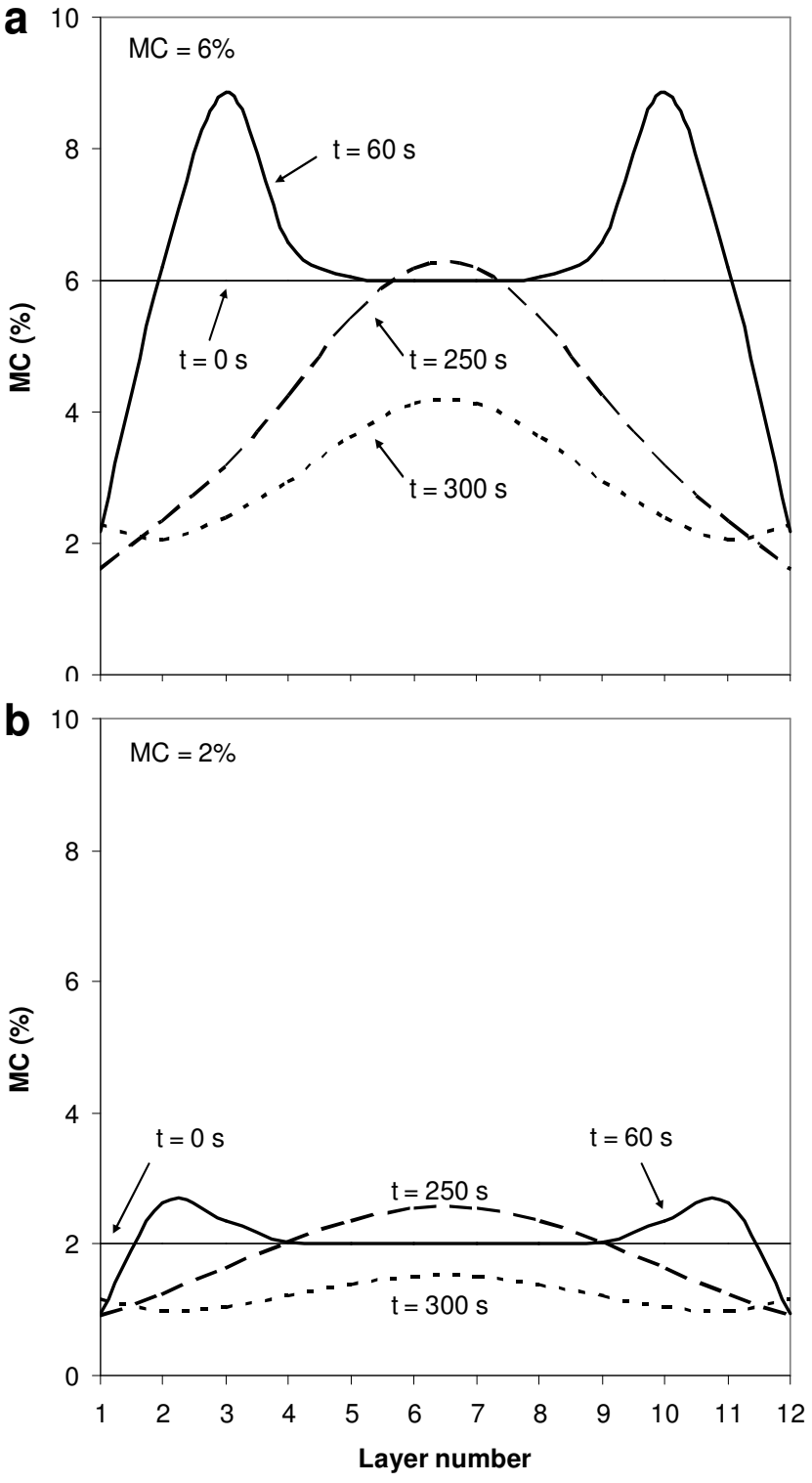

Figure 5.11 Predicted MC distributions inside the mat at various stages during hot pressing.

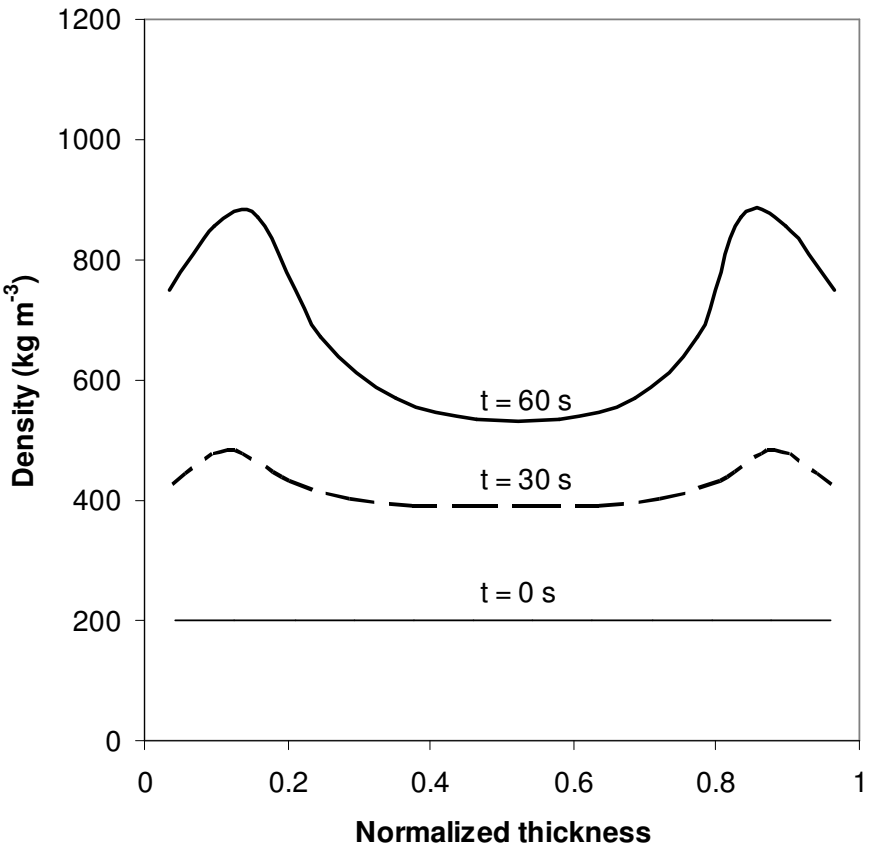

Figure 5.12 Development of the VDP in a strand mat at different times during press closing as predicted by the model (MC = 6%).

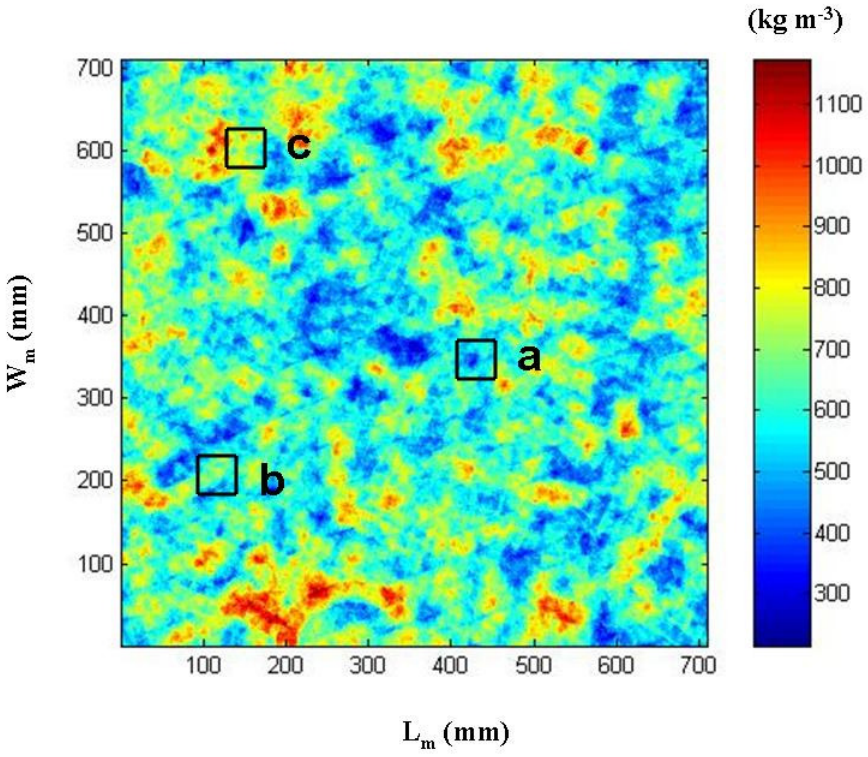

Figure 5.13 Horizontal density distribution within the mat at the target thickness (MC = 6%).

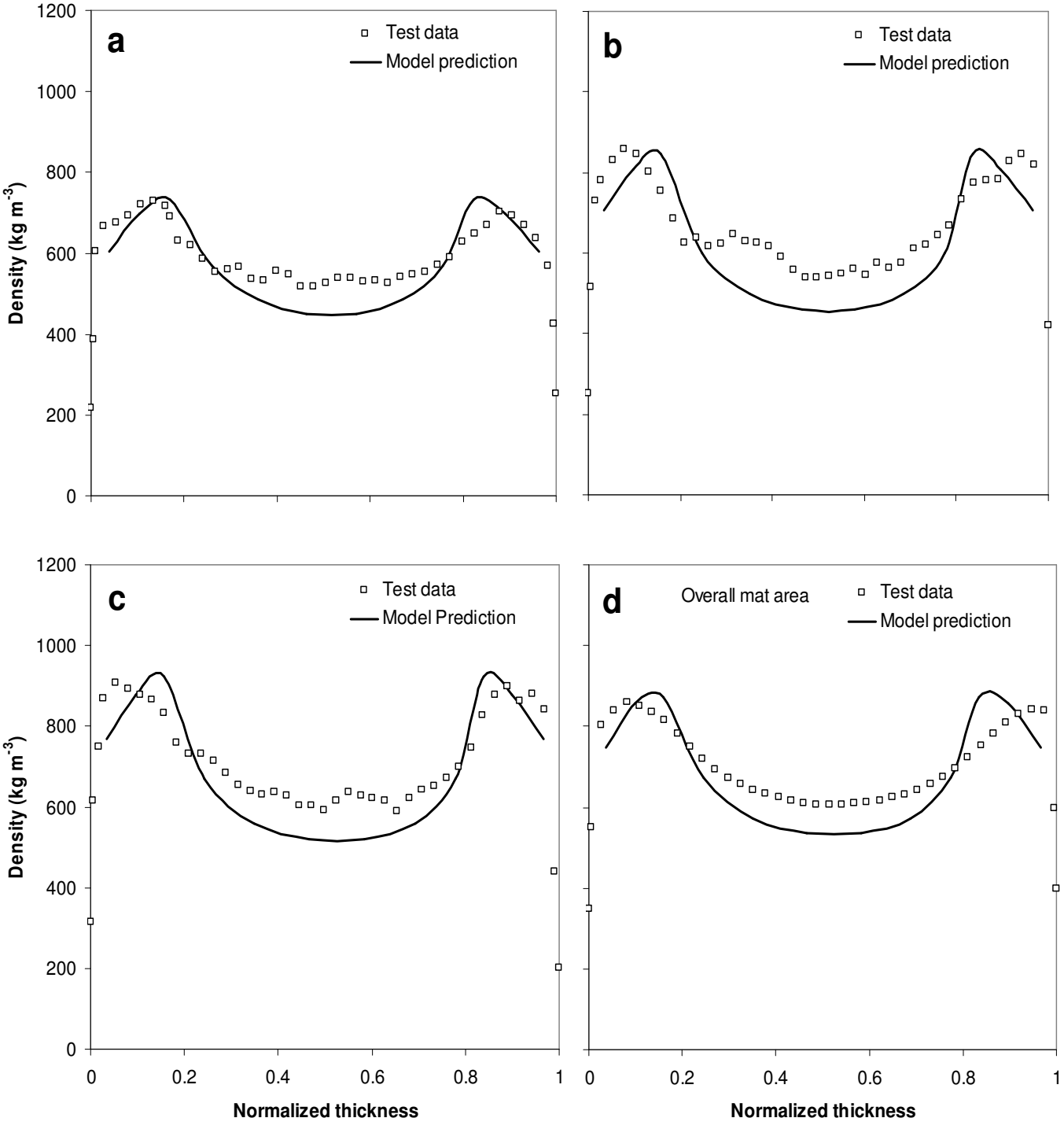

Figure 5.14 Comparison of predicted local VDP in Figure 5.13 with the measured data from 50 × 50 mm samples. (a) average local density = 591 kg m^{-3}, (b) average local density = 656 kg m^{-3}, (c) average local density = 713 kg m^{-3}, (d) overall mat density = 680 kg m^{-3}.

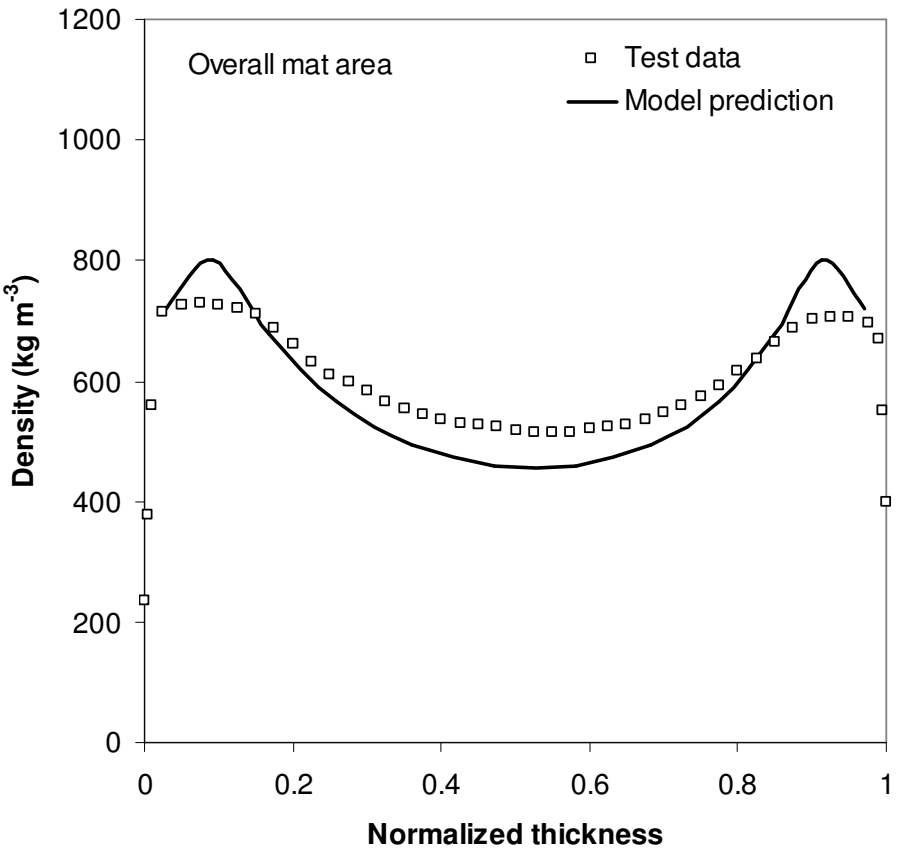

Figure 5.15 Comparison of the predicted VDP for a panel made from ovendry strands and the measured results from a panel made under the same conditions.

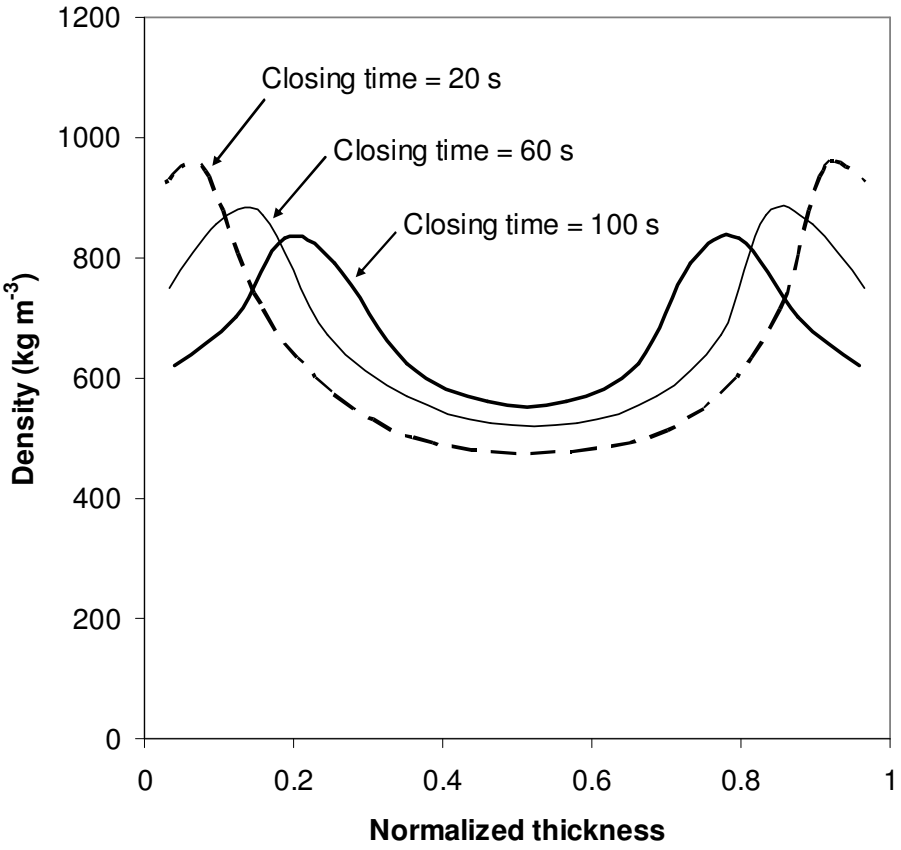

Figure 5.16 Comparison of the shape of the panel VDP for three press closing times.

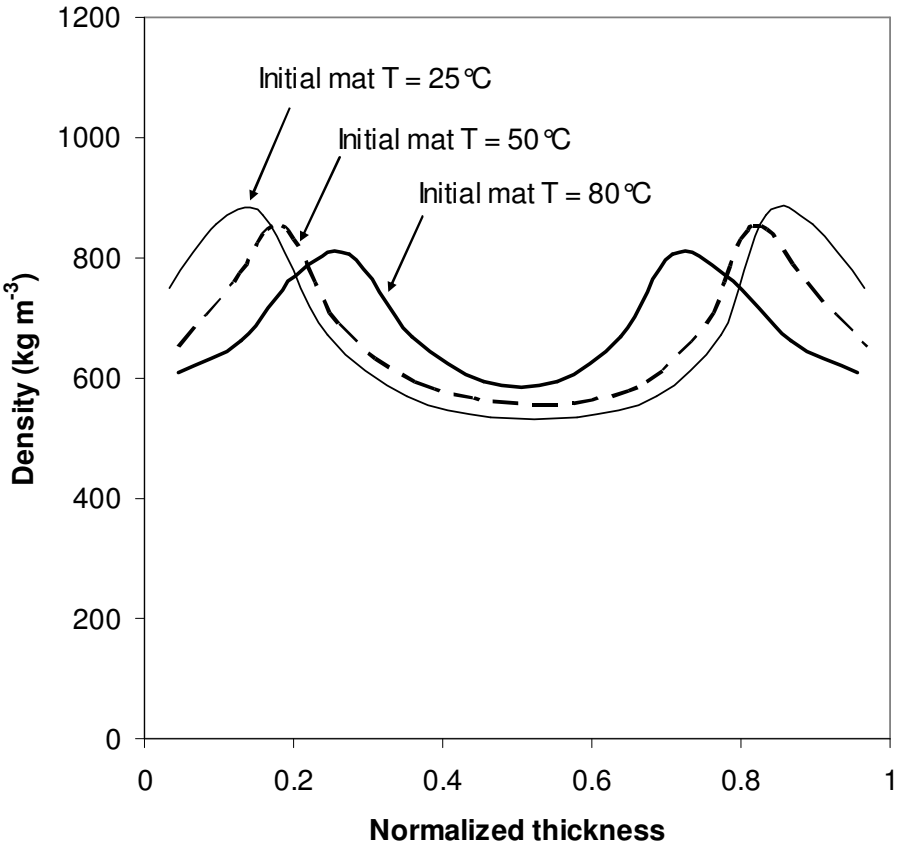

Figure 5.17 Comparison of the shape of the panel VDP for three initial mat temperatures.

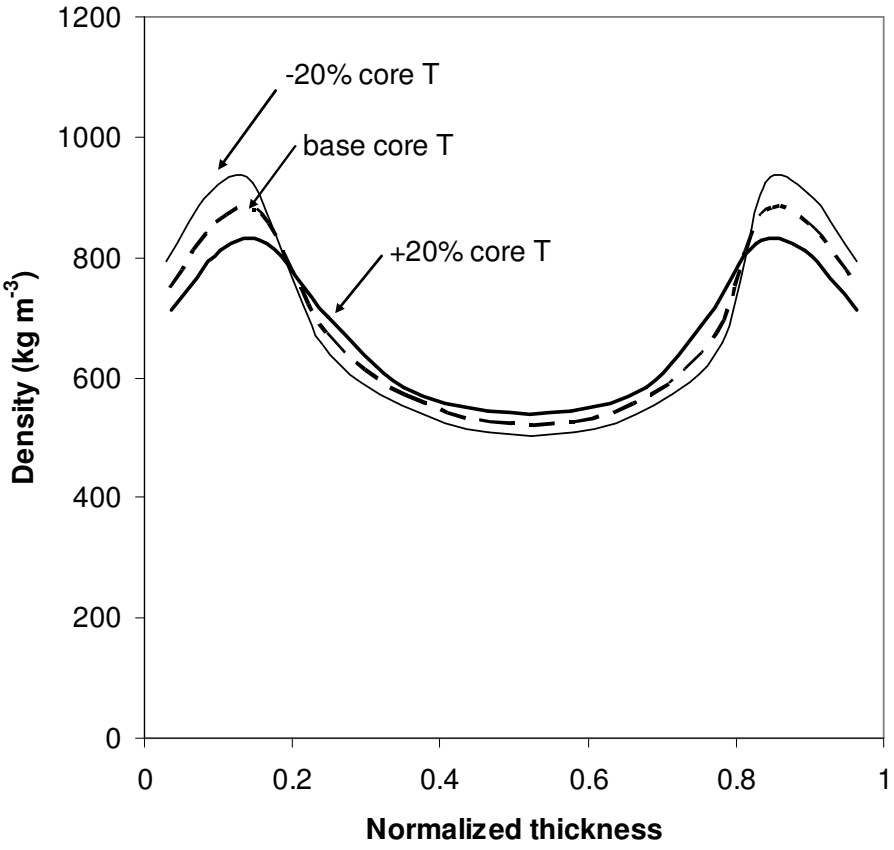

Figure 5.18 The effect of a 20% change in core temperatures on the shape of the panel VDP.

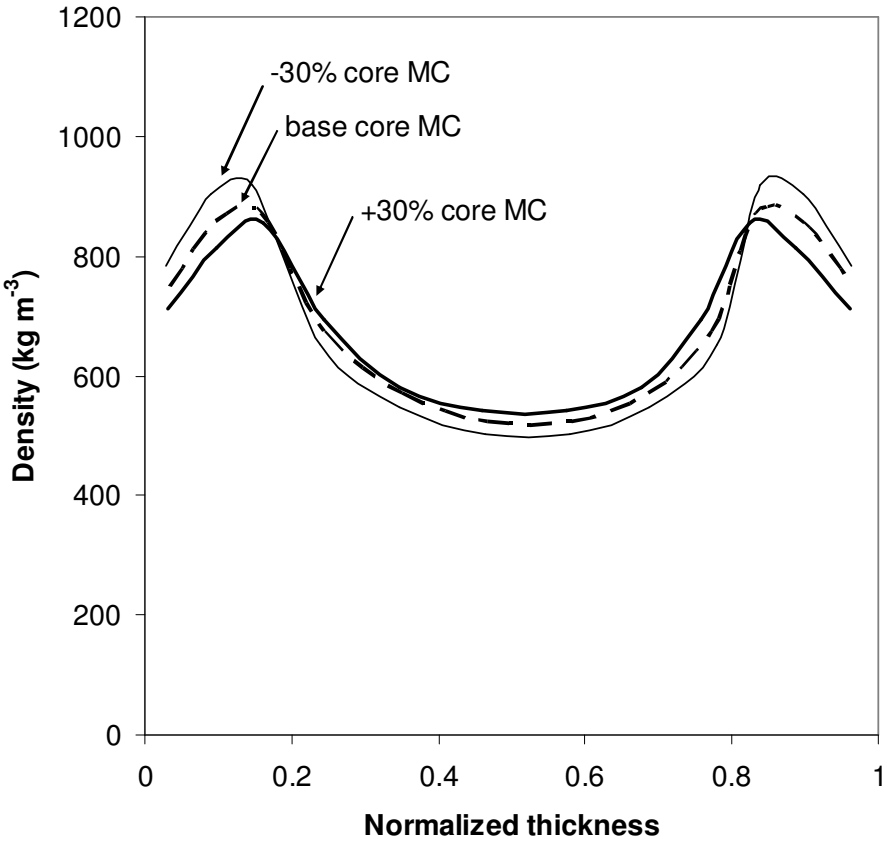

Figure 5.19 The effect of a 30% change in core MCs on the shape of the panel VDP.

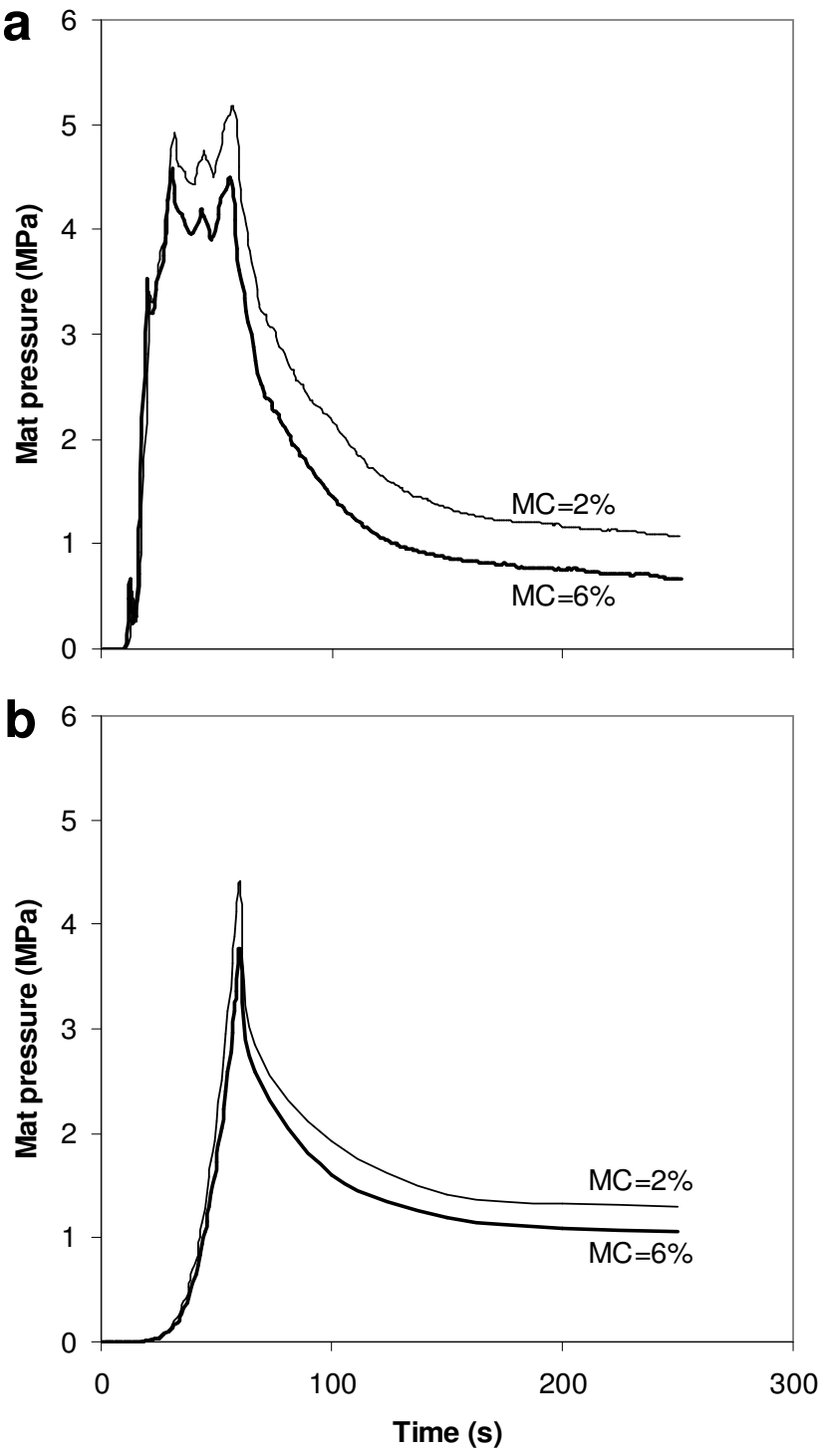

Figure 5.20 Stress relaxation behaviour of mat during hot pressing. (a) experimental results, (b) model predictions.

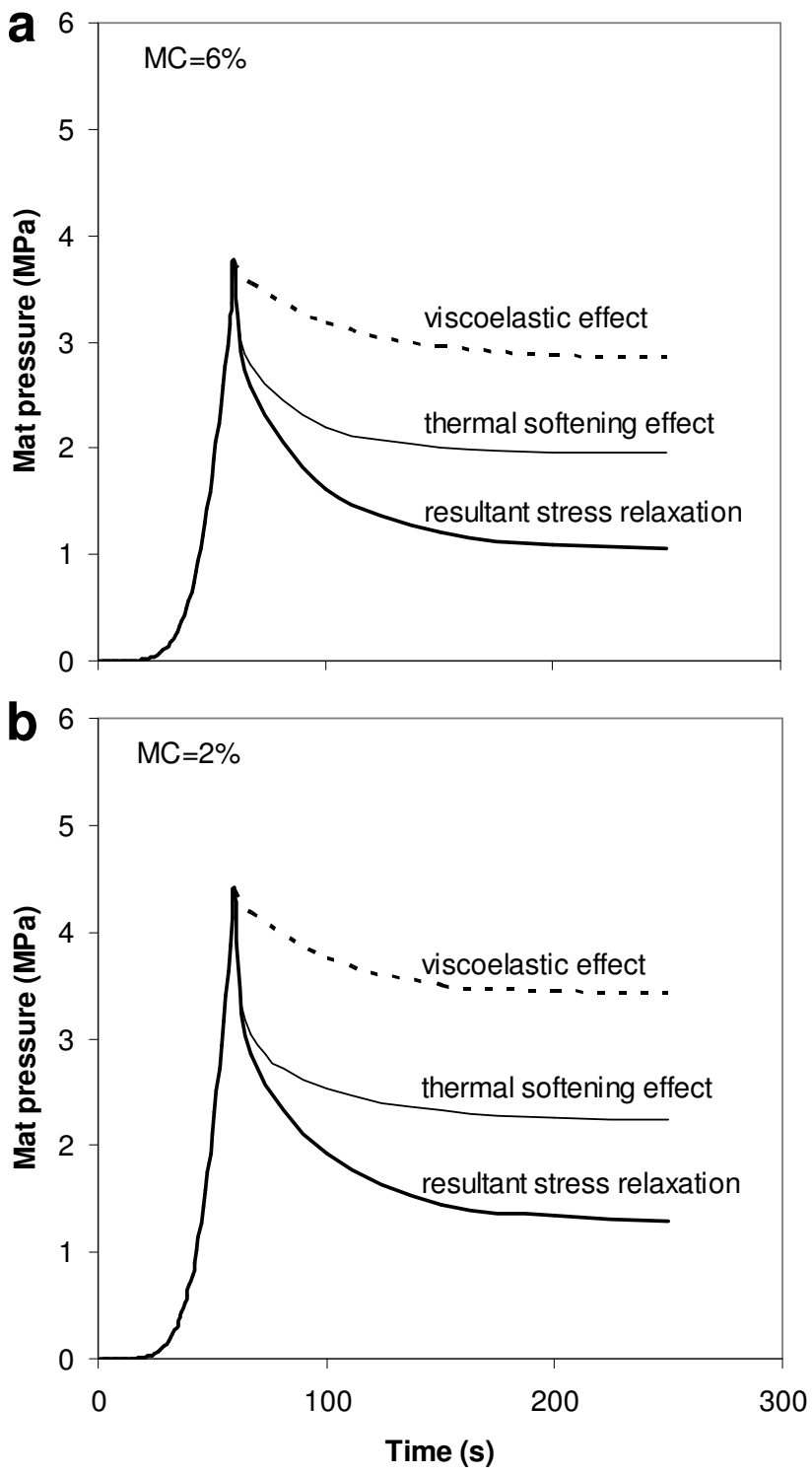

Figure 5.21 The mat pressure decrease as a coupled response of thermal softening and viscoelastic stress relaxation.

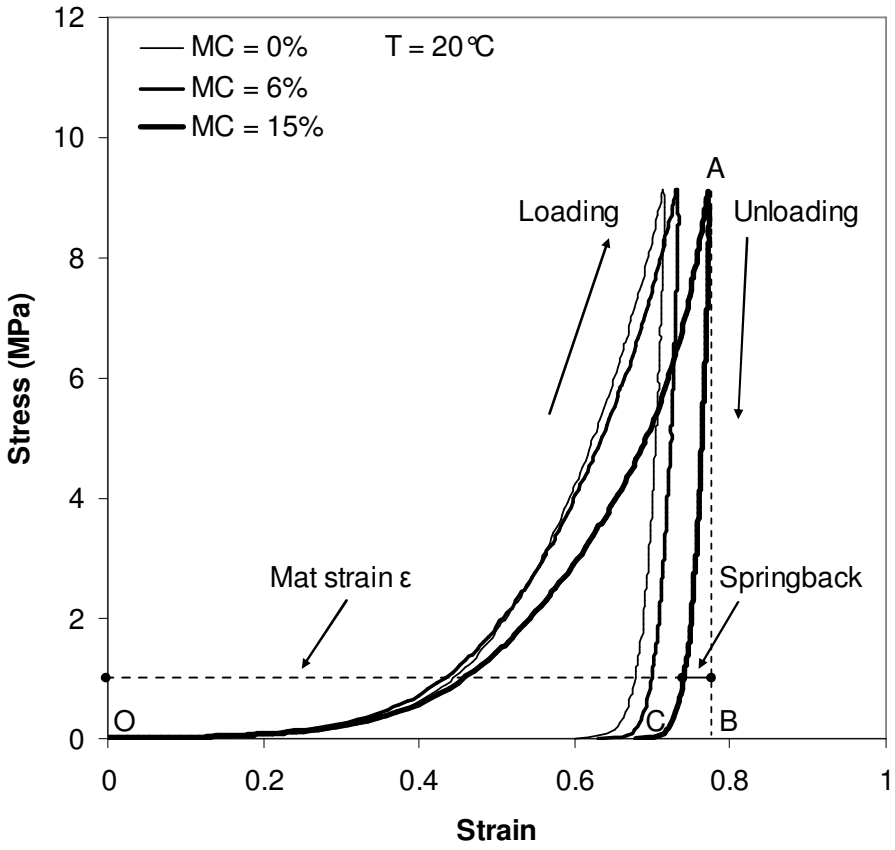

Figure 5.22 The elastoplastic behaviour of strand mat at various moisture levels.

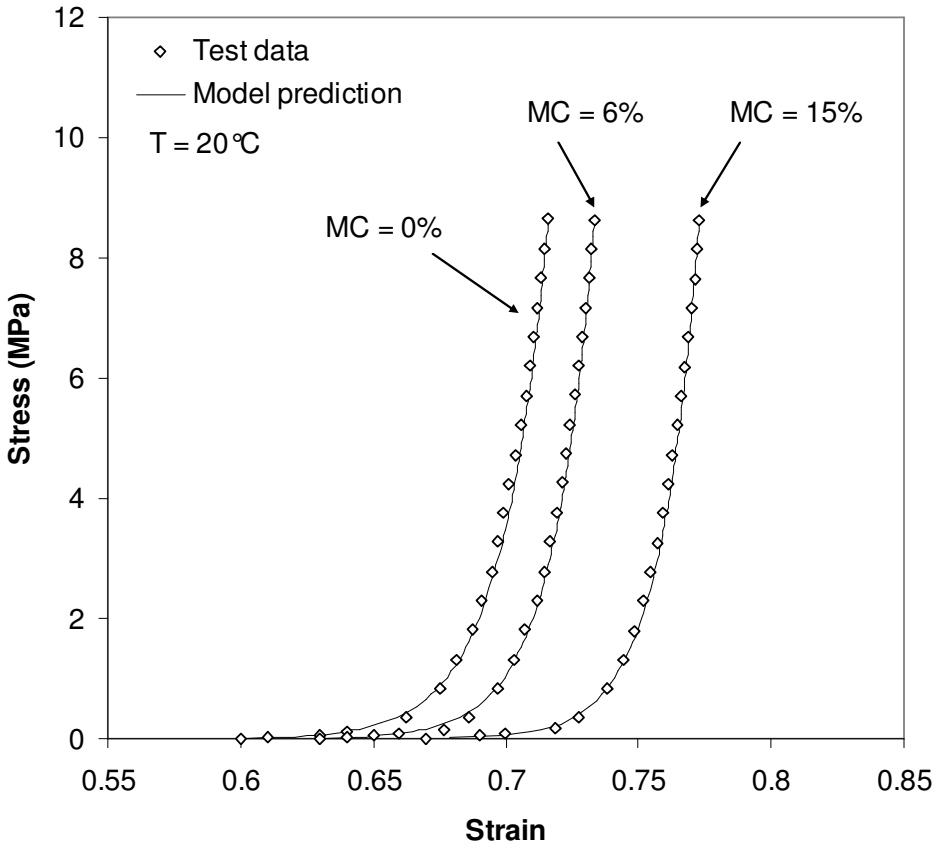

Figure 5.23 Comparison of stress-strain relationship during unloading between experimental results and model predictions.

5.7 Bibliography

Andrews, C.K., Winistorfer, P.M., Bennett, R.M. (2001) The influence of furnish moisture content and press closure rate on the formation of the vertical density profile in oriented strandboard. Forest Prod. J. 51:32-39.

Bolton, A.J., Humphrey, P.E. (1988) The hot-pressing of dry-formed wood-based composites. Part I. A review of the literature, identifying the primary physical process and the nature of their interaction. Holzforschung 42:403-406.

Carvalho, L.M.H., Costa, C.A.V. (1998) Modeling and simulation of the hot-pressing process in the production of medium density fiberboard (MDF). Chem. Eng. Comm. 170:1-21.

Carvalho, L.M.H., Costa, M.R.N., Costa, C.A.V. (2001) Modeling rheology in the hot-pressing of MDF: comparison of mechanical models. Wood Fiber Sci. 33:395-411.

Carvalho, L.M.H., Costa, M.R.N., Costa, C.A.V. (2003) A global model for the hot-pressing of MDF. Wood Sci. Technol. 37:241-258.

Dai, C. (2001) Viscoelasticity of wood composite mats during consolidation. Wood Fiber Sci. 33:353-363.

Dai, C., Steiner, P.R. (1993) Compression behavior of randomly formed wood flake mats. Wood Fiber Sci. 25:349-358.

Dai, C., Steiner, P.R. (1994a) Spatial structure of wood composites in relation to processing and performance characteristics. Part II. Modeling and simulation of a randomly-formed layer network. Wood Sci. Technol. 28:135-146.

Dai, C., Steiner, P.R. (1994b) Spatial structure of wood composites in relation to processing and performance characteristics. Part III. Modeling the formation of multi-layered random flake mats. Wood Sci. Technol. 28:229-239.

Dai, C., Steiner, P.R. (1997) On horizontal density variation in randomly-formed short-fibre wood composite boards. Composites Part A 28A:57-64.

Dai, C., Yu, C. (2004) Heat and mass transfer in wood composite panels during hot pressing: Part I. A physical-mathematical model. Wood Fiber Sci. 36:585-597.

Dai, C., Yu, C., Hubert, P. (2000) Modeling vertical density profile in wood composites during hot-pressing. In: Proceedings of 5th Pacific Rim Bio-based Composites Symposium. Canberra, Australia. pp. 220-226.

Dai, C., Yu, C., Zhou, X. (2005) Heat and mass transfer in wood composite panels during hot pressing: Part II. Modeling void formation and mat permeability. Wood Fiber Sci. 37:242-257.

Dai, C., Yu, C., Xu, C., He, G. (2007) Heat and mass transfer in wood composite panels during hot pressing: Part 4. Experimental investigation and model validation. Holzforschung 61:83-88.

Fenton, T.E., Budman, H.M., Pritzker, M.D. (2003) Modeling and simulation of oriented strandboard pressing. Ind. Eng. Chem. Res. 42:5229-5238.

García, P.J. (2002) Three-dimensional heat and mass transfer during oriented strandboard hot-pressing. Ph.D. dissertation, University of British Columbia, Vancouver, BC, Canada.

García, P.J., Avramidis, S., Lam, F. (2001) Internal temperature and pressure response to flake alignment during hot-pressing. Holz Roh Werkst. 59:272-275.

García, P.J., Avramidis, S., Lam, F. (2003) Horizontal gas pressure and temperature distribution responses to OSB flake alignment during hot-pressing. Holz Roh Werkst. 61:425-431.

Harless, T.E.G., Wagner, F.G., Short, P.H., Seale, R.D., Mitchell, P.H., Ladd, D.S. (1987) A model to predict the density profile of particleboard. Wood Fiber Sci. 19:81-92.

Haselein, C.R. (1998) Numerical simulation of pressing wood-fiber composites. Ph.D. dissertation, Oregon State University, Corvallis, OR.

Hood, J.P., Kamke, F.A., Fuller, J. (2005) Permeability of oriented strandboard mats. Forest Prod. J. 55:194-199.

Humphrey, P.E., Bolton, A.J. (1989) The hot pressing of dry-formed wood-based composites. Part II. A simulation model for heat and moisture transfer, and typical results. Holzforschung 43:199-206.

Kamke, F.A., Casey, L.J. (1988a) Gas pressure and temperature in the mat during flakeboard manufacture. Forest Prod. J. 38:41-43.

Kamke, F.A., Casey, L.J. (1988b) Fundamentals of flakeboard manufacture: internal-mat conditions. Forest Prod. J. 38:38-44.

Kelly, M. (1977) Critical review of relationships between processing parameters and physical properties of particleboard. Gen. Tech. Rep. FPL-GTR-10 USDA Forest Prod. Lab., Madison, WI.

Lang, E.M., Wolcott, M.P. (1996) A model for viscoelastic consolidation of wood-strand mats. Part II: Static stress-strain behaviour of the mat. Wood Fiber Sci. 28:369-379.

Lee, J.N., Kamke, F.A., Waston, L.T. (2007) Simulation of the hot-pressing of a multi-layered wood strand composite. J. Compos. Mater. 41:879-904.

Lenth, C.A., Kamke, F.A. (1996) Investigations of flakeboard mat consolidation. Part II. Modeling mat consolidation using theories of cellular materials. Wood Fiber Sci. 28:309-319.

Meinecke, E.A., Clark, R.C. Mechanical properties of polymeric foams. Technomic, Westport, CT, 1973.

Maloney, T.M. Modern particleboard & dry-process fiberboard manufacturing. Miller Freeman Inc. San Francisco, CA, 1993.

Painter, G., Budman, H., Pritzker, M. (2006) Predictions of oriented strand board properties from mat formation and compression operating conditions. Part 1: Horizontal density distribution and vertical density profile. Wood Sci. Technol. 40:139-158.

Schulte, M., Frühwald, A. (1996a) Shear modulus, internal bond and density profile of medium density fiber board. Holz Roh Werkst. 54:49-55.

Schulte, M., Frühwald, A. (1996b) Some investigations concerning density profile, internal bond and relating failure position of particleboard. Holz Roh Werkst. 54:289-294.

Strickler, M.D. (1959) Effects of press cycles and moisture content on properties of Douglas-fir flakeboard. Forest Prod. J. 9:203-215.

Suchsland, O. (1962) The density distribution in flake boards. Michigan Quart. Bull. 45:104-121.

Suchsland, O. (1967) Behavior of a particleboard mat during the press cycle. Forest Prod. J. 17:51-57.

Suchsland, O., Xu, H. (1989) A simulation of the horizontal density distribution in a flakeboard. Forest Prod. J. 39:29-33.

Suchsland, O., Xu, H. (1991) Model analysis of flakeboard variables. Forest Prod. J. 41:55-60.

Suo, S., Bowyer, J.L. (1994) Simulation modeling of particleboard density profile. Wood Fiber Sci. 26:397-411.

Thoemen, H. (2000) Modeling the physical processes in natural fiber composites during batch and continuous pressing. Ph.D. dissertation, Oregon State University, Corvallis, OR.

Thoemen, H, Humphrey, P.E. (2003) Modeling the continuous pressing process for wood-based composites. Wood Fiber Sci. 35:456-468.

Thoemen, H., Humphrey, P.E. (2006) Modeling the physical processes relevant during hot pressing of wood-based composites. Part I. Heat and mass transfer. Holz Roh Werkst. 64:1-10.

Thoemen, H., Ruf, C. (2008) Measuring and simulating the effects of the pressing schedule on the density profile development in wood-based composites. Wood Fiber Sci. 40:325-338.

Thoemen, H., Haselein, C.R., Humphrey, P.E. (2006) Modeling the physical processes relevant during hot pressing of wood-based composites. Part II. Rheology. Holz Roh Werkst. 64:125-133.

von Hass, G., Frühwald, A. (2000) Untersuchungen zum Verdichtungsverhalten von Faser-, Span-, und OSB-Matten. Holz Roh Werkst. 58:317-323.

von Hass, G., Frühwald, A. (2001) Untersuchungen zum rheologischen Verhalten von Faser-, Span-, und OSB-Matten. Holz Roh Werkst. 58:415-418.

Wang, S., Winistorfer, P.M. (2000a) Fundamentals of vertical density profile formation in wood composites. Part II. Methodology of vertical density formation under dynamic conditions. Wood Fiber Sci. 32:220-238.

Wang, S., Winistorfer, P.M. (2000b) Consolidation of flakeboard mats under theoretical laboratory pressing and simulated industrial pressing. Wood Fiber Sci. 32:527-538.

Wang, S., Winistorfer P.M. (2002) Monitoring *in-situ* density change for in-process measurement and control of hot pressing. Forest Prod. J. 52:77-82.

Wang, S., Winistorfer, P.M., Young, T.M. (2004) Fundamentals of vertical density profile formation in wood composites. Part III. MDF density formation during hot-pressing. Wood Fiber Sci. 36:17-25.

Wang, S., Winistorfer, P.M., Moschler, W.W., Helton, C. (2000) Hot-pressing of oriented strandboard by step-closure. Forest Prod. J. 50:28-34.

Wang, S., Winistorfer, P.M., Young, T.M., Helton, C. (2001a) Step-closing pressing of medium density fiberboard: Part 1. Influence on the vertical density profile. Holz Roh Werkst. 59:19-26.

Wang, S., Winistorfer, P.M., Young, T.M., Helton, C. (2001b) Step-closing pressing of medium density fiberboard: Part 2. Influences on panel performance and layer characteristics. Holz Roh Werkst. 59:311-318.

Winistorfer, P.M., Young, T.M., Walker, E. (1996) Modeling and comparing vertical density profiles. Wood Fiber Sci. 28:133-141.

Winistorfer, P.M., Moschler, W.W., Wang, S., DePaula, E., Bledsoe, B.L. (2000) Fundamentals of vertical density profile formation in wood composites. Part I. *In-situ* density measurement of the consolidation process. Wood Fiber Sci. 32:209-219.

Wolcott, M.P. (1990) Modelling viscoelastic cellular materials for the pressing of wood composites. Ph.D. dissertation, Virginia Polytechnic Institute and State University, Blacksburg, VA.

Wolcott, M.P., Kamke, F.A., Dillard, D.A. (1990) Fundamentals of flakeboard manufacture: viscoelstic behavior of the wood component. Wood Fiber Sci. 22:345-361.

Wolcott, M.P., Kamke, F.A., Dillard, D.A. (1994) Fundamental aspects of wood deformation pertaining to manufacture of wood-based composites. Wood Fiber Sci. 26:496-511.

Wong, E.-D., Zhang, M., Wang, Q., Kawai, S. (1998) Effects of mat moisture content and press closing speed on the formation of density profile and properties of particleboard. J. Wood Sci. 44:287-295.

Wong, E.-D., Zhang, M., Wang, Q., Kawai, S. (1999) Formation of the density profile and its effects on the properties of particleboard. Wood Sci. Technol. 33:327-340.

Yu, C., Dai, C., Wang, J.B. (2007) Heat and mass transfer in wood composite panels: Part 3. Predicted variations and interactions of the pressing variables. Holzforschung 61:74-82.

Zhou, C., Dai, C., Smith, G.D. (2008) A generalized mat consolidation model for wood composites. Holzforschung 62:201-208.

Zhou, C., Smith, G.D., Dai, C. (2009) Characterizing hydro-thermal compression behavior of aspen wood strands. Holzforschung 63:609-617.

Zhou, C., Dai, C., Smith, G.D. (2009) Viscoelasticity of aspen strands during hot pressing. Submitted to Holzforschung (under revision).

Zombori, B.G. (2001) Modeling the transient effects during the hot-pressing of wood-based composites. Ph.D. dissertation, Virginia Polytechnic Institute and State University, Blacksburg, VA.

Zombori, B.G., Kamke, F.A., Watson, L.T. (2003) Simulation of the internal mat conditions during the hot-pressing process. Wood Fiber Sci. 35:2-23.

Zombori, B.G., Kamke, F.A., Watson, L.T. (2004) Sensitivity analysis of internal mat environment during hot pressing. Wood Fiber Sci. 36:195-209.

CHAPTER 6 CONCLUDING REMARKS AND RECOMMENDATIONS

6.1 General Summary and Conclusions

Both modeling and experimental work were conducted to improve the fundamental understanding of mat consolidation of wood composite products. Unlike most of the existing models which treated the composite mat as a continuum material, this research aimed at developing a structural model by correlating the overall mat response to the behavior of individual wood strands and mat structure. As such, the mat consolidation behavior of wood composites during hot pressing can be predicted based on the compression properties of its wood constituents and the mat structure. The main conclusions and contributions are summarized as follows.

1) A generalized model was established to predict the mat consolidation behavior of wood composites at ambient conditions. In the model development, the composite mat was viewed as a system of bending units, in which the compressive force was transferred from the point contacts between adjacent wood elements. It is for the first time to apply this analytical model to investigate the mat consolidation in the filed of wood composites. This model provided good predictions of mat pressure-density relationship for fiber mats at low- and moderate-stress consolidation, where the fiber bending was the dominant mechanism. For the strand mat, the bending model predictions agreed well with the experimental results during low-stress consolidation, where the compression model (Dai and Steiner 1993) did not work well. Thus the entire consolidation process of the strand

mat could be predicted using these two models. Although this model did not give a mechanistic explanation, it provided a good fit for particle mat consolidation with some coefficient adjustments. This generalized model provided valuable insight into the understanding of the mechanisms during wood composite mat consolidation, which is useful especially for manufacturing low-density panel products.

2) The stress-strain relationship of wood strands in transverse compression was experimentally investigated at various temperatures and MCs. The quantitative relationship between the strand compression modulus and environmental conditions was described by a regression model. For the first time, the strain function of wood strands was found to be affected by high temperatures and MCs, which was previously assumed independent of environmental conditions (Dai and Steiner 1993, Wolcott et al. 1994). Nevertheless, a modified Hooke's law could still be used to predict the strand stress-strain response by modifying the strain function at elevated temperatures and MCs.

3) The stress relaxation behavior of wood strands in transverse compression was investigated at different combinations of strain level, temperature and MC. The results indicated that, on a log-log plot, the strand stress relaxation modulus and time followed a linear relationship for all conditions examined in the test. It was found that the relaxation rate was not only dependent on temperature and MC but also dependent on the initial strain level. The specific relaxation modulus of wood strands was found to be only dependent on environmental conditions. Based on these material properties, a model was established to predict the stress relaxation of wood strands during hot pressing. The

model described the strand viscoelastic behavior in terms of basic material properties such as relaxation modulus, relaxation rate, and strand thickness as well as loading rate.

4) The drop in mat pressure at the fixed mat thickness during hot pressing could be attributed to a coupled effect of hydro-thermal softening and viscoelastic stress relaxation. The former had a more significant impact than the latter. The mat elastoplasticity and springback were found to be dependent on mat MC. The mat deformation is much more plastic than elastic in nature. At normal densification, mat compression is highly irreversible, with only very small springback. The loading and unloading stress-strain relationship of strand mats had to be treated differently. A regression model was proposed to describe the mat stress-strain relationship during unloading, which gave some implications for the redistribution of layer densities after the mat reached the target thickness.

5) By linking the strain-strain relationship of wood strands in compression at elevated temperatures and MCs to the mat structure, together with a 3D heat and mass transfer model, a comprehensive simulation model was established to predict the VDP formation in strand-based wood composites during hot pressing. This VDP mode is novel because it took into account the non-uniform mat structure. As a result, it can predict not only the overall panel VDP but also the localized VDP of a given area within the panel. It is for the first time to link the horizontal density distribution to the vertical density distribution within the panel. The proposed model was validated by comparing its predictions with experimental data. It was found that the VDP of low-density area seemed to be more

uniform than that of high-density area. Furthermore, one capability of this VDP model is to predict the effects of some pressing variables on VDP formation in the form of a sensitivity analysis, which revealed that the face layer density increased for shorter press closing times with a corresponding decrease in core layer density; preheating of the mat was found to make the VDP of the panel more uniform.

This VDP model provided a fundamental approach to correlating the product properties to the production variables. As a result, it may become a valuable tool for the optimization of the manufacturing process with minimum trial-and-error experiments and their associated costs. For example, the effect of strand dimensions on VDP formation was not examined in this work, but it could be easily undertaken by a plant personnel. The input strand dimensions for the model can be varied systematically and the effect of these parameters on the predicted VDP determined. The plant would then be able to identify the strand parameters that have the most impact on VDP and then make modifications to their stranding process to obtain the required strand dimensions.

6.2 Recommendations and Further Research Work

The simulation model for VDP formation during hot pressing is developed based on the assumption of uniform strand size and random strand orientation. Further work is needed to take into account the combination of strand size and non-random orientation to better represent the actual conditions of OSB manufacture. Moreover, the current mat structure was constructed for a one-layer strand mat (purely random) and thus a multiple-layered

mat (combination of random layer and oriented layer) could be introduced into further model development. In addition, an uneven meshing technique could be used to more accurately simulate the VDP curve. Namely, the outer layers in the mat would be meshed into finer elements because they are more sensitive to the distributions of temperature, MC, and layer densities. Also, steam-injection heating would be incorporated into the model by modifying the heat and mass transfer model. Finally, asymmetric heating can be introduced by changing the boundary conditions to predict asymmetric VDP in real boards.

Due to the limitation of the testing apparatus, the compression behavior and viscoelasticity of wood strands were not fully investigated under the conditions of high temperatures and MCs. More effort is needed to acquire an environmental chamber, which can precisely control the temperature and humidity conditions and make them uniformly distributed inside the mat in a short time without any degradation occurring in wood. With this chamber mounted on an MTS load frame, the strand compression and stress relaxation tests can be conducted under the environmental conditions similar to the real panel manufacturing process, which will provide more accurate input parameters for the VDP model. Furthermore, the consolidation and stress relaxation tests for the whole mat at elevated temperature and MC can also be carried out with this environmental chamber, which will provide more comparable results with model predictions. Similarly, with the environmental chamber, the effects of temperature and resin curing need to be further investigated to more accurately describe the mat elastopalsticity and springback.

The proposed VDP model ignores the interactions between neighbouring strand columns. This simplification could affect the VDP model prediction. Additional work to incorporate between-column interactions would make the model more closely describe the actual pressing process. Further work could also be conducted on the mat creep behavior during mat pressure holding stage, which is not considered in the current model. Moreover, the effect of fines on VDP formation could be another interesting issue for further model development. With these expected improvements, a complete VDP formation process during hot pressing would be modeled with more accuracy.

In addition, all the experimental results in the present work were obtained from aspen wood strands, a diffuse-porous hardwood with no obvious growth rings (Bowyer et al. 2002). For other wood species, due to the anatomical differences such as rays and earlywood-to-laterwood ratio, their compression behavior could be different from that of aspen wood. The strain function is dependent on the cellular structure of the wood species and may be different for other species. As a result, to improve the applicability of this model, further experimental work is needed to characterize the mechanical responses of different wood species in transverse compression under various environmental conditions. When such a material property database is established, together with the other improved input parameters, this VDP model would have more realistic applicability in industry production.

6.3 Bibliography

Bowyer, J.L., Shmulsky, R., Haygreen, J.G. Forest products and wood science: An introduction. Iowa State Press, Ames, IA. 2002.

Dai, C., Steiner, P.R. (1993) Compression behavior of randomly formed wood flake mats. Wood Fiber Sci. 25: 349-358.

Wolcott, M.P., Kamke, F.A., Dillard, D.A. (1994) Fundamental aspects of wood deformation pertaining to manufacture of wood-based composites. Wood Fiber Sci. 26: 496-511.